1-1-2014

A Functional Approach to Resolving the Biogeocomplexity of Two Extreme Environments

Haydn Rubelmann III
University of South Florida, rubelman@mail.usf.edu

A Functional Approach to Resolving the Biogeocomplexity of Two Extreme Environments

by

Haydn Rubelmann III

A dissertation submitted in partial fulfillment
of the requirements for the degree of
Doctor of Philosophy
Department of Cell Biology, Microbiology and Molecular Biology
College of Arts and Sciences
University of South Florida

Major Professor: James R. Garey, Ph.D.
Randy Larsen, Ph.D.
Kathleen Scott, Ph.D.
David Merkler, Ph.D.

Date of Approval:
November 12, 2014

Keywords: environmental microbiology, extremophiles, shallow-water hydrothermal vents, anoxic marine pits

DEDICATION

I would like to dedicate this dissertation to three of my personal champions: my grandfather, Haydn Rubelmann Sr. (1929 - 2004), who encouraged me to pursue an academic career; my stepfather, Dale Jones (1954 - 2008), who was the best father anyone could ever hope for, and my husband, Eduardo Godoy, who suffered through not only 8 years of my doctoral tenure, but a grueling civil liberty injustice that almost wedged the Caribbean Sea between us.

ACKNOWLEDGMENTS

There are many people without which this dissertation would not be possible. I would be foolish to think I could include them all here, and will try to be brief in my gratitude. Foremost, I must acknowledge my mentor, Jim Garey, who is paramount in providing me the opportunity to research in his lab. I would like to acknowledge the graduate students in the Garey lab who preceded me and guided me in the bench work while I was an undergraduate – notably: Terry Campbell, Mike Robeson, and Brent Nichols. I would also like to thank the first two undergraduate researchers who worked with me for over two years: Matthew Trinidad and Christina Brown. Kathleen Scott's Winogradsky column provided me unlimited DNA without which my *dsr* primers would have never been perfected. I would like to thank Jody Harwood for allowing me to use her DGGE apparatus and Bionumerics software and Bina Nayak for taking me through the procedure for the first time. Thanks to Steven Enkemann who provided me bench space at Moffitt Cancer Research Center's Microarray Core as well as guidance in the analysis of microarray data. I would also like to emphasize my extreme gratitude to all of the undergraduates that were necessary for the field work required of this study: Mark Khuns, Urvish Patel, William Spencer, Monica Lazaro, Gabby Gauthier, Amanda Zimmerman, Amanda Diaz, Sean Jarvis, Matthew Manzi, and Paulo Portocarrero. Field work consisted of 16 hour days, in which all of these undergraduates exceeded any

expectations I had. My family, who has always supported me and given me comfort in times of despair, deserves crowns for their generosity. Specifically, my mother, Cheryl Jones, who infused me with creativity and a work ethic that allowed me to accomplish this dream. Eva Woodruff, my aunt, who answered all of my phone calls of frustration and my grandmother, Shirley Stevens who imbued values in me that have allowed me to make numerous and lasting friendships. Thank you to all.

TABLE OF CONTENTS

LIST OF TABLES

LIST OF FIGURES

ABSTRACT

The biodiversity of two distinct marine environments was observed to describe the biogeocomplexity of these extreme ecological systems. A shallow-water hydrothermal vent in Papua New Guinea served as a study of a thermophilic ecosystem influenced by arsenic rich vent fluids while a 60 m deep offshore primarily anoxic karst sink served as a study of an anaerobic sulfur-influenced habitat. Both environments support unique biological communities that are influenced by the physical and chemical pressures imposed on them by the harsh conditions of these systems. In Tutum Bay, Ambitle Isle, Papua New Guinea, a transect was created from a shallow hydrothermal vent that extended 120 m away from the vent. Previous studies have shown that the geochemistry of the system is heavily influenced by arsenic which is toxic to most organisms. In this study, macro- and meiofauna were collected and scored and combined with bacterial sequence data collected along the length of the transect. It was found that near vent sites harbored biological communities more similar than sites further from the vent. Many species were found only at sites near the hydrothermal vent. Near-vent communities were less diverse than those away from the vent, and biodiversity generally increased as distance from the vent increased. Distinct correlations between thermophilic organisms and temperature were observed. The metabolic repertoire of the microbial communities suggests that many strategies are

used to obtain energy and carbon. The relative abundance of bacteria containing genes to reduce arsenic was comparable to those able to reduce sulfur compounds. Primary production appeared to be a mix of chemo- and phototrophy. Food webs and association analysis suggest a complex interplay between macrofaunal, meiofaunal and bacterial communities. While the system is heavily influenced by arsenic, no specific correlation between the relative abundance of arsenic metabolizing organisms and the amount of arsenic in the system could be drawn. This is likely due to the fact that most of the arsenic produced by the system is readily adsorbed onto iron oxyhydroxides, reducing the arsenic's bioavailability.

The anoxic conditions at Jewfish sink provide a different hurdle than the hot arsenic conditions found in Papua New Guinea. The anoxic conditions are shared by other pit features found in karst geography, but the metabolic processes between Jewfish sink and these other karst habitats are different. The blue holes and black holes of the Bahamas are some of the most well-studied of these karstic pits. In these features, which are large circular pits with diameters of over 300 m, light and sulfur are used as a means of energy acquisition. Jewfish sink, having an opening only 6 m in diameter, is light restricted compared to these systems. As a result, the strategy of organisms dwelling in the anoxic conditions of the sink is different than those found at the well-studied holes in the Bahamas. Geochemical measurements were recorded over two time periods spanning a combined total of 6 years. The anoxic bottom waters of Jewfish sink remain stable and contained high levels of sulfide throughout most of the seasons studies. Sequence analysis of prokaryotes within the sink showed that sulfur reducers had the highest relative abundance compared to other functional guilds. To

monitor the changes of the microbial communities within the sink, bacterial communities were examined at 4 depths within the sink at 9 different intervals over a period of 685 days. Denaturing Gradient Gel Electrophoresis (DGGE) was used to fingerprint 16s rRNA bacterial communities and dissimilatory sulfite reducing communities by targeting the 16s rRNA bacterial gene and the *dsr* gene associated with dissimilatory sulfite reducing bacteria and archaea. The lowest depth studied within the sink (40 m) remained stable chemically and biologically until a turnover event occurred within the second winter of the study. This turnover event disrupted the biological communities at 40 m and led to a reestablished community comprised of different species that those found prior to the event. Upper waters within the sink show that clines establish themselves seasonally and partition zones that confine bacterial communities that are more similar to each other within these zones while excluding bacterial communities that are outside of these zones. Oxygenated water was shown to not contain prokaryotes containing the *dsr* gene. As the oxycline changed seasonally, dissimilatory sulfite reducing prokaryotes containing the *dsr* gene remained in the anoxic zone and required time to reestablish themselves whenever oxygenated water displaced them.

CHAPTER ONE: COMPARISON OF AN INACTIVE SUBMARINE SPRING WITH AN ACTIVE NEARSHORE ANCHIALINE SPRING IN FLORIDA

This chapter has been published as: Garman KM, Rubelmann H, Karlen DJ, Wu T and Garey JR. (2011). *Comparison of an inactive submarine spring with an active nearshore anchialine spring in Florida*. Hydrobiologia 677: 65-87. My part of this work was the processing (extraction, cloning, sequencing) and analysis of the bacterial and archaeal communities within Jewfish sink. I also wrote that section of the paper.

Abstract:

Jewfish Sink is a former anchialine karst feature located in the Gulf of Mexico off the coast of West Central Florida. Freshwater flowed from the feature until 1962 and it is now an anoxic marine basin. The current biodiversity within Jewfish Sink was examined in terms of Bacteria, Archaea and Eukaryota using a combination of 16S and 18S ribosomal RNA analysis from environmental samples. Analysis of 16S rRNA sequences from microbial mats in the anoxic zones revealed a broad diversity of bacteria (320 clones) and archaea (412 clones), many of which had been previously identified in anoxic environmental samples and are likely involved with sulfur, nitrogen and methane metabolism. Sequence analysis of 836 18S clones revealed that fungi and dinoflagellate sequences dominate the eukaryote sequences. Because Jewfish Sink

water is anoxic and high in sulfide we investigated the effect of Jewfish sink on the nearby shallow benthic environment. We compared the shallow benthic macrofauna near Jewfish Sink to that near Crystal Beach Spring, an active submarine spring. We found significantly higher species richness, abundance, and diversity of benthic fauna near the Jewfish Sink site compared near Crystal Beach Spring. This comparison suggests that higher rates of submarine groundwater discharge in an area with active submarine springs are a significant factor reducing the richness and diversity of the benthic community structure in the near shore, shallow marine environment.

Introduction:

Anchialine cave systems are characterized by the presence of freshwater or brackish water, a halocline that forms between waters of different salinities, and subterranean connections to a saltwater body (Iliffe 1992). Such mixing zones between waters of varying salinities in cave systems and other groundwater circulation systems have been referred to as the subterranean estuary by Moore (1999). Anchialine cave systems formed in limestone are found along the Gulf of Mexico coast of Florida, Bermuda, Cuba, the islands of the West Indies including the Bahamas, the Yucatan Peninsula, and Central America including Belize (Iliffe 1992). Along Florida's Gulf of Mexico coastline, some anchialine cave systems like Crystal Beach Spring discharge water as submarine springs. Over the last 50 years, many submarine springs off the coast of Florida such as Jewfish Sink have ceased flowing, becoming anoxic marine basins.

Anoxic marine basins:

Anoxic marine basins similar to Jewfish sink include Bahamian blue holes. Bottrell et al. (1991) studied Bahamian blue holes in which an oxic freshwater lens overlies anoxic saline water. They documented bacterially mediated sulfate reduction, which produces sulfide in the anoxic saline zone. They also identified bacterially mediated sulfide oxidation at the chemocline, which reduces pH and may enhance dissolution of the carbonate rock. Similar processes were also documented in cenotés of the Yucatan Peninsula (Stoessell et al. 1993; Schmitter-Soto et al. 2002).

The sulfide produced by sulfate reduction during the oxidation of organic carbon in anoxic marine basins readily reacts with reduced metals to form insoluble metal sulfide compounds such as the iron-sulfide pyrite. When sulfide reacts with metals, escapes the water column, or is converted to elemental sulfur by anoxic photoautotrophic sulfide bacteria, the water column remains basic, favoring the precipitation of calcium carbonate (Castanier et al. 1999). The sulfide can also support communities of chemolithoautotrophic sulfur-oxidizing bacteria at the chemocline where oxygen is present and in zones where nitrate is present (Moon et al. 2010). In this case, the end product of bacterial mediated sulfide oxidation is often sulfuric acid, which reduces the pH creating conditions in which calcium carbonate precipitation does not occur (Castanier et al. 1999). By these processes, the composition of microbial communities and the reactions of sulfide in anoxic marine basins are indicated by pH and by the presence or absence of calcium carbonate precipitation.

Submarine groundwater discharge:

Submarine groundwater discharge is estimated to be about 95% recirculated seawater (Santos et al. 2008). Studies by Johannes (1980), D'Elia et al. (1981), and Simmons (1992) indicate that groundwater seepage into shallow marine environments has higher levels of ions including nitrate than surface water discharges. This increase in ion concentration is caused by chemical transformations such as ammonification of organic nitrogen followed by nitrification in the subterranean estuary; and is thought to have a significant impact on benthic communities (Slomp and Van Cappellen 2004; Charette and Sholkovitz 2006; Santos et al. 2008).

Benthic macrofauna:

The West Central Florida area of the study reported here was included in the Florida West Coast province of Engle and Summers (2000) where benthic macroinvertebrates were examined from 870 estuaries along the Gulf of Mexico and the western Atlantic coasts of the United States to evaluate fauna provinces. In a literature review of benthic macrofauna assemblages that included the Gulf of Mexico, Brooks et al. (2006) identified polychaetes, specifically *Prionospio cristata*, *Nephtys incisa*, *N. picta*, and *Spiophanes bombyx*, as the principal taxa common to all assemblages. A study of estuaries in the northern Gulf of Mexico by Rakocinski et al. (1997) determined that the influence of natural gradients in depth, salinity and sediment composition made evaluating the impacts of sediment pollution difficult to identify in benthic macrofauna communities. During storm events in the Gulf of Mexico, scouring of the sediment and salinity changes have been identified as the primary factors contributing to changes in diversity and abundance of benthic macrofauna (Malin et al. 1999; Engle et al. 2009).

Seasonal hypoxic zones accompanied by sulfate reduction and sulfide formation were also found to decrease benthic macrofauna abundance, diversity, richness, and evenness (Rabalais et al. 2001; Montagna and Ritter 2006).

Benthic macrofauna can be useful indicators of environmental stress. Previous studies have focused on changes in benthic abundance and diversity due to natural or anthropogenic disturbance within a localized area (Zajac and Whitlatch 2003), or along an environmental or pollution gradient (Weston 1990; Simboura et al. 1995; Rakocinski et al. 1997; Rosenberg et al. 2001; Je et al. 2003; Stark et al. 2005; Karlen et al. 2010).

Jewfish Sink:

Jewfish Sink was a submarine spring near Aripeka, Florida (Figure 1.1), with flow at all tidal stages until the drought of 1961-62 when the spring ceased flowing. In 1960, salinity measurements at the water surface from the spring boil, where spring water had mixed with overlying Gulf of Mexico water, were 8.8 ppt (Wetterhall 1965; Rosenau et al. 1977; Waller 1985). Today, the former spring is an anoxic marine basin with sulfidic bottom water and surface water salinities in the vicinity of the sinkhole typically range from 16 to 27 ppt. The basin has a maximum depth of about 64 m and a diameter of about 76 m at the bottom compared to a diameter of about 6 m on the floor of the Gulf of Mexico, which is 0.6 to 2 m deep in the vicinity of the sinkhole (Garman and Garey 2005). Today, there are no visible conduits passable by a diver leading from the sinkhole to the aquifer, indicating that the spring had numerous smaller conduits or the main conduits have been filled with sediment since flow ceased.

The Jewfish Sink water column was found to have four distinct water quality zones during a previous study by Garman and Garey (2005). The four water column

zones include: the shallow oxic zone; the transition zone in which dissolved oxygen concentrations drop abruptly with depth to zero or near zero and salinity increases abruptly; an upper anoxic zone with some influence from trace oxygen concentrations when chilled surface water sinks in the winter; and relatively stable anoxic bottom water with elevated alkalinity, ammonia, and sulfide values compared to the upper anoxic zone and with relatively stable temperature (16 to 17°C) and salinity (33 to 35 ppt). These zones are illustrated schematically in Figure 1.2 and in more detail in Figures 1.3 through 1.6 which display Datasonde data relating depth to temperature over time (Figure 1.3), depth to salinity over time (Figure 1.4), depth to pH over time (Figure 1.5) and depth to dissolved oxygen over time (Figure 1.6). This data is from Garman and Garey (2005) but presented in a contoured format that was not previously prepared and illustrates how the physical and chemical parameters of the water change from season to season.

The oxic zone contains a variety of marine fish and macroinvertebrates. Within the oxic zone, there are sediment covered rock ledges that cut back into the sides of the sinkhole that may be influenced by sulfide seepage upward from the underlying anoxic zones, as the sponges, corals and tunicates that are common in the oxic zone on the sides of the sinkhole are scarce in the cut back ledges. The deeper anoxic zones are sulfide rich and contain no living fish or macroinvertebrates.

The Datasonde data show the sinking of cold oxygenated surface water in the winter. Another finding from the previous study is a dramatic increase in the pH of the upper anoxic zone during the summer months that is likely of biological origin (Figure 1.5). Analyses of particulates collected from the water column in the upper anoxic zone

and lower transition zone during the winter indicated the presence of two types of particles: aluminum silicate clay minerals; and aggregates of organic and inorganic particles rich in iron, sulfur and sea salts. During the winter months, pH values in the transition zone and upper anoxic zone are much lower than the summer values and normal seawater values indicating that chemolithotrophic sulfur oxidizing bacteria that convert sulfide to sulfate using oxygen as an electron acceptor in a reaction that reduces pH may be consuming most of the sulfide present in these zones (Garman and Garey 2005).

Crystal Beach Spring:

Crystal Beach Spring is an active brackish water spring with typical discharge salinity values of 2.9 to 5 ppt at the main spring vent in the floor of the near shore of the Gulf of Mexico (DeWitt 2003). Salinity values as low as 1.6 ppt have been measured in the cave passages unaffected by siphoning of Gulf water and the influx of saline groundwater. The spring opening is connected to anchialine cave passages that extend to the east beneath dry land and have a mapped length of over 2 km. Crystal Beach Spring begins as a 0.5 m opening at a depth of 6 m in a cone shaped basin with a diameter of about 15 m in the floor of Gulf. Cave passages are developed along bedding planes and are primarily located at depths between 15 and 42 m. Where the cave passages drop to a depth of 39 m there is a stable pycnocline in the water column with warmer, anoxic, saline groundwater (24.86 °C, salinity 33.3 ppt) below the freshwater spring flow (24.26 °C, salinity 2.29 ppt) (Garman et al. 1999; Garman 2000). Conduits feeding Jewfish Sink when it was an active spring were probably similar to the cave passages of Crystal Beach Spring.

Peak discharge occurs at the end of the wet season (typically September and October). Measurement of the discharge from the main spring vent in September 2003 showed a flow of 0.65 m^3/s. Tides in the Gulf of Mexico along the coast of West Central Florida are the mixed semidiurnal type with higher high and lower high tides as well as higher low and lower low tides possible each day (Yobbi 1992). At the end of the wet season, the spring siphons only during the highest high tides that occur during the full and new moon, if at all. Low discharge occurs at the end of the dry season (typically April and May). At this time of year, the spring generally experiences significant siphoning events at least once daily at the higher high tide (DeWitt 2003) when the flow out of the spring reverses and seawater flows into the spring.

The cave passages of Crystal Beach Spring contain a variety of fauna including five stygobitic crustaceans: the crayfish *Procambarus* sp. (probable new species, personal communication from Richard Franz, Florida Museum of Natural History) and *Troglocambarus* sp.; the isopod *Caecidotea* sp.; and the amphipods *Crangonyx hobbsi* and *C. grandimanus*. These stygobites represent the first cave-adapted animals found in a freshwater cave system flowing beneath a body of saltwater in Florida. Other macrofauna identified in the cave passages include: a hydroid, *Garveia franciscana*; entoprocts; clams *Mytilopsis leucophaeata* (Conrad 1831) and *Brachydontes exustus* (Linnaeus 1758); a hydrobiid snail *Littoridinops palustris*; and a worm *Stenoninereis martini* (Wesenburg-Lund 1958) (Garman 1997). The conduits and cave passages feeding the spring at Jewfish Sink likely contained a similar variety of fauna when the spring was active but currently no stygobitic macrofauna are associated with the sink.

Current study:

One goal of this project was to survey the prokaryotic and eukaryotic biodiversity within Jewfish Sink to test the hypothesis that the geochemical properties of the sink water are related to biological activity. We used a molecular profiling method (Wu et al. 2009) to characterize the prokaryotic and eukaryotic communities using 16S and 18S rRNA gene sequences from DNA extracted directly from environmental samples collected from sediments on cut back ledges in the sides of the sinkhole in the oxic zone of the sinkhole, the water column at the chemocline, and bacterial mats in the anoxic zones.

Jewfish Sink is located offshore from rural Pasco County without large point sources of environmental pollutants (Figure 1.1). In contrast, Pinellas County operates a spray irrigation and sludge disposal facility for sewage about 5 km north-northeast of Crystal Beach Spring. This facility has treated about 11,355,000 cubic meters of water per year since 1976. The disposal operations have created a potentiometric high in the Floridan aquifer at the disposal facility and elevated nitrate concentrations that exceed 10 mg/l have been detected in wells to the west of the facility (Trommer 1992). The geologic investigation for the Trommer study showed a high degree of conduit porosity development in the Floridan aquifer allowing rapid movement of effluent impacted groundwater to coastal discharge points. Studies in the Florida Keys, where there is also a high degree of conduit porosity, measured groundwater velocities exceeding 100 m/hr to discharge points offshore (Paul et al. 1995; 1997; 2000). The shallow benthic marine environment around Jewfish Sink is subject to potential impacts from sulfide production in the bottom water of the sinkhole and surrounding subterranean estuary

that may create a sulfide pump by diffusion of sulfide upward from the sink into the overlying and nearby sediments (Garman and Garey 2005). Additionally, the submarine groundwater discharge in the vicinity of Jewfish Sink should have less freshwater and anthropogenic influences compared to the submarine groundwater discharge near Crystal Beach Spring where a higher freshwater head is present and the spring is still active. These factors led to another goal of this project which was to study the influence Jewfish Sink and Crystal Beach Spring each have on their surrounding marine environments. They influence the surrounding environment not only by discharge from the main opening of the spring and sink, but also the more diffuse seepage from the underlying underground systems of which the sink and spring are a part. Therefore we examined the community structure of the benthic macrofauna in the vicinity of Jewfish Sink and compared it to the community structure of the benthic macrofauna in the vicinity of Crystal Beach Spring.

Materials and methods:

Certified divers affiliated with the National Association for Cave Diving, the National Speleological Society Cave Diving Section, and the Academic Diving Program at the University of South Florida performed the research dives for this study.

Physical characteristics:

HOBO recording thermometers (Onset Computer Corporation, 470 MacArthur Blvd., Bourne, Massachusetts) were installed in Jewfish Sink at ten fixed depths (3, 6, 9, 12, 18, 24, 31, 37, 46, and 61 meters) to record the water temperature every 4 hours from October 7, 2003 to July 26, 2004. The purpose of the thermometer installations was to obtain a more detailed evaluation of the winter sinking of cold surface water than

was obtained during previous studies using a Datasonde carried by divers. The 4 hour sampling interval was adequate for this evaluation. HOBO thermometers were encased in watertight 5-cm diameter plastic spheres weighted with lead to have slight negative buoyancy in saltwater. Each sphere was labeled with the desired installation depth. A nylon line was attached to a rock outcrop at a depth of 3.1 m where the first thermometer was installed. The thermometers were attached to the nylon line at each monitoring depth and the nylon line was attached to rock outcrops of opportunity so that the depth was fixed. Air temperature data were obtained from the Brooksville, Florida, weather station located about 22.5 km northeast of Jewfish Sink. Data were analyzed using Surfer version 9 (Golden Software, Golden, CO, USA)

Divers using 4 L containers collected samples of the particulate cloud. The containers were submerged, filled with distilled water. At the depth where the particulate cloud was observed to be the densest, the containers were purged with inert gas (laboratory grade helium rated 99.99 % pure) and filled with ambient water. Each container was purged three times as the diver moved forward and/or downward in the water column away from exhaust gases and previously purged contents of the sampling container. The samples were filtered onto a 0.2 µm filter and dried under a vacuum. Pieces of the filter (5 mm square) were examined in environmental mode of a scanning electron microscope (Hitachi S-3500N, Schaumburg, IL). Elemental analysis was performed using an energy dispersive X-ray analysis system with a light element prism detector (Princeton Gamma Technology, Rocky Hill, NJ). Dried filter samples were also sputter coated with gold for microphotography.

Seepage rates were measured in the vicinity of Jewfish Sink and Crystal Beach Spring in June 2006 using the method described by Lee (1977) and sampling procedures discussed in similar studies (Simmons and Netherton 1987; Shaw and Prepas 1990). Seepage was measured to evaluate large scale differences in the more diffuse submarine groundwater discharge beyond the entrances of the karst features in an area where a submarine spring has ceased flowing (low freshwater head) compared to an area where a submarine spring is still active (high freshwater head). The top third of a 55-gallon drum was buried with the edge 5 to 10 cm deep into the sediments in May 2005. At Jewfish Sink and Crystal Beach Spring, the seepage meters were installed 5 m and 15 m east (shoreward) of the rim of the sinkhole. Seepage rates were computed from the volume of water in the collection bag, the surface area of sediment enclosed by the meter, and the time that the collection bag was deployed. Local tide charts for the sampling period in June 2006 were obtained (Figure 1.7).

Macrofauna sample collection and processing:

At each location on August 8, 2004, benthic macrofauna samples were collected at four sites in the vicinity of the sink or spring: 5 m, 50 m, 100 m, and 1 km from the edge of each basin. At Jewfish Sink, the 5, 50, and 100 m samples were collected along a horizontal line running from the eastern edge of the sink eastward toward shore. The 1 km sample was collected to the west of the sink basin. At Crystal Beach Spring, the 5, 50, and 100 m samples were collected along a horizontal line running from the eastern edge of the spring basin eastward toward shore. The 1 km sample was collected to the north of the spring basin. At each site, a 1 m^2 grid was placed next to the sampling line. Three core samples (diameter = 7.62 cm; area = 45.6 cm2) were collected from the grid

at random positions by pushing the cores 10 cm into the sediments. The short push core samples were sieved through a 500 µm mesh sieve and the retained animals were fixed in 10% formalin with Rose Bengal stain for a minimum of 72 hours then transferred into 70% methanol for preservation. Organisms were sorted from the sediment under a dissecting microscope, identified to the lowest practical taxonomic level and enumerated.

Macrofauna data analysis:

All data was initially entered into a Microsoft Excel spreadsheet. Statistical analysis was conducted using SigmaStat ver. 3.5 (Systat Software, Richmond CA). Multivariate statistics, SIMPER analysis, and basic community indices were calculated using PRIMER ver 6 (Plymouth Marine Laboratory, U.K.). Abundance and richness between transects were analyzed using a Mann-Whitney rank sum test. Abundance among sampling sites was analyzed using a Kruskal-Wallis one-way analysis of variance on ranks. Shannon-Weiner diversity index and evenness between sampling sites were analyzed using a t-test. Shannon-Weiner diversity indices, evenness and richness among sampling sites were analyzed using a one-way analysis of variance with a Holm-Sidak pairwise multiple comparison procedure. Cluster analyses were performed using the Bray-Curtis similarity index that was calculated using a square root transform of the abundance data with PRIMER ver 6. Multi-dimensional scaling (MDS) using the Bray-Curtis similarity index was also used to show the community structure between transects and among sites along each transect.

Molecular analyses:

Samples were collected from the bacterial mats in the anoxic zones for analysis for bacterial and archaeal 16S rRNA and eukaryotic 18SrRNA, and sediment samples were collected from the cut back rock ledges within the sinkhole in the oxic zone for eukaryotic 18SrRNA.

Samples from the bacterial mat and water column were collected on March 30, 2002, by divers using sterile 60 mL capped syringes held below the diver during descent into the sinkhole to avoid contamination by exhaust gases, as described by Brigmon et al. (1994). Following the dive, the samples were stored in a cooler on ice until transferred to a -20°C freezer at the laboratory on campus. Sediment samples were collected by divers on July 22, 2002, and stored in a cooler on ice until transferred to a -20°C freezer at the laboratory on campus. Prior to DNA extraction, the water samples were vacuum filtered onto a 0.2 µm filter and the sediment samples were passed through a 500 µm sieve onto a 50 µm sieve.

DNA was extracted (Hempstead et al. 1990) by adding 5 mL extraction buffer (1M Tris-HCl, pH 8.0, 100mM EDTA, 3.5% SDS) to each sample and rotating for 10 to 20 min. A phenol extraction and ethanol precipitation was performed. The DNA pellet was dried and re-suspended in 500µL water.

The samples for eukaryotic 18S rRNA gene analysis were PCR amplified using conserved primers 18S4 (5' CCGGAATTCAAGCTTGCTTGTCTCAAAGATTAAGCC 3') and 18S5 (5' CCGGAATTCAAGCTTACCATACTCCCCCCGGAACC 3') representing approximately 800 base pairs of the 5 prime portion of the gene (Mackey et al., 1996). The samples for prokaryotic 16S rRNA gene analysis were PCR amplified using

conserved primers 8F (5' AGAGTTTGATCCTGGCTCAG 3') and 1492R (5' GGTTACCTTGTTACGACTT 3') (Baker et al., 2003, Reysenbach et al. 1994).The samples for archaeal 16S rRNA gene analysis were PCR amplified using conserved primers Arch21F (5' TTCCGCTTGATCCYGCCGGA 3') and Arch958R (5' YCCGGCGTTGAMTCCAATT 3') (Baker et al., 2003). For PCR amplification the following components were used: 39.5 µL nanopure water; 5 µL 10X reaction buffer (200 mM Tris-HCl pH 8.75, 100 mM KCl, 1mg/mL BSA); 1 µL dXTP mixture with 12.5 mM of each nucleotide; 0.5 µL (2.5 units) Taq polymerase; 0.5 µL of 5 µM of each primer; 2 µL 50 mM MgCl2; and 1 µL 1:20 dilution of environmental DNA. PCR conditions consisted of an initial denaturation at 94° C for 2 min, followed by 35 cycles of denaturation at 95° C for 15 s, annealing at 55° C for 1 min, extension at 72° C for 2 min, and a final extension of at 72° C for 5 min. Libraries of PCR amplified 18S rRNA gene fragments from each site were cloned using a TOPO TA Cloning Kit (Invitrogen Inc., Carlsbad, California). Individual clones were sequenced with a Beckman CEQ 8000 instrument (Beckman Co., Palo Alto, California). For sequencing, archaeal primer Arch21F, prokaryotic primer 27F (5' AGAGTTTGATCCTGGCTCAG 3') (DeLong 1992), and eukaryotic primer 18S4 were used.

Raw sequences were processed with custom software developed in our lab that finds a highly conserved region of the sequence as an anchor point and then trims upstream and downstream from that point. We optimized the trim points so that only the most accurate part of the sequences were used, and employed a filter that removed poor quality sequences. This optimization approach has been shown by Wu et al.

(2009) to produce highly accurate sequences by reducing the length of the read to 500 bp and discarding poor sequences.

The filtered sequences were analyzed using the program Sequencher (Gene Codes, Ann Arbor, MI) to group sequences into operational taxonomic units (OTUs) with 97% identity for prokaryotes (Schloss and Handelsman 2005) and 99% identity for eukaryotes (Wu et al. 2009). A representative sequence from each OTU was used as a query in a Genbank search and the nearest identified sequence match used to provisional identify each OTU. The sorting of prokaryote OTUs into groups with similar metabolic function was carried out by reviewing the literature for each provisionally identified prokaryote. Rarefaction curves and estimates of Shannon Diversity were calculated using EcoSim Software (Gotelli 2009).

Results:

Physical characteristics within Jewfish Sink:

Temperature data was recorded every 4 hours in Jewfish Sink from October 11, 2003 to July 26, 2004 (Figure 1.8). The data show that the water temperatures in the upper 9 m of the sinkhole vary in close relationship to the surface air temperature. Decreases in water temperature at depths of 6 and 9 m show a delay of about 10 days compared to decreases in water temperature at 3 m depth. The coldest temperatures in the upper 9 m were 10.6^{o}C on December 12, 2003, and 10.2^{o}C on January 1, 2004, at 3 m; 10.2^{o}C on December 21, 2003, and on January 12, 2004, at 6 m; and 10.9^{o}C on December 22, 2003, at 9m.

Figure 1.8 shows contoured temperature data from the HOBO recording thermometers. The sinking of denser, colder water was observed in the data from the

recording thermometers at depths of 12, 18, and 24m. At a depth of 12m, the temperature decreased 3.8^{o}C in 8 hours on December 3, 2003, and another 3^{o}C in 20 hours on December 6 and 7, 2003. At a depth of 18m, the temperature decreased 4.2^{o}C in 8 hours on December 7 and 8, 2003. At a depth of 24m, the temperature decreased 3.4^{o}C over 16 days from December 28, 2003, to January 13, 2004. The sinking surface water was not dense enough to influence temperatures at depths of 31m and deeper. At these deeper depths, the temperature was generally constant.

Previous analyses of the particulate cloud in Jewfish Sink were from samples collected in late winter 2004-2005 from the upper anoxic zone and lower transition zone. Additional samples were collected during the summer of 2005 to determine whether the composition of the particulate cloud changes in the summer when the pH of the water in the upper anoxic zone undergoes a dramatic increase. Electron microscopy revealed two kinds of particles in the cloud from the summer samples: iron sulfide minerals including pyrite framboids and a mineral composed of calcium, carbon, and oxygen identified as calcium carbonate (Figure 1.9). The summer composition of the particulate clouds is different from the winter composition of aluminum silicate clay minerals and aggregates of organic and inorganic particles (Garman and Garey 2005).

Molecular measures of biodiversity within Jewfish Sink:

The 413 archaeal sequences clustered into 205 OTUs based on 97% similarity and the results are summarized in Table 1.1. Shannon Diversity of archaeal sequences were lower (4.64) than bacterial sequences (4.81). Rarefaction curves suggest that sampling of both archaeal and bacterial sequences was incomplete (Figure 1.10). The closest sequences in Genbank for each OTU varied widely but included environmental

sequences from hypersaline waters, microbial mats, anoxic sediments, methane cold seeps and hydrothermal sediments. Archaeal sequences represented a variety of groups that included anaerobes, ammonia oxidizers, methanogens and sulfur reducers (Table 1.2).

The 320 bacterial sequences clustered into 164 OTUs based on 97% similarity. Results are summarized in Table 1.3. The closest sequences in Genbank for each OTU included environmental sequences from hypersaline microbial mats and waters, deep sea microbial mats, anoxic sediments, methane cold seep sediments, salt marshes, landfill leachate, hydrothermal sediments, seagrass sediments, and whale fall ecosystems. Bacterial sequences represented groups that included anaerobes, methane oxidizers, ammonia oxidizers, sulfur reducers and oxidizers.

The 836 eukaryotic sequences clustered into 149 distinct (OTUs) based on 99% similarity and the results are summarized in Table 1.4. Shannon Diversity of eukaryotic sequences within the anoxic mat is higher (3.42) than in the oxic sediment from the cut back ledges (2.53) while rarefaction curves suggested that sampling was incomplete (Figure 1.11). These sequences represent six eukaryotic super groups (based on Baldauf, 2003): Alveolates, Amoebozoa, Cercozoa, Heterokonts, Opisthokonts, and Plantae. The two most prominent groups are Alveolates (39% of OTUs and 34% of sequences) and Opisthokonts (34% of OTUs and 49% of sequences). The Opisthokont sequences were dominated by fungi (64% of OTUs and 93% of sequences) and metazoans comprised 18% of the OTUs and 3% of the sequences. The Alveolate sequences consisted of: Apicomplexa, Ciliophora, Cryptosporidium and Dinophyceae. The Heterokont sequences included diatoms and three other groups of algae:

Bolidophyceae, Raphidophyceae, and Thraustochytriidae. The Plantae included Chlorophyta and Streptophyta. The Cercozoa included Ascetosporea, Cercomonadida, Cryomonad, Ebridea, and Thaumatomonadida.

Seepage measurements in the vicinity of Jewfish Sink and Crystal Beach Spring:

At the time that seepage measurements were made, the surface water salinity at Jewfish Sink was 22 to 22.5 ppt compared to 28 to 30 ppt at Crystal Beach Spring. The Crystal Beach Spring site is behind a barrier island in the Intracoastal Waterway and salinities are higher in late spring and early summer compared to early winter measurements of 24 to 25 ppt. The samples collected from the Jewfish Sink area were greater than 50% coarse sand (>500 µm). At Crystal Beach Spring, the 5 m sample next to the spring basin was washed by the diffuse groundwater discharge near the main spring vent and contained greater than 50% coarse sand. The low flow in the Intracoastal Waterway behind the barrier island allows the accumulation of finer sediments away from the spring basin and the other sampling locations contained less than 10% coarse sand.

Two seepage readings were taken at Jewfish Sink. The first was over a period of 1500 min from a falling tide just below high tide through two high tides ending at a medium tide before a low tide (Figure 1.7). The second was over a period of 1215 minutes beginning at a medium tide before a low tide through two low tides and ending just before high tide. Seepage rates were between 0.008 and 0.020 l/min-m^2 at locations 5 m and 15 m east (shoreward) of the rim of the sinkhole, respectively.

Surface salinity at Jewfish Sink was 22 to 22.5 ppt; the same as the salinity of the seepage.

A seepage reading was taken at Crystal Beach Spring beginning at low tide through one low tide and ending on a rising tide near high tide. At Crystal Beach Spring, which is closer to shore and still actively discharging low salinity water, seepage rates were 0.080 l/min-m^2 at locations 5 m and 15 m east (shoreward) of the rim of the sinkhole. Surface salinity at Crystal Beach Spring was 28 ppt at low tide and 30 ppt at high tide compared to the seepage salinity of 27 to 28.5 ppt and salinity near the spring vent of 6 ppt.

Macrofauna in the vicinity of Jewfish Sink and Crystal Beach Spring:

A total of 833 individual specimens were identified from the sampling with 664 individuals from the Jewfish Sink site and 169 individuals from the Crystal Beach site. These specimens were not collected from within the sink and spring, but from the nearby benthic habitat. The macrofauna abundance and richness from each sample are shown in Figure 1.12. Both the number of taxa and overall abundance were greater at Jewfish Sink compared to Crystal Beach Spring ($p < 0.001$). The 1 km site at Crystal Beach Spring included more taxa than the samples collected closer to Crystal Beach Spring. Species richness was significantly higher at the Jewfish Sink transect compared to the Crystal Beach Spring transect ($p=0.003$). There were no statistically significant differences in species richness when sites within a transect were analyzed, but there were some statistical differences in richness for two sites at Jewfish Sink (50m and 100m) compared to three sites at Crystal Beach Spring (5m, 50m, and 100m).

The Shannon-Weiner diversity index (H'; $\log_e$) was higher at the Jewfish Sink transect compared to the Crystal Beach Spring transect (p=0.014). There were no significant differences among individual sites within either transect (Figure 1.13). The evenness was significantly higher at the Crystal Beach Spring transect compared to the Jewfish Sink transect (p=0.006) (Figure 1.13).

The cluster analysis of abundance data showed three major groups at 30% Bray-Curtis similarity (Figure 1.14). The Crystal Beach Spring 1 km samples and one of the Crystal Beach Spring 5 m replicates grouped with two replicates from the Jewfish Sink 1 km site and one replicate from the Jewfish Sink 5 m site (Group A). The remaining Jewfish Sink samples form Group B and the remaining Crystal Beach Spring samples excluding one replicate from the 100 m site form Group C. The same groupings were observed in an MDS plot (not shown).

SIMPER analysis (Table 1.5) of the cluster groups showed that the Group A sites had an average similarity of 36%, with Tubificidae and *Tectidrilus squalidus* accounting for 68% of the similarity. Group B sites had an average similarity of 36%, with Tubificidae and *Aricidea philbinae* accounting for 50% of the similarity. Group C sites had an average similarity of 22%, with *Cirrophorus* sp. accounting for 66% of the similarity.

Discussion:

Physical Characteristics within Jewfish Sink:

The sinking of cold surface water in the fall and winter did not influence the bottom water of the sinkhole during the study period (Figure 1.8). The salinity and high

concentrations of other solutes make the bottom water too dense for sinking winter surface water to mix with it.

Biodiversity and related processes within Jewfish Sink:

The seasonal changes in the composition of the particulate clouds in the water column appear to be related to the composition of the microbial communities. In the winter, the sinking of oxygenated surface water combined with the limited sunlight penetrating into the sinkhole opening from the low angle of the winter sun would allow sulfur-oxidizing bacteria in the upper anoxic zone to out-compete the anaerobic sulfide phototrophic bacteria. Sulfur oxidizers comprise 22% of the bacteria present in Jewfish sink winter water with *Thiomicrospira* and *Sulfurimonas* representing the most common genera (Tables 2 and 3). The chemoautotrophic bacteria use sulfide and convert it to sulfate, thereby reducing pH, as observed in the winter water column profile. The reduced pH favors bicarbonate and dissolved carbon dioxide rather than carbonate, and calcium carbonate precipitation does not occur (Castanier et al. 1999).

In the summer, when the bottom water pH is at a maximum and calcium carbonate is one of the principal components of the particulate clouds, dissolved oxygen is limited to the upper 15 m of the water column (Figures 2 and 6), limiting the habitat for sulfur oxidizing bacteria that require oxygen as an electron acceptor. At this time of the year, without trace oxygen and corresponding sulfur oxidizing bacteria activity in the upper anoxic zone, sulfide is not converted to sulfate and the pH in the upper anoxic zone increases (Figure 1.5). Dissimilatory sulfate reducers may increase pH by creating a proton sink during the creation of sulfide. It is possible then that sulfide can then be converted to elemental sulfur by anoxygenic phototrophic bacteria or metal sulfides

such as pyrite in chemical reactions if light is available. Although we examined water collected in late winter, we found at least one example of anoxygenic phototrophic bacteria (*Thioalkivibrio*) in low abundance as would be expected in the winter. Similarly, because the sink is predominantly anoxic during the summer, prokaryotes using dissimilatory sulfate reduction to produce hydrogen sulfide are expected to increase, resulting in a higher pH. In our winter sample, we found numerous prokaryotes capable of dissimilatory sulfate reduction (e.g. *Desulfovibrio*, *Desulfococcus*, *Desulfatibacillum*, *Moorella*). An increase in pH favors the presence of carbonate anion in solution instead of bicarbonate anion or dissolved carbon dioxide. The presence of both carbonate anion and calcium results in the passive precipitation of calcium carbonate (Castanier et al., 1999). It has been demonstrated that the cell wall of some prokaryotes plays a role in carbonate precipitation. The increased reactivity of cations adsorbed to the cell wall promotes nucleation of carbonate minerals such as calcium carbonate (Merz-Preiβ 2000). Cave divers in Florida often encounter particulate clouds associated with a strong sulfide odor, particularly at the freshwater/saltwater interface of anchialine environments as well as in anoxic marine sinks. This provides anecdotal evidence that the link between calcium carbonate precipitation and bacterial mediated sulfide production is widespread in marine-influenced anoxic environments.

In addition to the bacteria that contribute to calcium carbonate precipitation and sulfur reduction, 26.7% of archaeal sequences were potentially methanogenic (Table 1.2). Methanogenesis leads to an increase in alkalinity as well as a depletion of carbon dioxide. Subsequently, an increase in calcium carbonate precipitation is observed (Castanier 1999). The known syntrophy of certain methanogens with sulfur reducing

bacteria suggests that the sulfide peaks corresponding to an increase in sulfur reduction may also correlate to an increase in those methanogens. Indeed, both *Methanosarcinales* and *Desulfosarcina*, two genera known to participate in this type of syntrophy (Konhauser 2007), were found in the samples collected. Lastly, the production of carbonate and bicarbonate ions as a result of nitrogen cycling favors calcium carbonate precipitation. Ammonification, anoxic dissimilatory nitrate reduction and urea degradation not only produce the carbonate ions, but also lead to an increase in pH which induces the precipitation (Castanier et al. 1999). Roughly 22% of the prokaryotic sequences found represent taxa potentially involved in the cycling of nitrogen (Table 1.2).

The presence of iron sulfide minerals in the particulate cloud in the summer indicates that some sulfide is reacting with iron in an inorganic reaction. This reaction is mediated indirectly by both the high sulfide concentration caused by microbial sulfur reduction and the iron (II) that results from microbial iron reduction (Konhauser 2007). Sequences similar to known iron reducing prokaryotes were represented by approximately 2% of the bacterial sequences and 0.24% of the archaeal sequences found in Jewfish Sink. Bacteria within the water column may serve as a surface for the precipitation of iron sulfide, the precursor to the framboidal pyrite (Schoonen 2004). The sulfide concentration in the bottom water showed peaks in late winter (March) and late summer (August/September). The sulfide peaks occurred at times of large inputs of organic carbon into the sinkhole: the influx of bottom feeding horseshoe crabs and stingrays that fall into the sinkhole and die in late winter (Figure 1.15); and the influx of macroalgae from storm surges during the summer. The spikes in sulfide production are

believed to correspond to the development of condensed particulate clouds that were periodically observed in the sinkhole. The particulates created in conjunction with the sulfide spikes are biomineral aggregates in the winter and calcium carbonate and pyrite in the summer. It appears that seasonal biogeochemical cycles in the sinkhole cause large variations in pH and the onset and cessation of calcium carbonate precipitation.

The largest prokaryotic contributors found within the sink in our late winter samples were dominated by sulfur metabolizers. Members of the genera *Arcobacter*, *Clostridium*, *Desulfobacterium*, *Staphylothermus* (Tables 1 and 3) are associated with either sulfur reduction or sulfur oxidation. Both *Arcobacter* and *Clostridium*, the two dominant bacterial taxa found (21% of bacterial sequences), are genera known to contain human pathogens. Among the Archaea, *Methanobrevibacter* and *Nitrosocaldus*, both ammonia oxidizers, were also abundant. While the percentage of nitrogen oxidizers exceeds that of nitrogen reducers, the anoxic environment is primarily composed of anaerobic organisms using terminal electron acceptors other than oxygen, with sulfur reducers comprising half of all prokaryotes sequenced (Table 1.2). The sink, never becoming completely oxic or anoxic, sustains a functionally diverse consortium of prokaryotes; the successions of which manifest the geochemical cycles observed.

Bacterial Shannon Diversity was slightly higher (4.81) than Archaea (4.64). Rarefaction curves (Figure 2.9) demonstrate that sampling was incomplete in that the number of OTUs continues to increase with the addition of new sequences. Rarefaction curves using Shannon Diversity (not shown) did not increase much with the addition of new sequences, suggesting that most of the new sequences being added were rare.

This is consistent in that most of the bacterial and archaeal OTUs (with 97% match criteria) were represented only one time in our data.

The eukaryotes within Jewfish Sink were diverse, representing 6 super groups, ophisthokonts, avleolates, heterokonts, plants, and one amoebozoan (Table 1.4). The 836 sequences clustered into 164 OTUs, most of which were provisionally identified using GenBank Blast searches. In some cases, the sequence identity to known GenBank entries was low, so the provisional identification was sometimes imprecise as seen in the Plantae detail in Table 1.4 where a fern (Polypodiaceae) and flowering plant (Alliaceae) sequence were “identified.” However, provisional identifications did provide an overview of the eukaryotic community in Jewfish Sink.

The eukaryote sequences originated from two locations. There were 394 sequences from microbial mat collected from the vertical wall of the sink the anoxic zone below a depth of 30 m, and 442 sequences from sediment on horizontal cut back ledges in the oxic zone. No metazoan sequences were found in the anoxic zone, and only 14 of 442 sequences from the oxic zone sediment (3%) represented metazoans. Table 1.4 indicates that 9 provisionally identified eukaryote groups were found only in the microbial mat sample, 17 were found only in the oxic zone sediment samples, while 8 groups were found in both environments. The dominant eukaryote group in terms of sequence number was fungi that composed 65% of the sediment sequences. Although fungi were also the most common type of sequences in the microbial mat, they represented only 24% of those sequences. Dinoflagellates were equally predominant in the microbial mat (24%), followed by ciliophorans (16%). An analysis of the Shannon Diversity revealed that the diversity of eukaryotic sequences in the anoxic zone

microbial mats (3.42) was higher than in the oxic zone sediment (2.53), most likely due to the predominance of a few fungi OTUs in the oxic zone sediment. Rarefaction analysis revealed that although Shannon Diversity of eukaryotes was higher in the microbial mat sample, more OTUs were present in the oxic zone sediment than in the anoxic zone mat. The rarefaction analysis also suggested that sampling was far from complete because the number of OTUs continued to increase with increasing numbers of sequences (Figure 1.11). As with the prokaryote sequences, Shannon diversity became relatively stable with increasing number of sequences (not shown). Examination of fresh samples of microbial mat under a microscope revealed numerous dinoflagellates and ciliates that appeared to be grazing on the mat material. Several provisionally identified taxa including some alveolates and cercozoans in Table 1.4 have been reported to feed on diatoms and dinoflagellates (Massana and Pedros 1994; Schnepf and Kühn 2000;Taylor 1987), so our analysis suggests that Jewfish Sink provides a thriving and diverse environment for anaerobic eukaryotes.

Macrofauna in the vicinity of Jewfish Sink and Crystal Beach Spring:

The original hypothesis based on previous work at Jewfish Sink (Garman and Garey 2005) was that the benthic macrofauna community surrounding Jewfish Sink would be potentially influenced by the effects of the sulfide seeping upward from the anoxic zones of the sinkhole and surrounding subterranean estuary, creating a community with lower abundance and diversity compared to the community surrounding Crystal Beach Spring, an active submarine spring. Contrary to this initial hypothesis, the sampling sites near the basin of Crystal Beach Spring had relatively few taxa and low overall abundance compared to sampling sites near Jewfish Sink. This condition is likely

a result of higher submarine groundwater discharge in an area where freshwater hydraulic head is still high enough to support an active submarine spring. Seepage rates in the vicinity of Crystal Beach Spring are an order of magnitude greater than those in the vicinity Jewfish Sink. At Jewfish Sink, where spring flow has ceased and seepage rates are an order of magnitude lower, there was higher species abundance and diversity. Pinellas County in the vicinity of Crystal Beach Spring is more developed than the rural, sparsely populated area near Jewfish Sink. Group B of Figure 1.14 consisted entirely of samples from the area near Jewfish Sink while group C contained only samples from near Crystal Beach, suggesting that the sites near Crystal Beach Spring had benthic macrofauna communities that are distinct from those near Jewfish Sink. However, the sites that were 1 km distant from Jewfish Sink and Crystal Beach Spring mostly fell into group A, meaning that the macrofauna communities most distant from Jewfish Sink were more similar to the macrofauna communities most distant from Crystal Beach Spring than they were to sites closer to Jewfish Sink. This suggests that the measurable effect of the both Crystal Beach Spring and Jewfish Sink on the surrounding marine benthic community extends only about 1 km from the respective sink or spring. Similarity of macrofaunal communities at different sites was due to the contribution of only a few taxa with overlap between group A and B caused primarily by a species of Tubificidae. The other taxa that contributed to group A (*Tectidrilus squalidus* and *Prionospio heterobranchia*) did not contribute significantly to group B structure and none of the main contributors to the structure of group C were contributors to either A or B (Table 1.5).

Conclusions:

Jewfish sink represents a former anchialine system that transitioned to an anoxic sulfur-cycling marine basin in the early 1960s. Similar environments are found along the west coast of Florida from the Anclote River in northern Pinellas County extending along Pasco County at least to the Weeki Wachee River in Hernando County (Figure 1.1). The biota within the deep anoxic zones of Jewfish sink currently consist entirely of prokaryote and eukaryote microbes and are similar to those found in other anoxic environments (Tables 1-4). No metazoan macrofauna were found in the deep anoxic zone and metazoans made up only 3% of the eukaryote sequences in the shallower oxic zone of the sink. The prokaryote community is rich in anaerobic taxa that metabolize sulfur, iron, nitrogen and methane. The prokaryote community is clearly related to the geochemistry of Jewfish Sink. The dominant eukaryotes in both the deep anoxic zone and the shallower oxic zone appear to be fungi and dinoflagellates. The reduction in freshwater hydraulic head that leads to the cessation of spring flow also results in a corresponding reduction in the magnitude of submarine groundwater discharge in the vicinity of the spring that has ceased flowing. The overall influence of the geochemistry of the subterranean estuary on the surrounding benthic marine ecosystem is significantly lower in an area of reduced freshwater hydraulic head at which submarine spring flow has ceased like Jewfish Sink compared to an area of higher freshwater hydraulic head with active submarine spring flow like Crystal Beach Spring. Both Jewfish Sink and Crystal Beach Spring appear to affect the benthic macrofaunal communities to a distance of 1 km.

This study suggests that through features such as Jewfish Sink, aquifer overuse on land can affect near shore benthic macrofauna, which in turn could affect fisheries

that depend on the macrofauna. In addition, offshore springs that continue to function can transport nutrients from populated areas that could decrease macrofauna diversity, again with a potential impact on fisheries.

References:

Baker, G. C., J. J. Smith, and D. A. Cowan, 2003. Review and re-analysis of domain-specific 16S primers. Journal of Microbiological Methods. 55: 541-555.

Baldauf, S. L., 2003. The deep roots of eukaryotes. Science. 300: 1703-1706.

Bottrell, S. H., P. L. Smart, F. Whitaker, and R. Raiswell. 1991. Geochemistry and isotope systematics of sulfur in the mixing zone of Bahamian blue holes. Applied Geochemistry 61: 97-103.

Brigmon, R. L., H. W. Martin, T. L. Morris, G. Bitton, and S. G. Zam., 1994. Biogeochemical ecology of Thiothrix spp in underwater limestone caves. Geomicrobiology Journal. 12: 141-159

Brooks, R. A., C. N. Purdy, S. S. Bell, and K. J. Sulak, 2006. The benthic community of the eastern US continental shelf: A literature synopsis of benthic faunal resources. Continental Shelf Research. 26: 804-818.

Castanier, S., G. Le Metayer-Levrel, and J. P. Perthuisot, 1999. Ca-carbonates precipitation and limestone genesis – the microbiogeologist point of view. Sedimentary Geology. 126: 9-23.

Charette, M. A., and E. R. Sholkovitz, 2006. Trace element cycling in a subterranean estuary: Part 2. Geochemistry of the pore water. Geochimica et Cosmochimica Acta. 70: 811-826.

D'Elia, C. F., K. L. Webb, and J.W. Porter, 1981. Nitrate-rich groundwater inputs to Discovery Bay, Jamaica: A significant source of N to local coral reefs? Bulletin of Marine Science. 31: 903-910.

Delong, E. F., 1992. Archaea in coastal marine environments. Proceedings of The National Academy of Sciences (U.S.A.) 89: 5685-5689.

DeWitt, D., 2003. Submarine springs and other karst features in offshore waters of the Gulf of Mexico and Tampa Bay. Southwest Florida Water Management District.

Engle, V. D. and J. K. Summers. 2000. Hydrobiologia. Biogeography of benthic macroinvertebrates in estuaries along the Gulf of Mexico and western Atlantic coasts 436 (1-3): 17-33.

Engle, V. D., J. L. Hyland, and C. Cooksey. 2009. Effects of Hurricane Katrina on benthic macroinvertebrate communities along the northern Gulf of Mexico coast. Environmental Monitoring and Assessment. 150 (1-4): 193-209.

Gotelli, N.J. and G.L. Entsminger. 2009. EcoSim: Null models software for ecology. Version 7. Acquired Intelligence Inc. & Kesey-Bear. Jericho, VT 05465.

Garman, K. M., 1997. The Crystal Beach Spring ecosystem. Journal of Cave and Karst Studies. 59: 167.

Garman, K. M., J. Paul, V. Harwood, and L. Robbins, 1999. Chemolithotrophic based ecosystem in the Crystal Beach Spring Cave System. 4th International Symposium on Subsurface Microbiology Abstract Book.

Garman, K. M., 2000. Estimates of seepage rates of reduced, saline, groundwater into the Dragon's Lair Tunnel of the Crystal Beach Spring Cave System. Journal of Cave and Karst Studies. 62: 36.

Garman, K. M., and Garey, J. R., 2005. The Transition of a Freshwater Karst Aquifer to an Anoxic Marine System. Estuaries. 28: 686-693.

Hempstead, P. G., S. C. Regular, and I. R. Ball, 1990. A method for the preparation of high-molecular-weight DNA from marine and fresh-water triclads Platyhelminthes, Turbellaria. DNA and Cell Biology. 9: 57-61.

Iliffe, T. M. 1992. Anchialine cave biology. In A. M. Camacho (Ed.), The Natural History of Biospeleology, 680 pp.
Je J.-G., T. Belan, C. Levings, and B. J. Koo, 2003. Changes in benthic communities along a presumed pollution gradient in Vancouver Harbour. Marine Environmental Research. 57: 121-135.

Johannes, R. E., 1980. The ecological significance of submarine discharge of groundwater. Marine Ecology Progress Series. 3: 365-373.

Karlen, D.J., R. E. Price, T. Pichler, and J. R. Garey, 2010. Changes in benthic macrofauna associated with a shallow-water hydrothermal vent gradient in Papua New Guinea. Pacific Science. 64: 391-404.

Konhauser, K., 2007. Introduction to Geomicrobiology. Blackwell Science Ltd., Massachusetts.

Lee, D., 1977. A device for measuring seepage flux in lakes and estuaries. Limnology and Oceanography. 22: 140-147.

Mackey, L.Y., B. Winnepenninckx, R. DeWachter, T. Backeljau, P. Emschermann, and J. R. Garey, 1996. 18S rRNA suggests that Entoprocta are protostomes, unrelated to Ectoprocta. Journal Of Molecular Evolution. 42: 552-559.

Mallin, M. A., M. H. Posey, G. C. Shank, M. R. McIver, S. H. Ensign, and T. D. Alphin, 1999. Hurricane effects on water quality and benthos in the Cape Fear watershed: Natural and anthropogenic impacts. Ecological Applications, 9: 350–362.

Masana, R. and C. Pedros-Alio., 1994. Role of anaerobic ciliates in planktonic food webs: abundance, feeding, and impact on bacteria in the field. Applied and Environmental Microbiology. 60: 1325-1334.

Merz-Preiβ, M., 2000. Calcification of cyanobacteria. In Riding, R.E. and Awramik, S. M. (eds), Microbial Sediments. Springer-Verlag, Berlin: 51-56.

Montagna, P. A. and C. Ritter. 2006. Direct and indirect effects of hypoxia on benthos in Corpus Christi Bay, Texas, USA. Journal Of Experimental Marine Biology And Ecology 330 (1): 119-131.

Moon, H. S., D. Shin, K. Nam, and J. Y. Kim. 2010. Distribution of the microbial community structure in sulfur-based autotrophic denitrification columns. Journal of Environmental Engineering 136 (5):481 -486.

Moore, W. S. 1999. The subterranean estuary: A reaction zone of ground water and sea water. Marine Chemistry 65: 111-125.

Paul, J. H., J. B. Rose, J. Brown, E. A. Shinn, S. Miller, and S. R. Farrah, 1995. Viral tracer studies indicate contamination of marine waters by sewage disposal practices in Key Largo, Florida. Applied and Environmental Microbiology. 61: 2230-2234.
Paul, J. H., J. B. Rose, S. C. Jiang, X. Zhou, P. Cochran, C. Kellogg, J. B. Kang, D. Griffin, S. R. Farrah, and J. Lukasik, 1997. Evidence for groundwater and surface marine water contamination by waste disposal wells in the Florida Keys. Water Research. 31: 1448-1454.

Paul, J. H., M. R. McLaughlin, D. W. Griffin, E. K. Lipp, R. Stokes, J. B. Rose, 2000. Rapid movement of wastewaters from on-site disposal systems into surface waters in the lower Florida Keys. Estuaries. 23: 662-668.

Rabalais, N.N., L.E. Smith, D.E. Harper Jr., and D. Justic, 2001. Effects of seasonal hypoxia on continental shelf benthos. Coastal and Estuarine Studies, 58: 211–240.

Rakocinski C. F., S.S. Brown, G. R. Gaston, R. W. Heard, W. W. Walker, J. K. Summers, 1997. Macrobenthic responses to natural and contaminant-related gradients in northern Gulf of Mexico estuaries. Journal of Applied Ecology. 7: 1278-1298.

Reysenbach, A. L., 1994. Phylogenetic analysis of the hyperthermophilic pink filament community in Octopus Spring, Yellowstone-National-Park. Applied and Environmental Microbiology. 60: 2113

Rosenau, J. C., G. L. Faulkner, C. W. Hendry, and R. W. Hull, 1977. Springs of Florida. State of Florida, Department of Natural Resources, Bureau of Geology, Bulletin No. 31. 461.

Rosenberg R., H. C. Nilsson, and R. J. Diaz, 2001. Response of benthic fauna and changing sediment redox profiles over a hypoxic gradient. Estuarines, Coastal and Shelf Science. 53: 343-350.

Santos, I. R., W. C. Burnett, J. Chanton, B. Mawashote, I. G. N. A. Suryaputra, and T. Dittmar, 2008. Nutrient biogeochemistry in a Gulf of Mexico subterranean estuary and groundwater-derived fluxes to the coastal ocean. Limnology and Oceanography. 53 (2): 705-718.

Schloss, P.D. and J. Handelsman, 2005. Introducing DOTUR, a computer program for defining operational taxonomic units and estimating species richness. Applied and Environmental Microbiology. 71: 1501-1506.

Schmitter-Soto, J. J., F. A. Comin, E. Escobar-Briones, J. Herrera-Silveira, J. Alcocer, E. Suarez-Morales, M. Elias-Guitierrez, V. Diaz-Arce, L. E. Marin, and B. Steinich. 2002. Hydrogeochemical and biological characteristics of cenotes in the Yucatan Peninsula SE Mexico. Hydrobiologia 467: 215-228.

Schnepf, E. and S. F. Kóhn, 2000. Food uptake and fine structure of Cryothecomonas longipes sp. nov., a marine nanoflagellate incertae sedis feeding phagotrophically on large diatoms. Helgoland Marine Research. 54: 18-32.

Schoonen, M. A. A., 2004. Mechanisms of sedimentary pyrite formation. In Amend, J. P., Edwards, K. J., and Lyons, T. W. (eds), Sulfur Biogeochemistry- Past and present. Geological Society of America Special Paper 379, Boulder, Colorado: 117-134.

Shaw, R.D. and E.E. Prepas, 1990. Groundwater-lake interactions: I. Accuracy of seepage meter estimates of lake seepage. Journal of Hydrology. 119: 105-120.

Simboura N., A. Zenetos, P. Panayotidis, and A. Makra, 1995. Changes in benthic community structure along an environmental pollution gradient. Marine Pollution Bulletin. 30: 470-474.

Simmons, Jr. G. M. and J. Netherton, 1987. Ground water discharge in a deep coral reef habitat—evidence for a new biogeochemical cycle? In C. T. Mitchell (ed), Proceedings of the American Association for Underwater Science. American Association for Underwater Science, Costa Mesa, California: 1-12.

Simmons, G. M., 1992. Importance of submarine groundwater discharge and seawater cycling to material flux across sediment/water interfaces in marine environments. Marine Ecology Progress Series. 84: 173-184.

Slomp, C. P., and P. Van Cappellen, 2004. Nutrient inputs to the coastal ocean through submarine groundwater discharge: controls and potential impact. Journal of Hydrology. 295: 64-86.

Stark, J. S., I. Snape, M. J. Riddle, and S. C. Stark, 2005. Constraints on spatial variability in soft-sediment communities affected by contamination from an Antarctic waste disposal site. Marine Pollution Bulletin. 50: 276-290.

Stoessell, R. K., Y. H. Moore, and J. G. Coke. 1993. The occurrence and effect of sulfate reduction and sulfide oxidation on coastal limestone dissolution in Yucatan cenotes. Ground Water 31 (4): 566-575.

Taylor, F. J. R., 1987. The Biology of Dinoflagellates. Blackwell Scientific Publications, Oxford, 785 pp.

Trommer, J.T., 1992. Effects of effluent spray irrigation and sludge disposal on ground water in a karst region, northwest Pinellas County, Florida. U.S. Geological Survey Water-Resources Investigation Report 91-4181, 32.

Waller, B.G., 1985. Drought of 1980-82 in Southeast Florida with comparison to the 1961-62 and 1970-71 droughts. U.S. Geological Survey Water-Resources Investigation Report 85-4152, 29.

Weston, D. P., 1990. Quantitative examination of macrobenthic community changes along an organic enrichment gradient. Marine Ecology Progress Series. 61:233-244.

Wetterhall, W. S., 1965. Reconnaissance of Springs and Sinks in West-Central Florida. Florida Geological Survey, Report of Investigations No. 39. 42.

Wu, T., Ayres, E., Li, G., Bardgett, R. D., Wall, D. and Garey J. R., 2009. Molecular profiling of soil animal diversity in natural ecosystems: incongruence of molecular and morphological results. Soil Biology and Biochemistry. 41:849-857.

Yobbi, D. K. 1992. Effects of tidal stage and ground-water levels on the discharge and water quality of springs in coastal Citrus and Hernando Counties, Florida. U.S. Geological Survey Water-Resources Investigations Report 92-4069, 44.

Zajac, R. N., and R. B. Whitlatch, 2003. Community and population-level response to disturbance in a sandflat community. Journal of Experimental Marine Biology and Ecology. 294: 101-125.

Table 1.1. Archaeal Sequences found at Jewfish Sink by Phylum and Genus.

	Abundance	**Richness**	
Phyla	**# Species**	**# OTUs**	**Match Percentage**
Crenarchaeota	276	139	78-89
Euryarchaeota	135	64	80-97
Korarchaeota	1	1	77
Genera	**# Species**	**# OTUs**	**Match Percentage**
Staphylothermus	218	92	81-88
Methanobrevibacter	62	26	81-87
Nitrosocaldus	31	24	80-85
Methanobacterium	26	4	82-83
Aciduliprofundum	24	13	81-85
Thermofermentum	15	15	81-85
Methanothermobacter	13	12	80-83
Thermofilum	6	6	82-85
Methanolobus	5	4	95-97
Caldisphaera	2	2	78-83
Fervidococcus	2	2	85-87
Aeropyrum	1	1	89
Desulfurococcus	1	1	86
Geoglobus	1	1	82
Korarchaeum	1	1	77
Methanococcoides	1	1	85
Methanoplanus	1	1	92
Methanopyrus	1	1	89
Methanosarcina	1	1	97

Table 1.2. Potential Functional Properties of Prokaryotes at Jewfish Sink. The percentages add up to more than 100% because some prokaryotes fit into multiple categories.

	Archaea		Bacteria		
	Sequences	*Percentage*	*Sequences*	*Percentage*	*Total Percentage*
Anaerobes	341	82.77	183	57.19	71.58
Aerobes	32	7.77	110	36.25	19.40
Methanogens	110	26.70	0	0.00	15.03
Obligate Methane Oxidizers	0	0.00	14	4.38	1.91
Sulfur Reducers	247	59.95	116	36.25	49.59
Sulfur Oxidizers	0	0.00	70	21.88	9.56
Unknown	39	9.47	27	6.56	9.02
Nitrogen Reducers	26	6.31	3	0.93	3.96
Nitrogen Oxidizers	93	22.57	37	11.56	17.76
Iron Reducers	1	0.24	7	2.19	1.09

Table 1.3. Bacterial Sequences found at Jewfish Sink by Phylum and Genus.

	Abundance	**Richness**	
Phyla	**# Species**	**# OTUs**	**Match Percentage**
Proteobacteria	179	164	80-99
Firmicutes	58	34	78-99
Bacteroidetes	14	14	82-98
Actinobacteria	13	9	78-85
Spirochaetes	21	9	84-100
Chloroflexi	12	7	82-100
Verrucomicrobia	9	6	79-84
Planctomycetes	7	5	83-88
Nitrospirae	2	2	80-81
Aquificae	1	1	80
Cyanobacteria	1	1	88
Cyanophora	2	1	83
Synergistetes	1	1	84
Genera	**# Species**	**# OTUs**	**Match Percentage**
Arcobacter	40	10	85-93
Clostridium	28	14	87-99
Desulfobacterium	26	11	82-91
Spirochaeta	19	8	84-100
Dehalococcoides	15	7	84-100
Desulfosarcina	12	4	91-94
Pseudomonas	8	1	98
Thiomicrospira	8	5	91-97
Verrucomicrobia	7	5	79-84
Unkown	6	5	
Catabacter	5	4	89-93
Cytophaga	5	3	88
Desulfomonile	5	2	83-89
Desulfovibrio	5	5	83-88
Methylobacter	5	2	93-99
Pelobacter	5	2	85-91
Planctomycetales	5	3	88
Sulfurimonas	5	2	80-91
Sulfurovum	5	1	93
Desulfatibacillum	4	2	83-89
Syntrophomonas	4	1	81

Table 1.4. Eukaryotic sequences found at Jewfish Sink.

	Abundance			Richness			
Super Group Summary	# Sequences			# OTUs			
	Total	**Mat**	**Sediment**	**Total**	**Mat**	**Sediment**	**Both**
Opisthokonts	409	102	307	50	17	36	3
Alveolates	272	199	73	58	39	28	9
Heterokonts	65	32	33	21	6	15	0
Cercozoa	54	43	11	10	5	6	1
Plantae	35	18	17	9	4	6	1
Amoebozoa	1	0	1	1	0	1	0
Alveolates Detail	**Total**	**Mat**	**Sediment**	**Total**	**Mat**	**Sediment**	**Both**
Dinophyceae	144	94	50	30	16	19	5
Ciliophora	61	61	0	12	12	0	0
Apicomplexa	44	33	11	10	4	8	2
Cryptosporidium	8	8	0	3	3	0	0
Unknown	15	3	12	3	2	1	1
Heterokonts Detail	**Total**	**Mat**	**Sediment**	**Total**	**Mat**	**Sediment**	**Both**
Diatoms	26	2	24	13	2	11	0
Algae, Bolidophyceae	19	18	1	2	1	1	0
Algae, Thraustochytriidae	13	11	2	3	2	1	0
Algae, Raphidophyceae	6	0	6	2	0	2	0
Unknown	1	1	0	1	1	0	0
Opisthokonts Detail	**Total**	**Mat**	**Sediment**	**Total**	**Mat**	**Sediment**	**Both**
Fungi, Sordariomycetes, saprobe degrades algal polysaccharides	297	31	266	13	2	13	2
Fungi, Tremellomycetes, deep-sea methane cold seep sediment	40	29	11	7	3	5	1
Fungi, Saccharomycetes, fermentation	18	18	0	3	3	0	0
Fungi, Ustilaginomycetes, plant parasite	12	12	0	1	1	0	0
Fungi, Dothideomycetes, plant pathogen or saprobe	9	0	9	3	0	3	0
Protist, Ichthyosporean	9	6	3	5	3	2	0
Metazoa, Mollusk	5	0	5	1	0	1	0
Fungi, Mucoromycotina, oxygen depleted marine	4	4	0	3	3	0	0
Fungi, Eurotiomycetes	2	2	0	2	2	0	0
Metazoa, Platyhelminthes marine	2	0	2	2	0	2	0
Metazoa, Annelid-2	2	0	2	2	0	2	0
Protist, Apusomonadidae, marine flagellate	2	0	2	2	0	2	0
Metazoa, Gnathostomulid	2	0	2	1	0	1	0
Glomeromycetes	1	0	1	1	0	1	0
Metazoa, Annelid-1, Capitella capitata	1	0	1	1	0	1	0
Metazoa, Copepod	1	0	1	1	0	1	0
Metazoa, Nemertea	1	0	1	1	0	1	0
Protist, Eccrinales	1	0	1	1	0	1	0
Cercozoa Detail	**Total**	**Mat**	**Sediment**	**Total**	**Mat**	**Sediment**	**Both**
Ebriidae	35	35	5	1	1	0	0
Thaumatomastigidae	7	0	7	2	0	2	0
Cryothecomonas	6	5	1	2	2	1	1
Cercomonadidae	4	3	1	3	2	1	0
Paradinium	2	0	2	2	0	2	0
Plantae Detail	**Total**	**Mat**	**Sediment**	**Total**	**Mat**	**Sediment**	**Both**
Pycnococcaceae	15	3	12	4	1	4	1
Pyramimonadales	12	0	0	2	2	0	0
Chlorellaceae	4	0	4	1	0	1	0
Alliaceae	3	3	0	1	1	0	0
Polypodiaceae	1	0	1	1	0	1	0
Amoebozoa Detail	**Total**	**Mat**	**Sediment**	**Total**	**Mat**	**Sediment**	**Both**
Hartmannellidae	1	0	1	1	0	1	0

Table 1.5. Simper analysis of macrofauna.

Group A: Average Similarity: 35.91		
Macrofauna Identification	**Contribution%**	**Cumulative%**
Tubificidae	40.85	40.85
Tectidrilus squalidus	27.58	68.42
Prionospio heterobranchia	10.86	79.28
Mysidacea	6.51	85.79
Cirrophorus sp.	5.06	90.86
Group B: Average Similiarity: 36.20		
Macrofauna Identification	**Contribution%**	**Cumulative%**
Tubificidae	26.74	26.74
Aricidea philbinae	22.97	49.71
Tectidrilus squalidus	8.60	58.30
Kinbergonuphis sp.	6.15	64.45
Chone americana	5.86	70.31
Group C: Average Similiarity: 21.57		
Macrofauna Identification	**Contribution%**	**Cumulative%**
Cirrophorus sp.	66.22	66.22
Nemertea	15.96	82.18
Ampelisca sp. A	4.69	86.87
Magelona pettiboneae	3.93	90.80

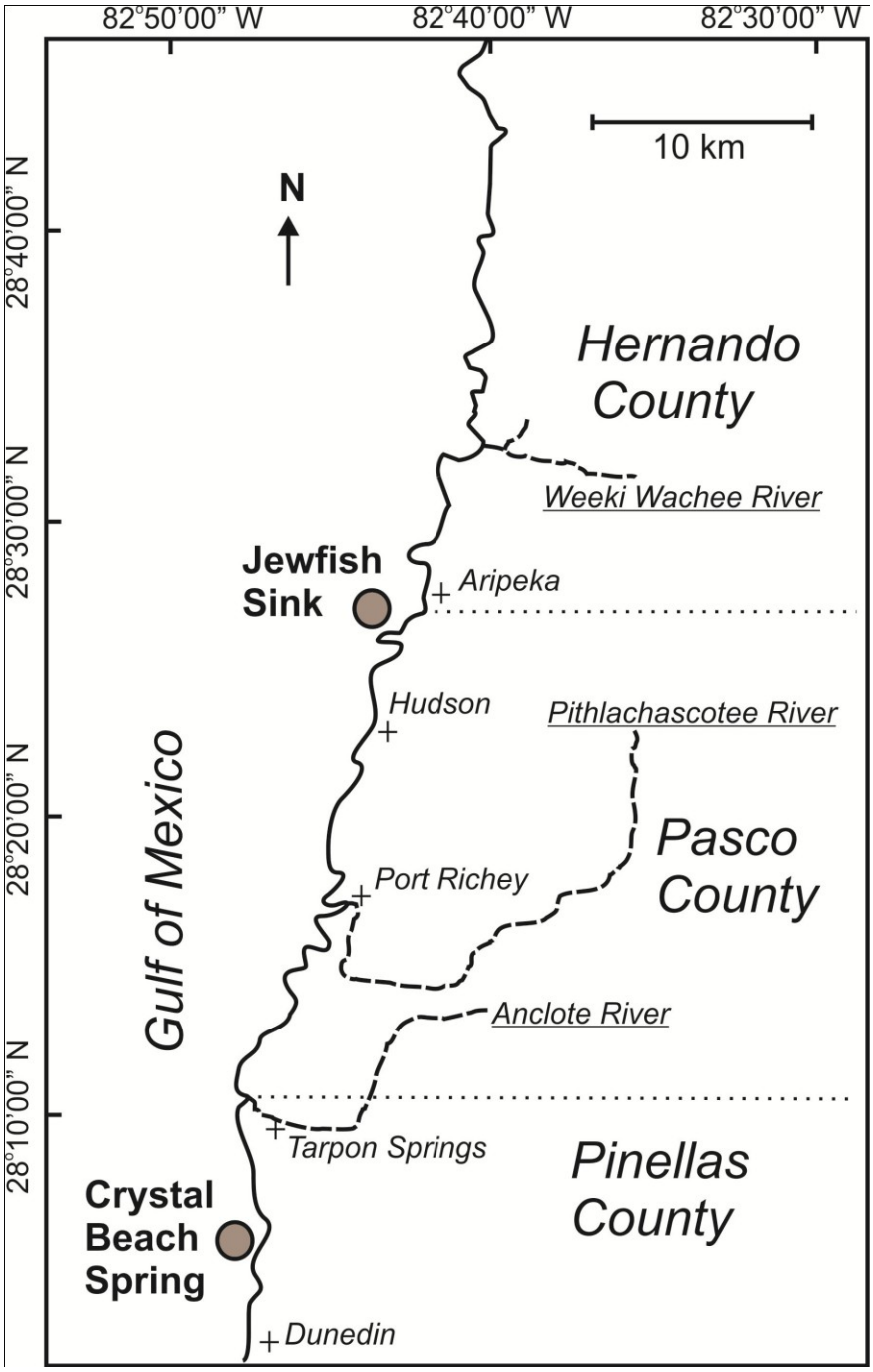

Figure 1.1. Map of the West Florida region showing the location of Jewfish Sink and Crystal Beach Spring. County boundaries are indicated with dotted lines, rivers are shown as dashed lines and coastal city/town centers are designated with a + symbol.

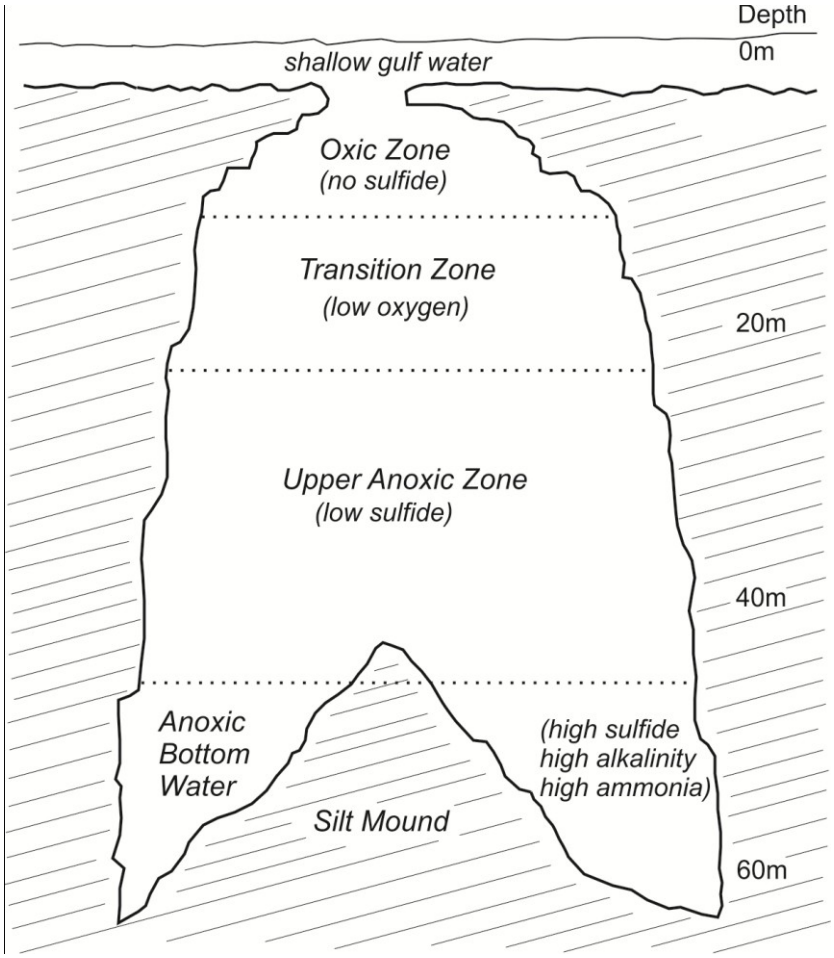

Figure 1.2. Schematic side view of Jewfish Sink showing the four zones described in the text. The depth of the zones varies with the season. Limestone rock containing the sink is shown shaded while the water column is not shaded. The approximate depth below the surface of the Gulf of Mexico is shown in meters along the right side.

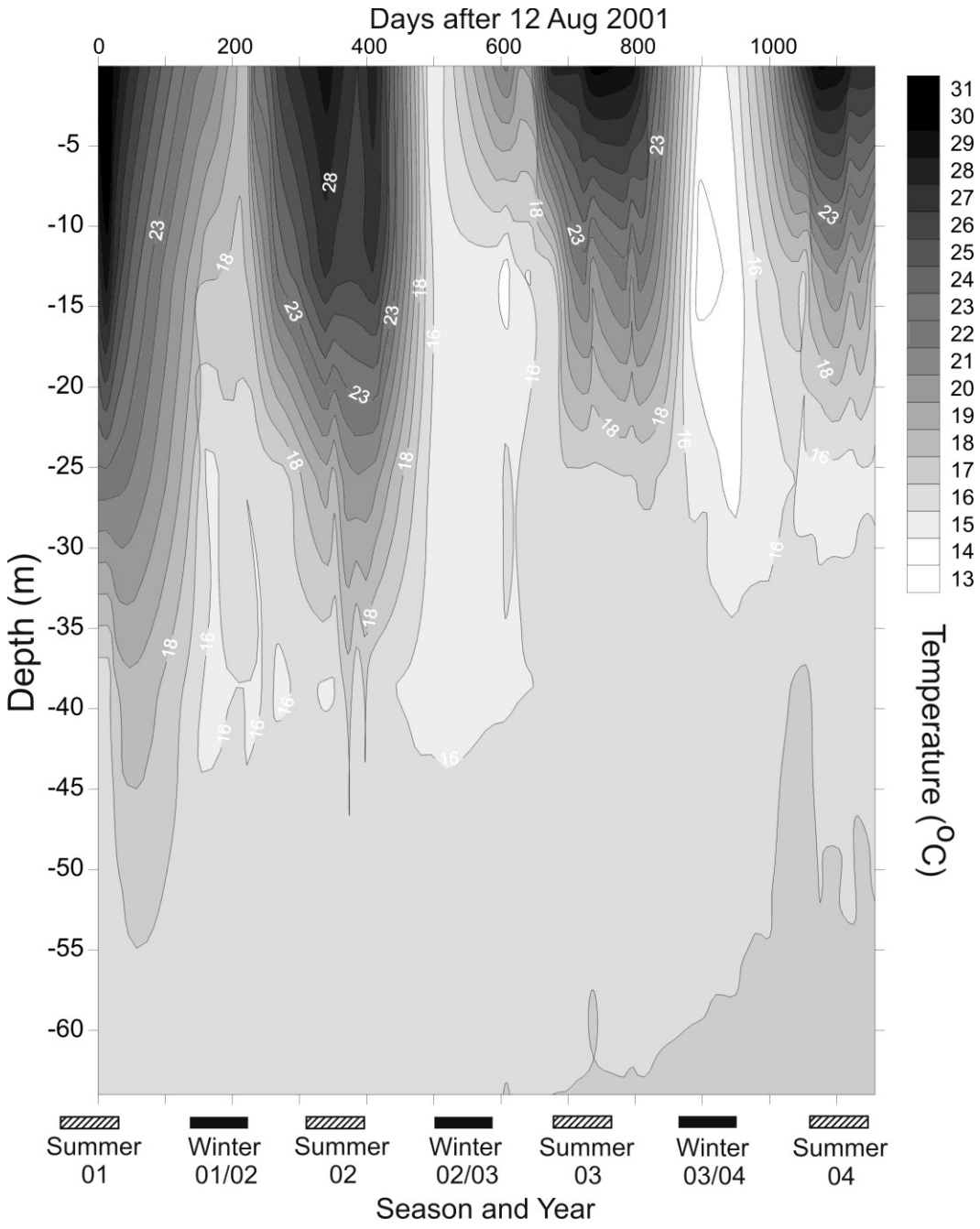

Figure 1.3. The relationship of temperature (^{0}C) and depth over time in Jewfish Sink derived from 29 hydrolab profiles between 22 August 2001 and 30 August 2004 (data from Garman & Garey, 2005). The X axis is labeled with the number of days elapsed from the first data collection (top) and annotated with summer and winter seasons (bottom).

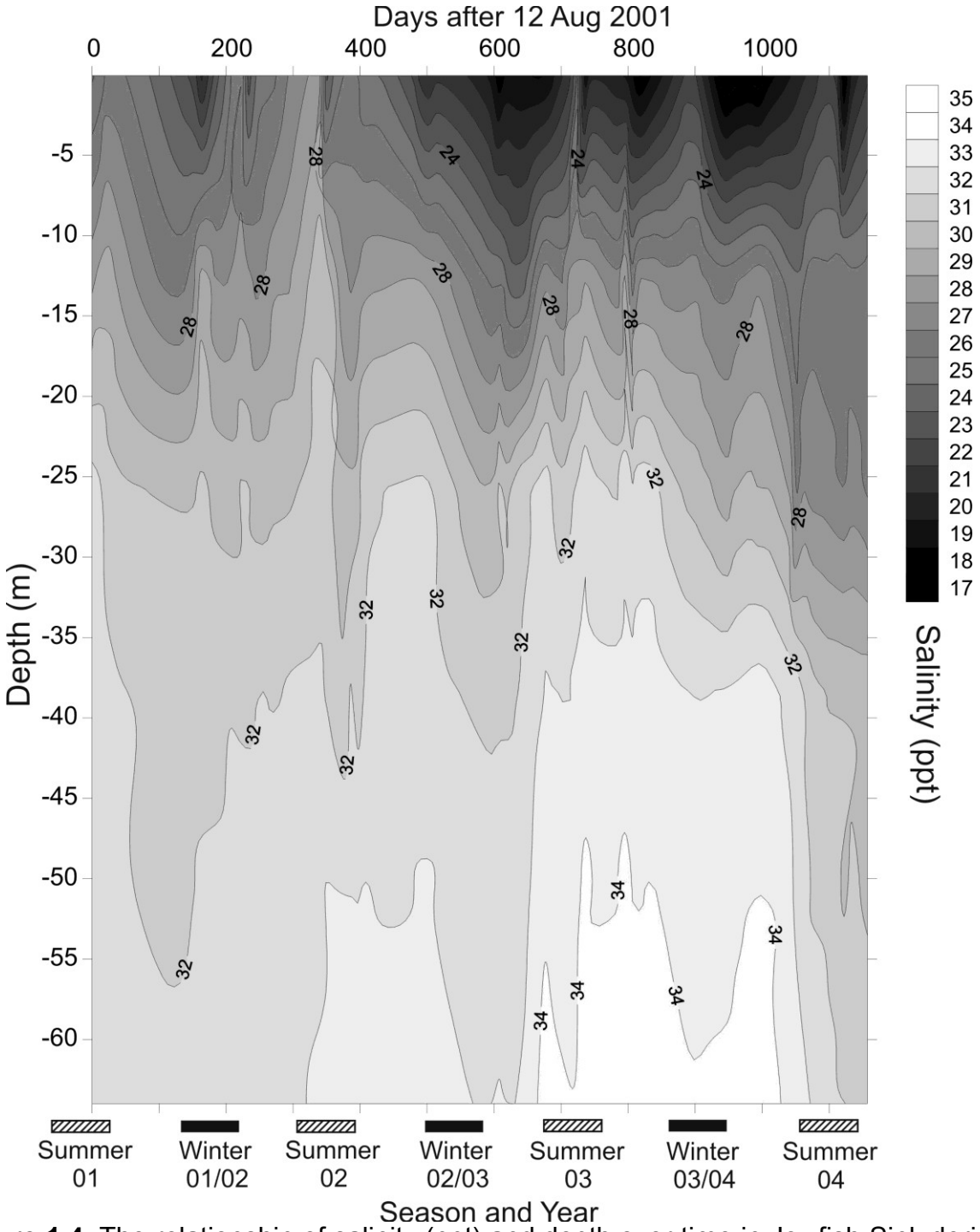

Figure 1.4. The relationship of salinity (ppt) and depth over time in Jewfish Sink derived from 29 hydrolab profiles between 22 August 2001 and 30 August 2004 (data from Garman & Garey, 2005). The X axis is labeled with the number of days elapsed from the first data collection (top) and annotated with summer and winter seasons (bottom).

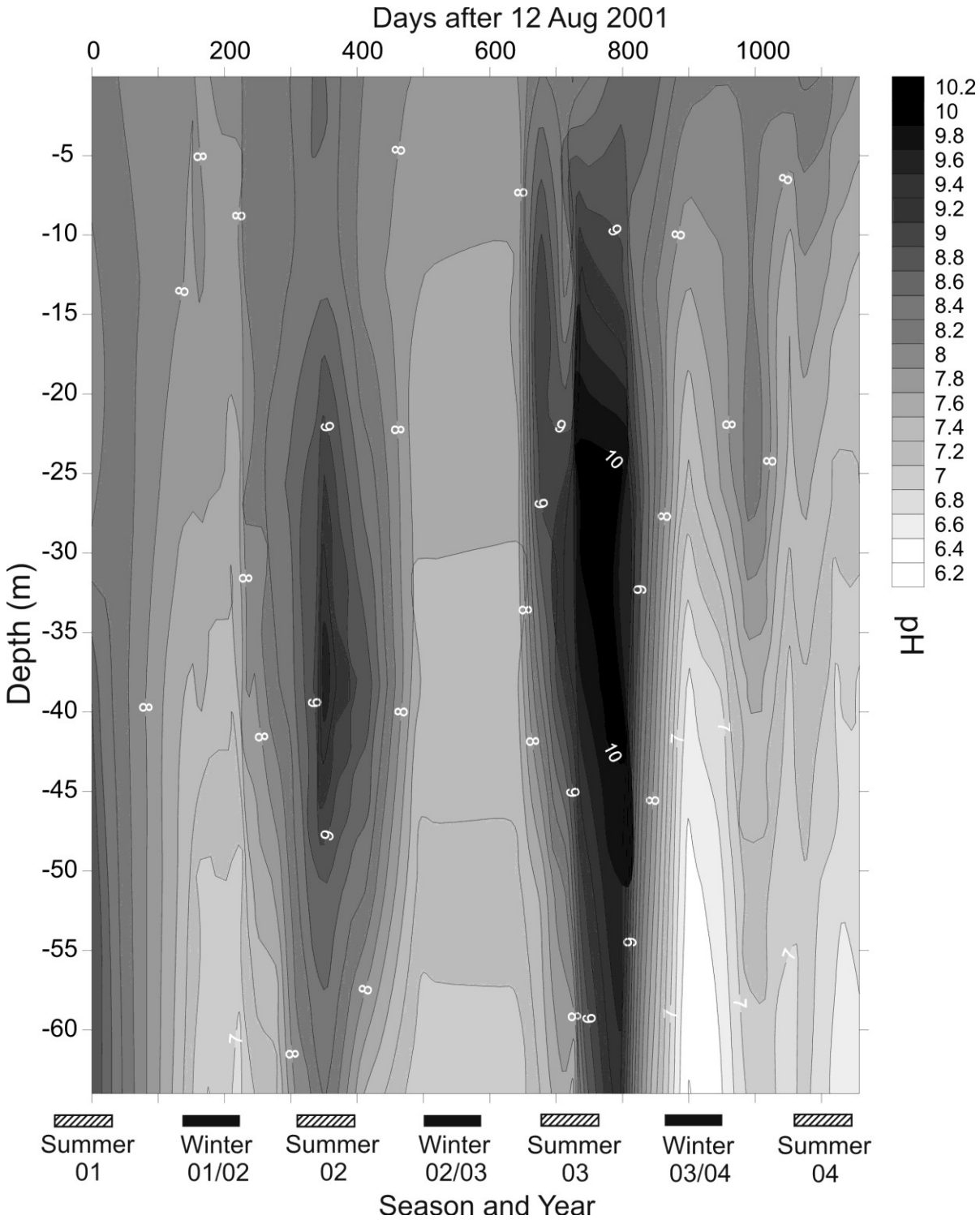

Figure 1.5. The relationship of pH and depth over time in Jewfish Sink derived from 29 hydrolab profiles between 22 August 2001 and 30 August 2004 (data from Garman & Garey, 2005). The X axis is labeled with the number of days elapsed from the first data collection (top) and annotated with summer and winter seasons (bottom).

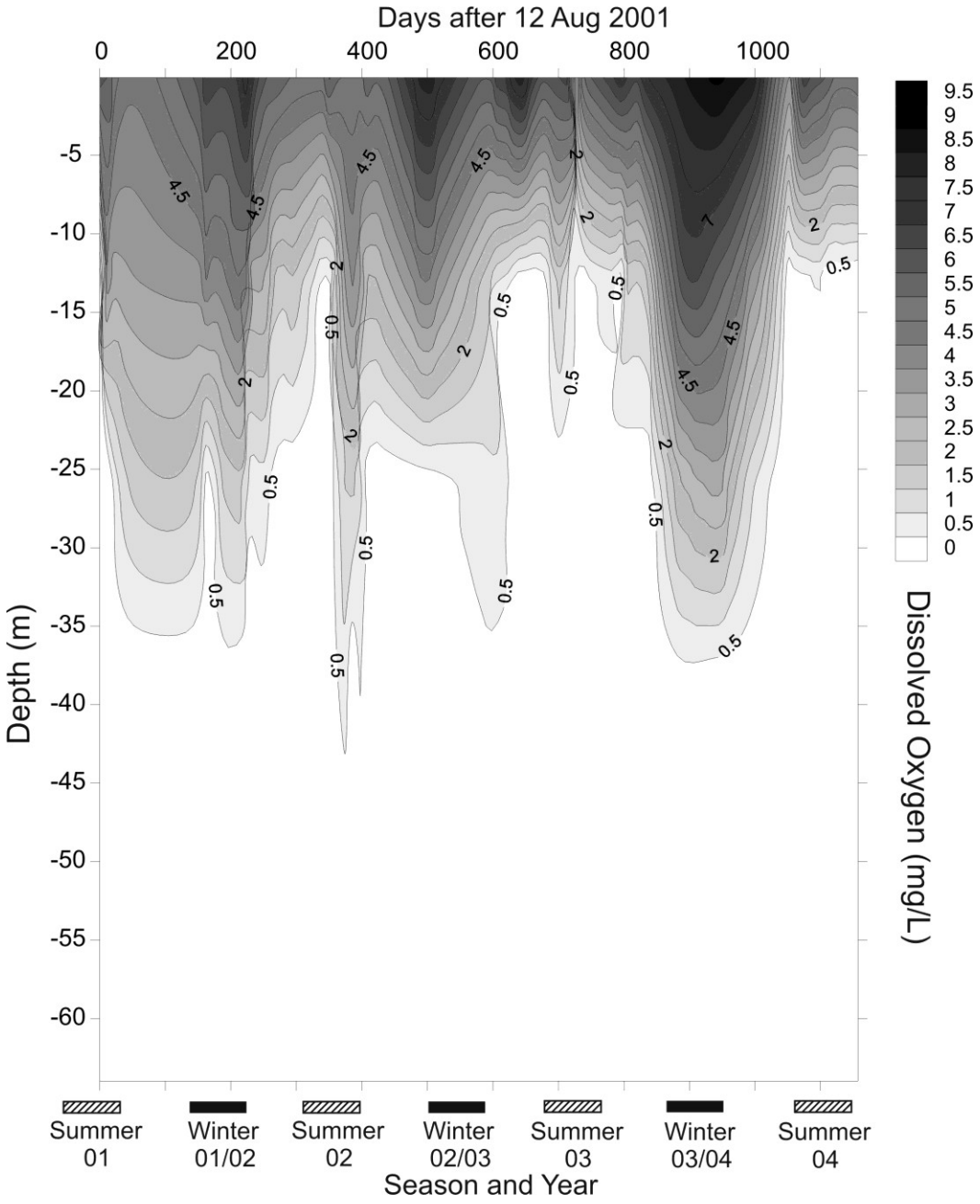

Figure 1.6. The relationship of dissolved oxygen (mg/L) and depth over time in Jewfish Sink derived from 29 hydrolab profiles between 22 August 2001 and 30 August 2004 (data from Garman & Garey, 2005). The X axis is labeled with the number of days elapsed from the first data collection (top) and annotated with summer and winter seasons (bottom).

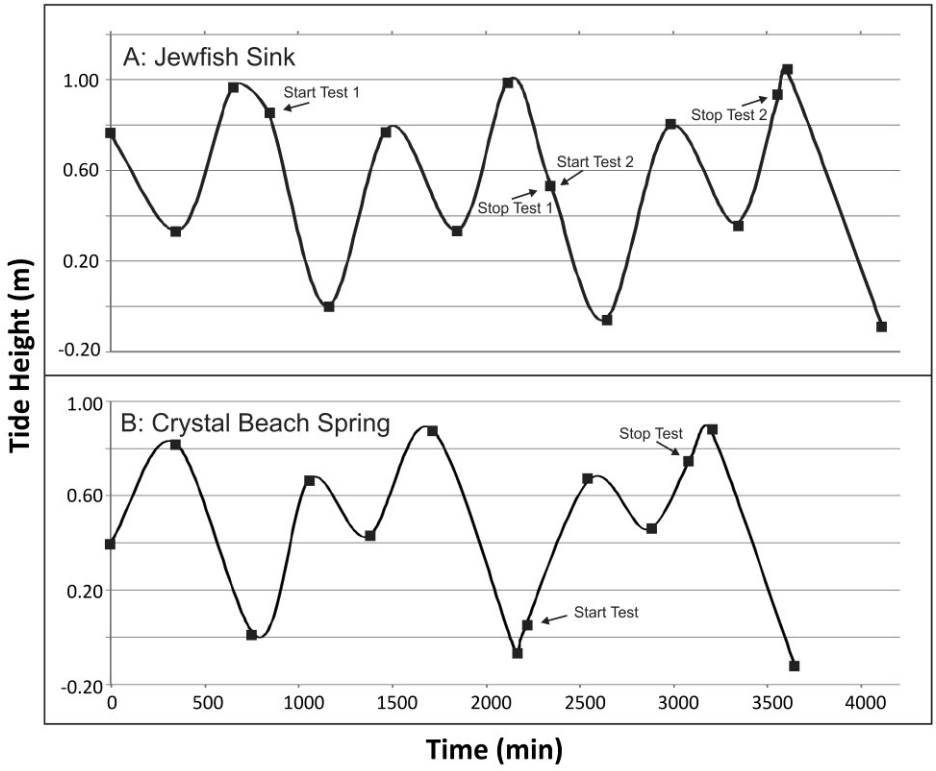

Figure 1.7. Seepage meter sampling. The tidal height is shown beginning on 7 October 2005 for Jewfish Sink (A) and Crystal Beach Spring (B). Two seepage meter tests were carried out at Jewfish sink and the start and stop points of each test are indicated with arrows in panel A. A single test was carried out at Crystal Beach Spring as indicated in panel B.

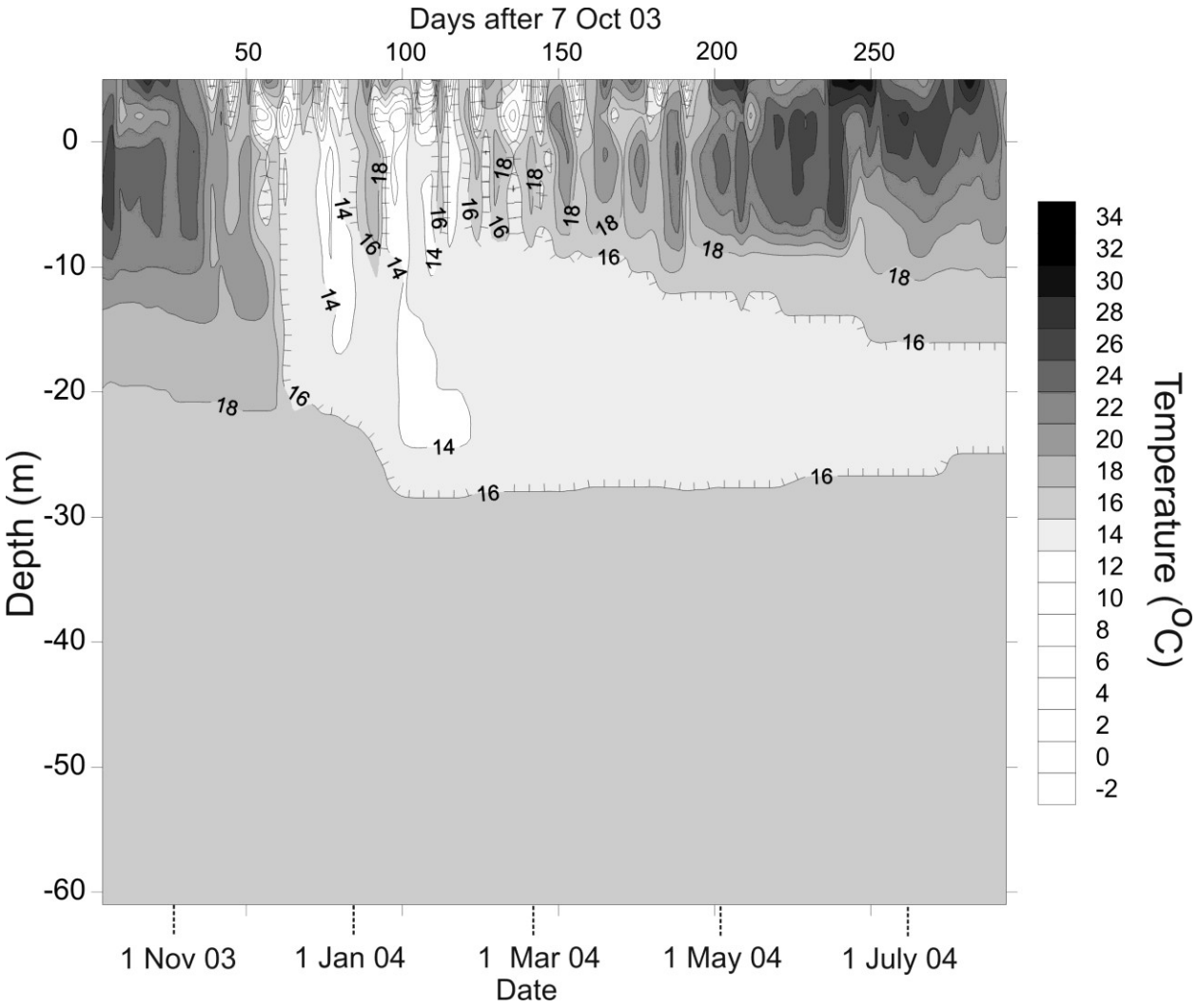

Figure 1.8. Temperature contours of Jewfish sink at different depths measured every four hours from 7 October 2003 through 26 July 2004. Measurements were taken at 3, 6, 9, 12, 18, 24, 37, 46 and 61m. Days from the first measurement are shown on the top, with the first day of each month shown at the bottom.

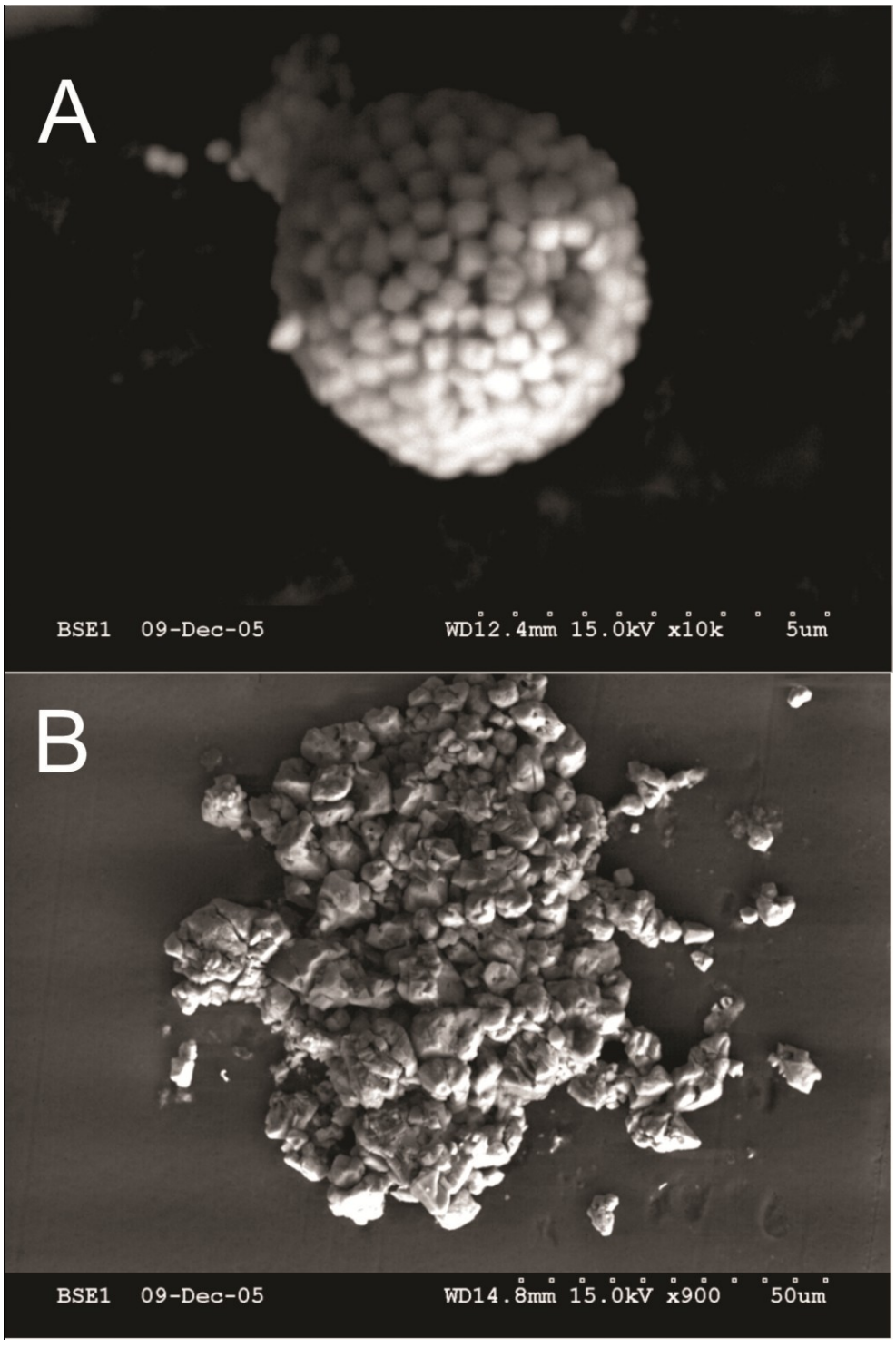

Figure 1.9. Two major types of particles found in Jewfish Sink Summer water: A. Pyrite framboid particle. B. Calcium Carbonate particles.

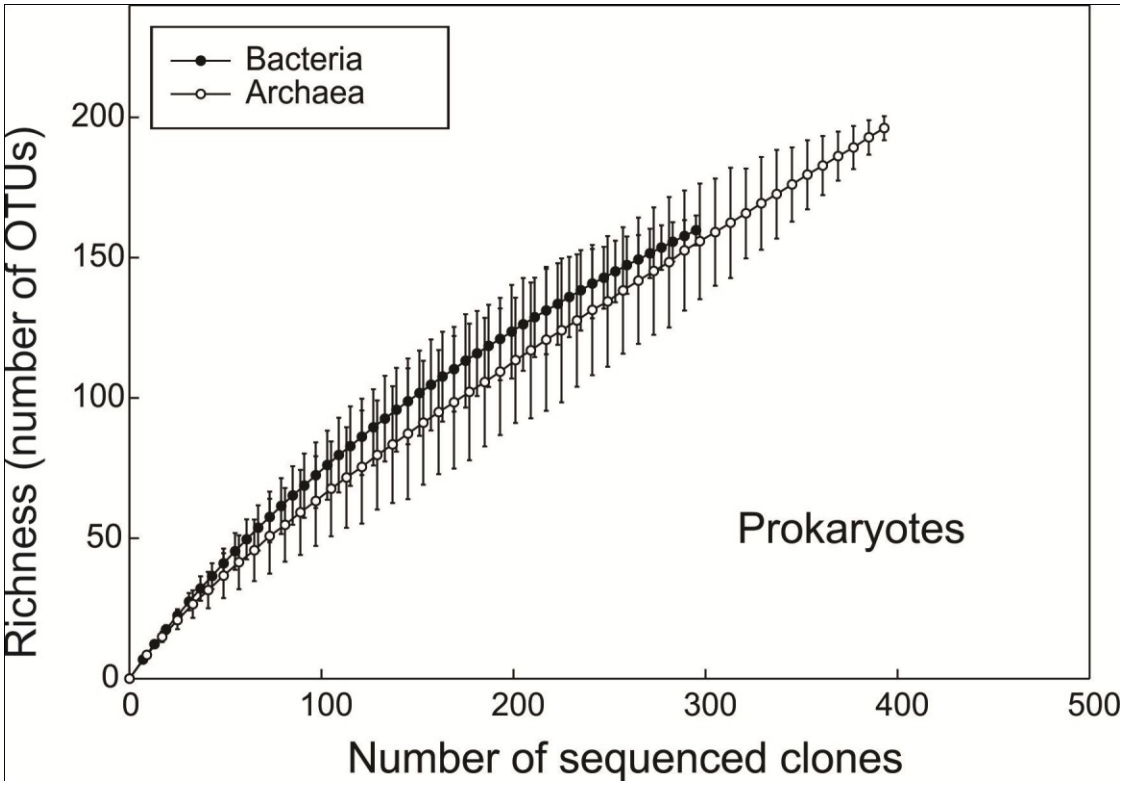

Figure 1.10. Rarefaction analyses of prokaryote 16S rRNA richness based on the number of OTUs. Mat samples from the vertical wall of Jewfish Sink were collected from the anaerobic zone. Error bars represent variance.

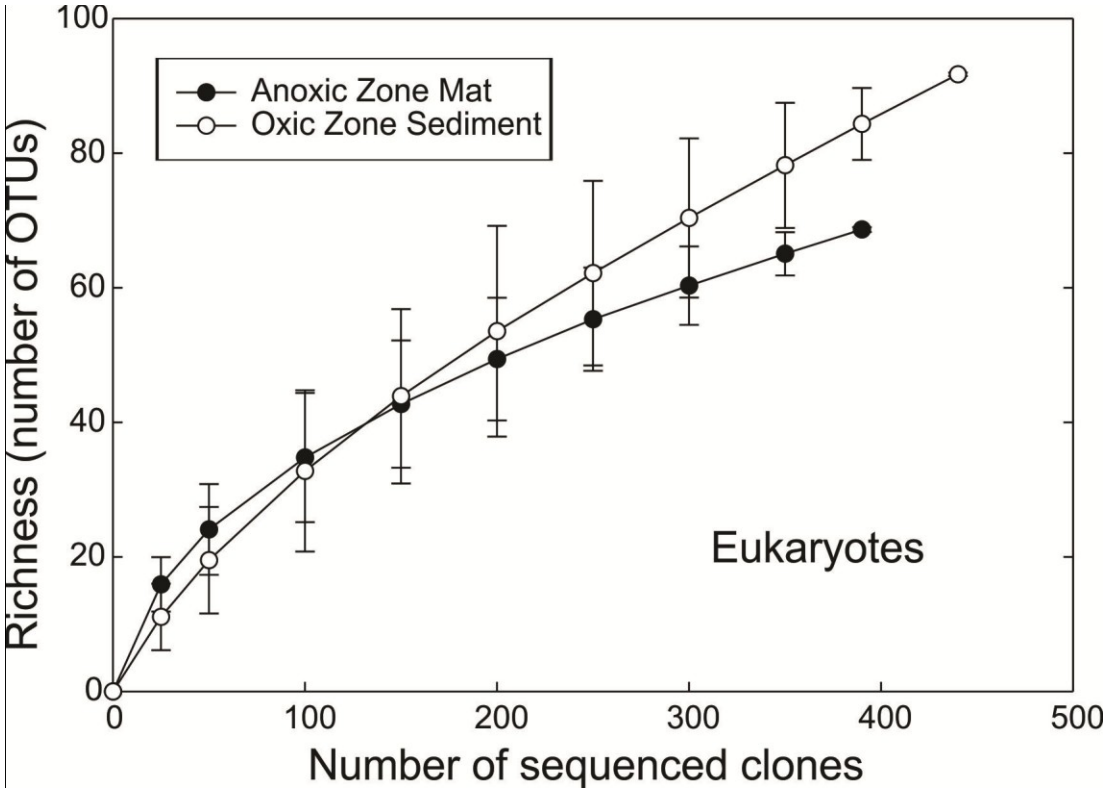

Figure 1.11. Rarefaction analyses of eukaryote 18S rRNA richness based on the number of OTUs. Mat samples from the vertical wall of Jewfish Sink were collected deep within the anaerobic zone. Sediment samples were collected from horizontal ledges in the shallow oxic zone. Error bars represent variance.

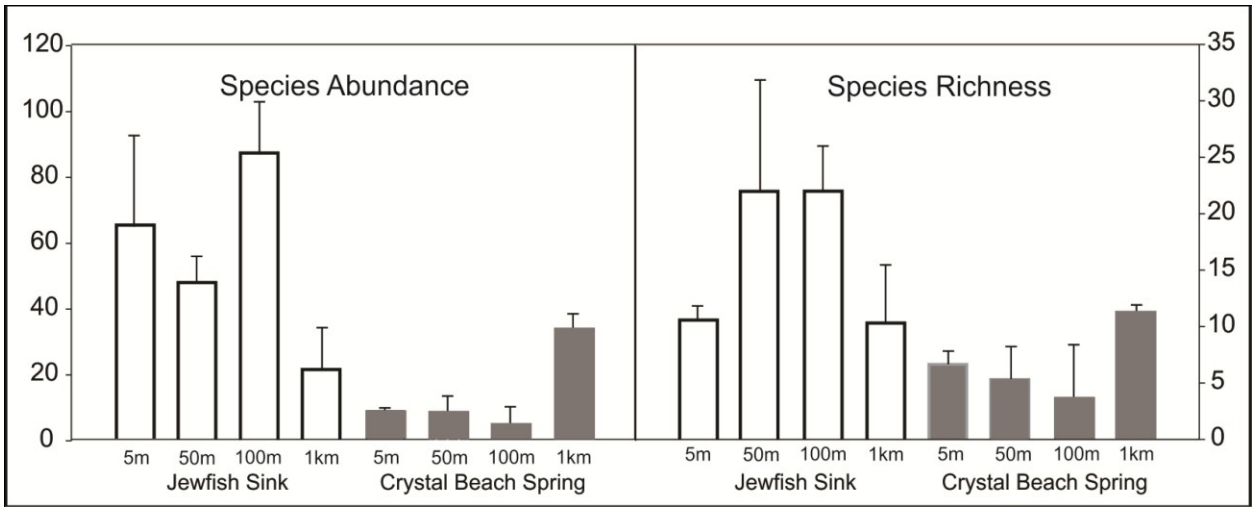

Figure 1.12. Species Abundance and Species Richness of macrofauna from transects at Jewfish Sink (white bars) and Crystal Beach Spring (gray bars). Distance along each transect from the entrance are shown.

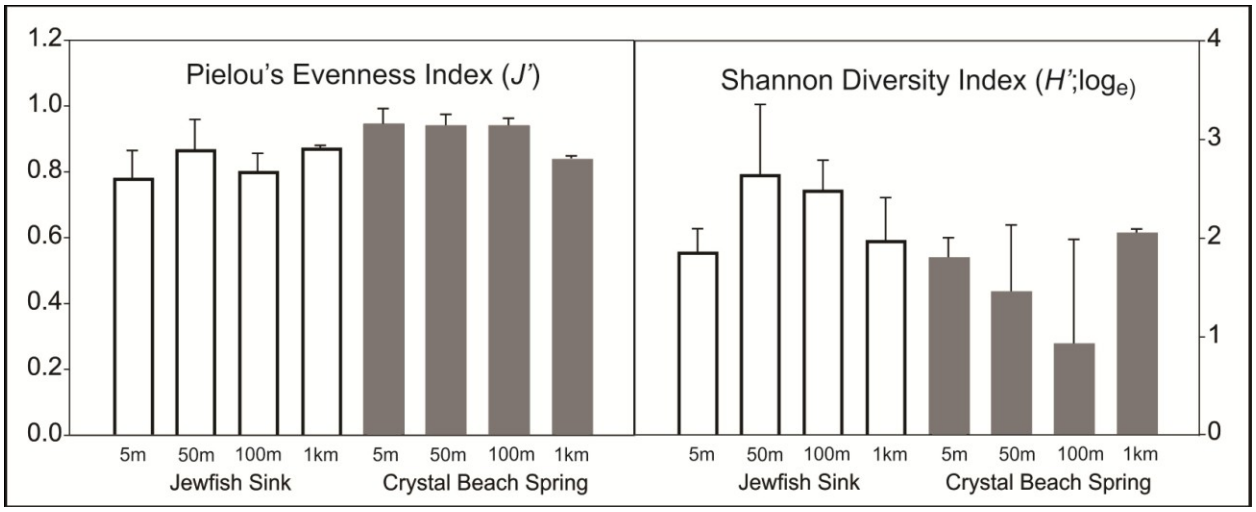

Figure 1.13. Evenness and Shannon Diversity of macrofauna from transects at Jewfish Sink (white bars) and Crystal Beach Spring (gray bars). Distance along each transect from the entrance are shown.

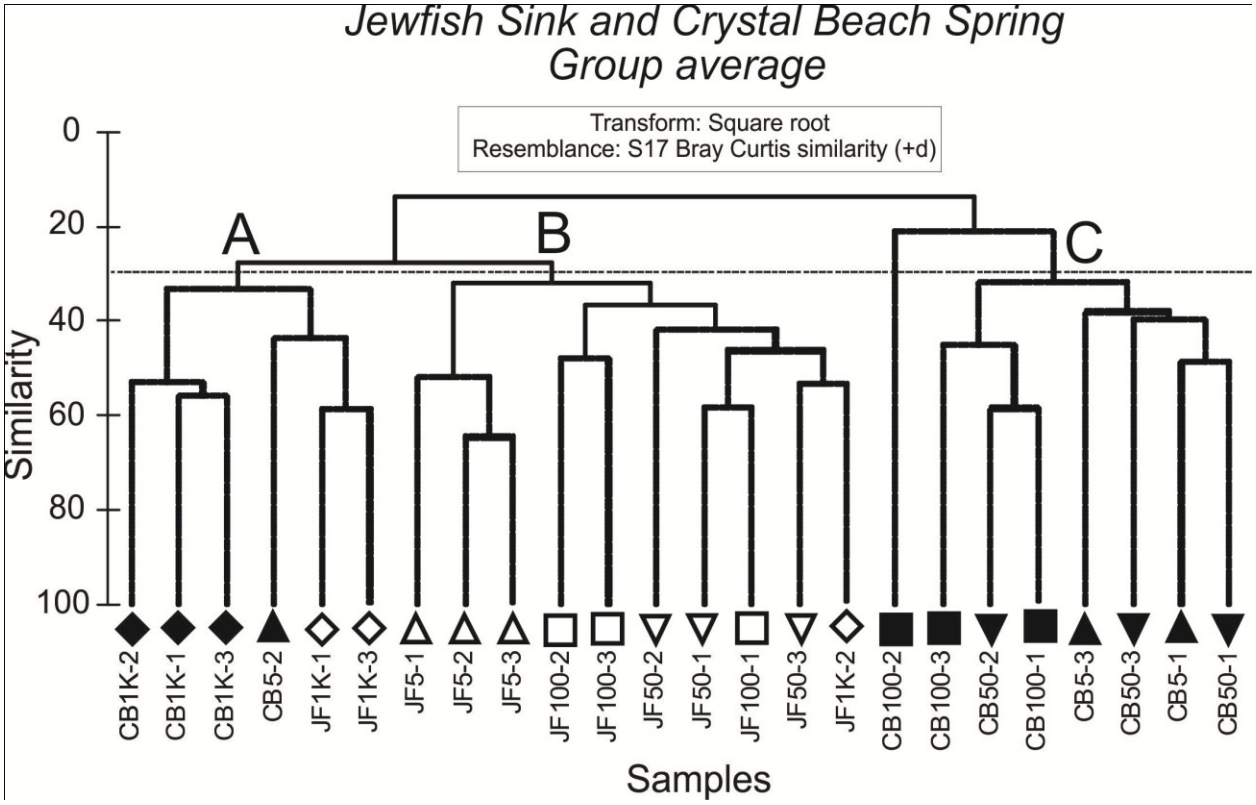

Figure 1.14. Cluster analysis of similarity among samples along the transect from Jewfish sink (JF, open symbols) and Crystal Beach Spring (CB, filled symbols). Distances from the sink or spring (5=5m, 50=50m, 100=100m, 1K=1000m) and the replicate number

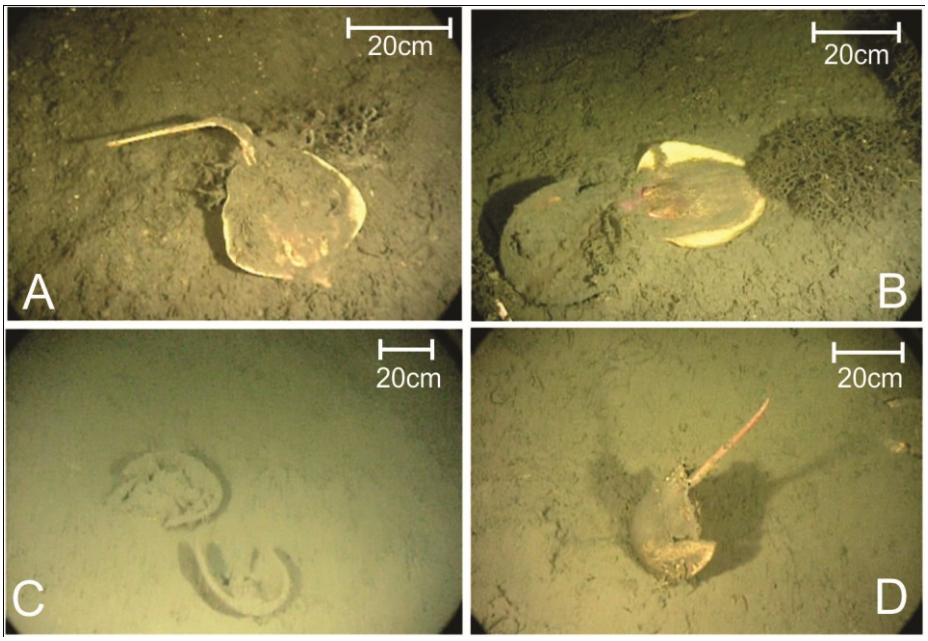

Figure 1.15. Stingrays, horseshoe crabs and macroalgae are commonly trapped in the bottom of Jewfish Sink where they die from anoxia. Soft tissues decay within a week or two. A: Dead stingraw and remnants of macroalgae, B: dead horseshoe crab, stingray, and macroalgae, C: dead horseshoe crabs exoskeletons partially covered with sediment, D: dead horseshoe crab, partially buoyant from gases evolved within the carapace from decomposition.

CHAPTER TWO: CLINE PARTITIONING OF MICROBIAL COMMUNITIES AND TURNOVER DISRUPTION IN AN ANOXIC KARST MARINE BASIN

Introduction:

Florida's gulf coast is one of many regions on earth dominated by a karst landscape. Characterized by caves and underground water systems, soluble porous rocks such as limestone and gypsum form much of the landforms that typify karst terrain. Found not only in Florida, karst aquifers provide roughly 20 – 25% of the global population with water (Ford & Williams, 2007). The distinctive hydrology inherent within karst systems leads to the formation of characteristic features such as springs, caves, and sinkholes. Both terrestrial and marine sinkholes are found in karst landscapes including the blue holes of the Bahamas. The term blue hole is usually used to describe circular sinkholes that can be on or off shore with a characteristic blue color. They usually have connected cave conduits and unique water-flow characteristics. The term "blue hole" is often used to describe many karst systems sharing a general morphological similarity. More recent narrower definitions emphasize the formation of the hole in carbonate rock with the majority of the pit below sea level with a tidal influence and possibly with conduits connected to the hole (Mylroie, Carew, & Moore, 1995). Similar to blue holes, but limited to interior onshore regions, are karst features called black holes. Besides the color, which is due to a horizontal microbial layer of purple sulfur bacteria, the main difference between a blue and a black hole is the

absence of lateral passages in black holes. This makes the hydrology of black holes relatively stable due to limited water exchange (Schwabe & Herbert, 2004).

Other karstic pit features, perhaps less familiar than blue and black holes, are common and can be found many places including Florida's Gulf coast. One such karst sink located approximately 1 km offshore from Aripeka, Florida in the Gulf of Mexico (N 28°25'42.9", W 82°42'29.7") is called Jewfish sink (Figure 2.1). Jewfish sink, while not having the characteristic wide circular opening of the black and blue holes of the Bahamas, shares some similarity to those well-studied features. Once a spring, it used to be fed freshwater from the conduits underlying the coastal region of the Gulf of Mexico before a drought in 1961-1962 caused it to stop discharging freshwater. Overuse of the groundwater eventually led to the sink becoming stagnant, receiving no detectable freshwater flow through (Garman & Garey, 2005). Jewfish sink has a 6 m opening but widens to a base diameter of 76 m (Figure 2.2). The total depth of the sink is approximately 64 m. Within the sink, horizontal zones establish themselves along a vertical axis, creating unique chemistry within each zone. Bacterial mats occupy the lower anoxic portion of the sink walls and recede or flourish as the clines that partition the zones change throughout the seasons. Particulate clouds form at certain times throughout the year and have been previously shown to have different compositions depending on the season. During the summer, framboidal pyrite and calcium carbonate composed the particulate clouds. During the winter, the particulates are aluminum silicate clay minerals along with organic and inorganic aggregates (Garman, Rubelmann, Karlen, Wu, & Garey, 2011). Sulfide is characteristic of the anoxic zones

and is normally found in relatively high concentrations in the anoxic bottom water (Garman & Garey, 2005) .

The microbiology of Jewfish Sink has been explored (Garman et al., 2011) and a provisional explanation of the biocomplexity at Jewfish Sink has been established. Of the prokaryotes sequenced, the majority predicted using phylotypes (70%) were anaerobic using sulfur (45%) as a reducing equivalent in energy production. After aerobes, sulfur oxidizing bacteria, also aerobic, comprised the third largest guild representing about 15% of the sequences examined. While present, methanogens, nitrogen metabolizers and iron reducers had a lower relative abundance than sulfur metabolizers highlighting the importance of sulfur metabolism within the sink.

Prokaryotes use a wide variety of mechanisms to reduce or oxidize sulfur (Figure 2.3). In the black holes of the Bahamas, sulfur oxidation has been shown to play an important role in the creation of the microbial layer responsible for coloring the holes black. Specifically, the purple sulfur bacteria belonging to the genera *Thiocapsa* and *Allochromatium* were isolated and cultured from the microbial layer. These genera are thought to play a significant role in the sink by harvesting light and using reduced sulfur as an electron donor to drive energy production (Schwabe & Herbert, 2004). These organisms oxidize sulfide to elemental sulfur which is stored internally until further oxidation of sulfur is needed. Neither of these genera were found in previous studies of Jewfish sink. The relatively small (D = 6 m) entrance of the sink does not allow for the amount of light received by the larger (D = 300 m) black hole of South Andros, Bahamas (Schwabe & Herbert, 2004). While both phototrophic sulfur oxidizers and

chemolithotrophic oxidizers were found at Jewfish Sink, their relative abundance was low compared to sulfur reducing bacteria.

Sulfur reducing prokaryotes have many strategies resulting in using sulfur as a terminal electron receptor in their electron transport chain (Figure 2.3). Various sulfur compounds can be reduced by a number of different enzymes. Not all prokaryotes share a similar method or pathway to accomplish this goal, which makes holistic modeling of sulfur cycling in any given system problematic. Perhaps two of the most studied strategies for reducing sulfur are the assimilatory and dissimilatory sulfate reduction pathways. The assimilatory pathway reduces sulfate to sulfide which is then used in the synthesis of sulfur containing cell components such as cysteine (Simon & Kroneck, 2013). This pathway shares some enzymes with the dissimilatory pathway but the enzymes are phylogenetically different enough from one another that they can be distinguished by careful sequence analysis. The dissimilatory pathway involves 3 major conversions that ultimately take sulfate (oxidation state +6) to sulfide (oxidation state -2) (Figure 2.4). The last step of this reaction utilizes the enzyme dissimilatory sulfite reductase (DSR) and is phylogenetically distinguishable from its assimilatory counterpart. Further complicating the matter, certain organisms use a form of the DSR enzyme in reverse, oxidizing the reduced sulfur. The genes encoding the reverse form of DSR were excluded from this study through careful primer design. The sulfide released from the cell at the end of the dissimilatory reductive pathway is responsible for the sulfur smell of many anaerobic environments. The seasonal variation of sulfide concentrations recorded at Jewfish sink suggests that this pathway is important to the ecology and productivity of the microbial communities dwelling within the sink. Chemical

profiles within Jewfish Sink were recorded on 9 sample days spanning a period of 685 days starting on September 17, 2009 in order to investigate seasonal variation of microbial communities within the sink. Microbial communities were examined at depths of 10 m, 20 m, 30 m, and 40 m for each sample date using both 16s rRNA and *dsr* targeted DGGE fingerprinting. This study will expand and describe the biogeocomplexity of less-studied karst features compared to more well studied blue holes and black holes.

Materials and Methods:

Site description:

Jewfish sink is located approximately 1 km offshore from Florida's gulf coast near the coastal town of Aripeka (Figure 2.1). The sea level around the entrance to Jewfish Sink ranges between 1.5 m and 3.0 m depending on the tide. The entrance to the sink is about 6 m in diameter and appears as a circular dark hole on the seafloor in the Gulf of Mexico. The total depth of the sink is around 60 m, although a debris mound in the center of the entrance is reached at a depth of around 40 m (Figure 2.2).

Sample collection:

Samples were collected at 9 different time points over the period of 685 days. Sample dates were as follows: September 17th, 2009, December 13th, 2009, January 29th, 2010, April 23rd, 2010, June 9, 2010, October 22nd, 2010, February 19, 2011, June 18th, 2011, and August 2, 2011. A Van Dorn bottle was used to retrieve water column samples from 4 depths within Jewfish Sink and surface water (0 m) from the channel leading to the sink. The Van Dorn bottle was attached to cave line marked at 5 m intervals. 1 L of water column was collected in 5 replicates at depths of 10 m, 20 m, 30

m, and 40 m (Figure 2.2). The water samples were stored in 1 L Nalgene bottles previously sterilized with 70% ETOH. The samples were stored on ice until processed back in the lab later that evening.

Water column chemistry and physical factors:

A Datasonde (Hydrolab-Hach Company Brand, Loveland, CO, USA) was programmed to record dissolved oxygen (DO), salinity, total dissolved solids (TDS), temperature, pH, oxidation-reduction potential (ORP), and depth at intervals of 30 seconds. The Datasonde was lowered into Jewfish Sink slowly to ensure accurate and sufficient data collection along the vertical axis of the sink. The maximum depth of data collection was 40 m to prevent interaction of the Datasonde with the debris mound. Data was recorded both on the descent and on the subsequent ascent of the Datasonde within Jewfish Sink. Data points on the descent were used in the analysis of the water column chemistry shown here.

The sulfur metabolites sulfite, thiosulfate and sulfide were tested using kits obtained from CHEMetrics (CHEMetrics, Inc., Calverton, VA, USA). The tests were performed on the boat as the samples were being collected to ensure the least amount of influence from prolonged exposure to air or oxygenated water. Each test was performed on 3 of the 5 replicates at any given depth.

The water chemistry was visualized using the software Surfer 11.0 (Golden Software, Golden, CO, USA).

Density of the water column was calculated based on methods described by El-Dessouky and Ettouny (2002). Rainfall data and air temperatures were collected from

public data available through the National Oceanic and Atmospheric Administration's website.

Bacterial community analysis:

500 mL of each replicate was filtered onto a 0.2 µm Isopore Membrane Filter (filter code GTTP) (EMD Millipore, Darmstadt, Germany). Cells were resuspended from each filter using 3 mL of a sterile phosphate buffered saline solution. Cell suspensions were pelleted by centrifugation and subsequently resuspended in 50 µL of the extraction buffer provided in the MoBio UltraClean Soil DNA extraction kit (Mo Bio Laboratories, Carlsbad, CA). DNA extraction was performed on all 5 replicates from each depth using the MoBio UltraClean Soil DNA extraction kit.

PCR targeting the 16s rRNA gene was perfomed on 3 of the 5 replicates. Primers 27F (5' - AGAGTTTGATCCTGGCTCAG - 3') and 1492R (5' - GGTTACCTTCTTACGACTT - 3') were used with an annealing temperature of 45° C (DeLong, 1992). PCR conditions consisted of an initial denaturation at 95° C for 2 min, followed by 40 cycles of denaturation at 95° C for 15 s, annealing at 45° C for 1 min, extension at 72° C for 2 min, and a final extension of at 72° C for 7 min. Gel purification of bands representing the 16s rRNA gene was performed on all samples using the QIAquick Gel Extraction Kit (Qiagen, Venlo, Netherlands).

Denaturing gradient gel electrophoresis (DGGE) was performed on the gel extracted 16s rRNA amplicons using primers 1070F (5' – ATGGCTGTCGTCAGCT -3') and 1392R (5'-CGCCCGCCGCGCCCCGCGCCCGGCCCGCCGCCCCCGCCCCACGGGC GGTGTGTAC – 3') (Ferris, Muyzer, & Ward, 1996). PCR conditions consisted of an initial denaturation at 94° C for 3 min, followed by 30 cycles of denaturation at 94° C for

45 s, annealing at 55° C for 45 s, extension at 72° C for 1 min, and a final extension of at 72° C for 5 min. Denaturation gradient gels were made using 15 mL of 40% (17.5 mL bis acrylamide, 2.0 mL 50X TAE, 24 mL formamide, 25.2 g urea brought to 100 mL total volume with nanopure water) denaturing agent combined with 150 µL of 7% ammonium persulfate and 15 µL of TEMED along with 15 mL of 60% (17.5 mL bis acrylamide, 2.0 mL 50X TAE, 16 mL formamide, 16.8 g urea brought to 100 mL total volume with nanopure water) combined with 150 µL of 7% ammonium persulfate and 15 µL of TEMED. These two mixtures were placed into a mixing apparatus that established the denaturing gradient along the vertical axis of the gel. The gels were run using the Bio-Rad DCode Universal Mutation Detection System (Bio-Rad Laboratories, Hercules, CA, USA) which contained 1X TAE. The gels were run for 16 hours at 44 volts and 60° C. Gels were stained with ethidium bromide and imaged using a Kodak DC 290 digital camera mounted to a Kodak EDAS 290 adapter for UV illumination and analyzed in the Kodak Molecular Imaging Software v 4.5.0 (Rochester, NY, USA). Band identification and gel normalization was performed using the Bionumerics software package (v. 4.6) (Applied Maths, Sint-Martens-Latem, Belgium). All sample sites and dates were normalized using DGGE markers made from pure cultures of *Escherichia coli*, *Ralstonia solanacearum*, *Streptococcus mutans*, *Salmonella typhimurium*, *Salmonella abony*, and *Desulfovibrio vulgaris*. The normalized fingerprint data was imported into Microsoft Excel. Each band from every sample was binned into 1 of 100 categories based on the normalized position it was found along the gel. Presence of a band at a position was given a numerical value of 1, while absence of a band at a position was given a value of

0. This data was then imported into the Primer-E software (Clarke & Gorley, 2006) for statistical analysis.

Dissimilatory sulfite reductase (dsr) community analysis:

10 forward primers and 10 reverse primers (Table 2.1) were designed from alignments of all known *dsr* genes found in the Intergrated Microbial Genomes (IMG) database (Bacteria and Archaea). The primers targeted a 1.9 kb fragment that spanned across both *dsrA* and *dsrB* (Figure 2.5). An equimolar mixture was created for both forward and reverse primers. PCR conditions consisted of an initial denaturation at 94° C for 2 min, followed by 10 cycles of denaturation at 94° C for 30 s, annealing at 55° C for 1 min, extension at 72° C for 4 min, and then 30 cycles of denaturation at 94° C for 30 s, annealing at 50° C for 1 min, extension at 72° C for 4 min and a final extension at 72° C for 3 min. Genomic DNA from *Desulfovibrio vulgaris* was used as a positive control.

Bands representing the *dsrAB* PCR product were excised from the gel using the QIAquick Gel Extraction Kit (Qiagen, Venlo, Netherlands). This purified PCR product was used in the DGGE PCR as the template. The primers used in the DGGE PCR of *dsr* were DSRp2060F (5' – CGCCCGCCGCGCCCCGCGCCCGGCCCGCCGCCC CCGCCCGCAACATCGTYGAYACCCAGGG – 3') (Geets et al., 2006) and DSR4R DGGE (5' – GTGTAGCAGTTACCGCA – 3') (Wagner, Roger, Flax, Brusseau, & Stahl, 1998) which amplified a 350 bp region of *dsrB* (Figure 2.5). PCR conditions consisted of an initial denaturation at 94° C for 3 min, followed by 30 cycles of denaturation at 94° C for 45 s, annealing at 55° C for 45 s, extension at 72° C for 1 min, and a final extension of at 72° C for 5 min.

DGGE gels were prepared, processed and analyzed as described for the bacterial community analysis.

Statistical analysis:

Fingerprints were imported into the Primer-E software package as presence and absence, therefore no data transformation was done prior to calculating the Bray-Curtis similarity. The similarity measures were used in cluster analysis and in the creation of Multi-Dimensional Scaling (MDS) plots.

Abiotic factors for each replicate at each depth and date were normalized within the Primer-E software package. Each date was analyzed independently of the other dates. Similarity was measured using Euclidian distance. The similarity was then used in cluster analysis. Euclidean distances between depths of ≥ 4 were considered clines in this study.

Results:

Water column chemistry and physical factors:

The Datasonde was used to record temperature, dissolved oxygen, total dissolved solids, pH, oxidation-reduction potential and salinity on 9 sample dates ranging from September 17th, 2009 (day 1) until December 14th, 2011 (day 685) (Figure 2.6). On the first day of the study, the temperature ranged from 27.5 °C at 14 m within the sink to 19.8 °C at 40 m deep within the sink. The dissolved oxygen concentrations measured from 0.1 mg/L at the maximum depth to around 5 mg/L at the surface. The oxidation-reduction potential remained negative at all depths within the sink and ranged from -200 to -700 mV. pH ranged from 8.0 at 10 m within the sink to 7.7 at 40 m. Sulfide, thiosulfate and sulfite tests recorded measurable quantities at 20 m depths and

below (Figure 2.7). Sulfide concentrations ranged from 0.7 mg/L (20 m) to 4 mg/L (40 m) while sulfite concentrations ranged from 4.5 mg/L (20 m) to 15.7 mg/L (40 m) (Table 2.2).

On the second sample day, December 13, 2009 (day 78), water temperatures were lower overall than on the prior sample day. The temperature ranged from 21 °C at surface waters to 17 °C at 15 m within the sink. Temperatures increased from the minimum reading at 15 m to 20 °C around 30 m and 19.8 °C at 40 m. Oxygenated water was found deeper within the sink than on the previous sample day, with 1.59 mg/L of DO found at a depth of 33 m. At 34 m the DO lowers to 0.98 mg/L and continues to decrease until a minimum concentration of 0.08 mg/L is reached at 40 m. The pH is markedly increased from the September sample day, ranging from 9 at surface waters to 7.9 at 40 m. Sulfide, sulfite and thiosulfate concentrations were only detected within the 40 m sample (Table 2.2).

By the third sample day at the end of January (day 135) the temperatures within the sink had cooled to a minimum of 12.8 °C around 23 m within the sink. The temperature profile shows cooler waters reaching depths of 27 m within the cave along with relatively high dissolved oxygen concentrations (still above 1.0 mg/L) (Figure 2.6). However, the lowest depths within the sink retained some warmth and never fell below the 19.8 °C recorded in the previous sample day. The oxidation-reduction potential increased and remained positive until reaching 39 m within the sink, where negative potentials were recorded. pH ranged from 8.7 to 7.5 showing a slight decrease from the previous sample date, especially at lower depths. Sulfide, sulfite and thiosulfate were all detected but only at the 40 m depth (Table 2.2).

In April (day 219), waters closer to the surface of the sink warmed. A pocket of cooler water still resided around the center of the sink, but bottom waters retained some warmth (Figure 2.6). Dissolved oxygen profiles showed an anoxic zone beginning at 7 m from the surface. Here oxygen concentrations were recorded at 0.54 mg/L and decreased to 0.15 mg/L at 12 - 15 m within the sink. Oxygen levels increased from 20 m to 22 m (0.6 mg/L to 0.9 mg/L) before falling again back below 0.1 mg/L at the bottom depths of the sink. A decrease in salinity was recorded with salinity measurements of 23 ppt found at a depth of 18 m within the sink, at least 4 units lower than salinity readings at that depth on any previous sample day. Sulfide and thiosulfate were only detected at 40 m within the sink (Figure 2.7), while sulfite was detected at low mean concentrations (0.7 mg/L) at 20 m. Sulfite was not detected at 30 m, but was again detected at 40 m (Table 2.2).

By June, water temperature increased in the upper 20 m of the sink (Figure 2.6). A small region of the water column (22 to 28 m) was cooler than the water above and below it. The oxidation-reduction potential was negative throughout the water column and ranged from -350 mV to -650 mV. The region from 22 to 28 m was less negative than the waters directly above or below it. The salinity in the upper portion of the sink increased from the previous sample date (Figure 2.6). Sulfide was detected at 20m and 40 m within the sink while sulfite was detected at 20 m, 30 m and 40 m (Figure 2.7). Thiosulfate was detected only at the 40 m depth at concentrations of 25.8 mg/L (Table 2.2).

On day 401 of the study (October 22, 2010), water temperature had decreased slightly in the upper portion of the sink (Figure 2.6). Dissolved oxygen concentrations

were as high as 2.42 mg/L at 14 m within the sink, but decreased to below 1 mg/L by 19 m within the sink. pH ranged from 8.0 to 7.4 within the sink, reaching a minimum at maximum depth. Only sulfide and sulfite were detected and only at depths of 40 m. The mean sulfide concentration was low (0.02 mg/L) while the mean concentration of sulfite was 4.3 mg/L (Table 2.2).

On February 19, 2010 (day 521) temperatures cooled at all depths within the sink when compared to the previous sample day. Temperatures ranged from 18.9 °C at the surface to 12.2 °C at a depth of 15 m within the sink. Dissolved oxygen concentrations remained above 0.9 mg/L until after 40 m within the sink. This turn over event is noticeable in Figure 2.6. The salinity of the sink ranged from 18 to 31 ppt but above 40 m only reached a salinity maximum of 28 ppt. No sulfide, sulfite or thiosulfate was detected at any depth (Figure 2.7, Table 2.2).

On day 618 (June 18, 2011), the temperature of the upper water increased to 30 °C at 5 m and reached a minimum of 16.5 °C at 23 m within the sink. Bottom water was slightly warmer at 17.5 °C. The salinity increased in the upper portion of the sink from the previous sample day as did the pH (Figure 2.6). Sulfide was not detected at any depth. Sulfite and thiosulfate was detected only at the 40 m depth (Table 2.2).

On the last day of the study, August 2, 2011, the temperature profile remained similar to the previous sample day with a maximum temperature of 30 °C at 4 m and a minimum of 16.6 °C at 29 m within the sink. pH ranged from 7.7 to 7.1. Sulfide, sulfite and thiosulfate were all detected but only at a depth of 40 m (Table 2.2).

Bacterial community structure:

DGGE gels of the 16s rRNA fragments each containing 3 replicates for 4 depths, along with a control and marker for a specific sample date were combined with gels containing fingerprints from other sample dates and normalized (Figure 2.8). MDS ordinations were constructed using the fingerprints and were compared to environmental clustering of the chemical components of the water (Figures 2.9-2.11). Provisional clines were drawn where the Euclidean distance of the abiotic factors between two depths was ≥ 4. A cluster diagram of all 16s rRNA DGGE fingerprints from the study was created (Figure 2.12). BIO-ENV was used to determine abiotic factors that most likely contribute to the biological MDS ordination observed at each date (Table 2.3). Fingerprints of the 16s rRNA DGGE at 40 m depths were clustered separately (Figure 2.13) and are highlighted to show groupings prior to and after the event in February where oxygen concentrations were recorded ≥ 0.9 mg/L down to a depth of 39 m within the sink.

PCR results of the *dsr* gene were overlaid on the DO profile for the length of the study (Figure 2.14). In areas where DO was low, the gene was amplified and the *dsr* fragment was observed. Where DO was above 3 mg/L, amplification of the *dsr* gene was not possible and no bands representing the *dsr* fragment were observed. Of the dates and depths where *dsr* was successfully amplified, DGGE fingerprints were created (Figure 2.15). The resulting fingerprints were clustered into provisional groupings (Figure 2.16). The node shaded in blue contains all sample dates prior to the column turnover event in February, 2011. While the *dsr* gene was not detected within

the sink during February, 2011, PCR detected the presence of *dsr* after the event. Those samples are designated red (Figure 2.16).

Discussion:

Water column chemistry and physical factors:

Previously, four provisional zones were established representative of the geochemical gradients present within Jewfish Sink: a shallow oxic zone closest to surface water, a transition zone with relatively low oxygen, an upper anoxic zone which is influenced by the occasional oxygenated water that descends during the winter, and a stable anoxic zone in the deepest portions of the sink (Garman et al., 2011). These zones, described primarily by oxyclines, may represent an oversimplified model of the true cline stratification present within the sink. In this study, additional geochemical variables were recorded. These were compared at the 4 depths relative to this study and several strong chemical gradients were noted on different sample days (Figures 2.9-2.11) and did not appear to correspond solely to an oxycline. BIO-ENV correlations (data not shown) provided high correlation values (≈ 1) for many of the abiotic factors measured, with sulfur metabolites suggested as a major component on most days causing the dendogram topography observed in the abiotic cluster diagrams (Figures 2.9-2.11). This suggests some level of interdependency between the physical and chemical parameters measured.

Temperature, salinity, pH and dissolved oxygen profiles from the 2011 publication spanned from summer 2001 until summer 2004 (Garman et al., 2011). During that time, an event around days 500 - 600 (January 4, 2003 - April 14, 2003) of the study recorded temperatures below 16 °C reaching depths of over 40 m. This event

was the only time within the 3 year study where minimum water temperatures reached that depth within the sink. This event was accompanied by a universal decrease in the pH of the sink during those same days and represented an incursion of more dense water from the surface down into the sink, perhaps analogous to the seasonal turnover of water within inland lakes. In the current study, a similar phenomenon is noted around days 470 - 570 (December 31, 2010 - April 10, 2011). Both temperature and pH decrease within the sink. This suggests a turnover event with a possible link to the presence or absence of particular microbial metabolic processes that affect the pH of the sink. As the cooler winter waters descended into the sink, dissolved oxygen was carried with it likely impacting the microbial species relying on anaerobic processes. Density calculations based on salinity and temperature did not show the incursion, however, which suggests that it most likely occurred between sample dates, prior to the February 2011 collection. Other than the 2 turnover events that spanned both studies, the relative stability of the bottom water (≥ 45 m) with respect to temperature was observed throughout the seasons from 2001 to 2004. In this (2009 – 2011) study, from September 2009 until October of 2010 there was also no change in temperature in the lower depths (≥ 40 m) of the sink (Figure 2.6). Studies of the black and blue holes in the Bahamas have established that a microbial contribution of heat to water columns is linked to prokaryotic sulfur metabolism and could possibly explain the warmer bottom waters of Jewfish sink. While most likely not the same chemical mechanism as the well-studied species of the black hole in South Andros, a similar pathway may contribute to the warmer bottom waters of Jewfish sink as cooler or warmer surface waters had little effect on the lowest portion of the water column. During certain days, like day 78, the

water column appeared to have temperature profiles that fluctuated along the vertical axis of the sink such that pockets of cold or warm water were found potentially corroborating this theory. These thermoclines are seen in the black holes of the Bahamas and have been found to be a direct result of low electron transport efficiency of certain species of phototrophic purple sulfur bacteria (Herbert et al., 2008).

Prior to the turnover event, sulfur metabolite concentrations were robust throughout the sink and always present in the lowest depth of the sink. In February of 2011, when cool oxygenated water reached deep within the sink, the sulfur metabolites measured were undetectable (Figure 2.7, Table 2.2). It was not until the following sample days when they were observed again at a depth of 40 m.

Biocomplexity of the sink:

With one exception, all replicates during the course of this study showed consistent similarity in the fingerprint patterns created during the DGGE process (Figures 2.9-2.11). On the first sample day in September of 2009, the 10 m and 0 m clustered by themselves with less than 20% similarity between any other sample depth. The 20 m, 30 m, and 40 m sites clustered loosely at 20% similarity (Figure 2.9). The provisional cline on that sample date between 20 m and 30 m did not directly correspond to the biological clustering of the 20 m, 30m and 40 m samples. Biologically, the communities appeared most distant between 10 m and 20-40 m. Superimposing the abiotic clustering analysis onto the biological MDS ordination, the cline can be seen dividing the community into upper and lower layers within the sink. Here, Euclidean distance of 3 is sufficient to distinguish the upper and lower microbial communities. The

abiotic factors best explaining the MDS ordination of bacterial communities were pH, salinity and dissolved oxygen (Table 2.3).

In December of 2009, the microbial communities of the control site, 10 m, 20 m and 30 m clustered together with 20% similarity (Fig 9). The 10, 20 and 30 m sites shared 40% similarity. Only the 40 m site clustered alone sharing less than 20% similarity with any other site. The cline at this date was observed between 30 and 40 m. This recapitulates the biological clustering of the bacterial communities and can be seen when abiotic clustering is overlayed on the biological MDS (Figure 2.9 bottom panel). The abiotic factors best explaining the MDS ordination of the bacterial communities at this date were depth, sulfide, sulfite, thiosulfate and oxidation-reduction potential (Table 2.3).

In January of 2010, the microbial community at 20 m clustered by itself and shared less than 20% similarity with other sites (Figure 2.9). 40 m and 30 m samples clustered with 40% similarity while the control site was most similar to the 10 m sample. The cline remained between 30 and 40 m but did not appear to correlate to the biological clustering. It is important to note that provisional clines were determined based on Euclidean distances greater than 4. In this instance, the Euclidean distance between the 30 m site and the 10 – 20 m cluster is approaching 4. This suggests the possibility of two clines present at this particular day but still does not correlate to the tight clustering of 30 and 40 m bacterial communities. The abiotic factors owing to the biological MDS ordination are temperature, pH and dissolved oxygen (Table 2.3).

In April of 2010, the 40 m fingerprints clustered with the 30 m samples sharing 20% similarity (Figure 2.10). The 10 and 20m samples shared 40% similarity with the

exception of one replicate which only shared 20% similarity. The cline still appeared between 30 and 40 m but did not correspond to the bacterial community clustering. The abiotic factors contributing to the biological MDS ordination were sulfide, sulfite, thiosulfate and pH.

In June of 2010, the 40 m fingerprints were all variable (Figure 2.10). It is possible that the Van Dorn bottle trapped some debris from the debris mound at the base of the sink when collecting a few of the replicates, potentially bringing microbes from decaying organic matter that are not normally found in the water column. The 30 and 40 m samples cluster with 40% similarity while the 10 m sample clustered alone. The warm summer waters established another provisional cline in the upper portion of the sink which corresponds to the bacterial community MDS where the 10 m sample clusters alone. Ignoring the variability of the 40 m fingerprints, the 3 zones created by the chemical and physical parameters correspond to the biological clustering of the bacterial communities. The abiotic factors that best explain the biological MDS are sulfide, thiosulfate, dissolved oxygen and pH (Table 2.3).

In October of 2010, 20 and 30 m bacterial communities cluster together with 40% similarity while 40 m samples cluster alone (Figure 2.10). The 10 m replicates are variable, but mostly cluster independent of the other samples. With two provisional clines established, the biological data correlates to the 3 zones created by the physical and chemical parameters. The abiotic factors best explaining the ordination pattern of the bacterial communities are sulfide, sulfite and salinity.

In February of 2011, the chemical profiles show a turnover event. 20 and 30 m bacterial communities cluster together with 60% similarity, while 10 m clusters

independently (Figure 2.11). The 40 m replicates cluster loosely (20% similarity) with the control site. The clines within the sink are not observed as all of the abiotic factors are more similar, with Euclidean distances between them < 3. The bacterial community clustering does not appear to correlate in any way to the clustering of depths based on abiotic factors. BIOENV analysis suggests depth, salinity and temperature are the factors most likely responsible for the MDS ordination pattern of the bacterial communities.

In June of 2011, the bacterial community cluster pattern is less clear (Figure 2.11). Fingerprints within each depth had some variability that resembled patterns of samples at neighboring depths. This suggests clines or bioclines that are not completely horizontal and the clines observed the previous years had not yet been completely reestablished since the turnover event observed in February 2011. Since replicates require dropping the Van Dorn water sampler down to the same depth 5 times, it is possible that some horizontal variance occurs during this process. If a biocline or cline establishes itself at different depths along the horizontal width of the sink, this may explain the variance observed on this day. It also is the first sample day after the turnover of the sink occurred, so many factors could contribute to this type of scenario as the sink returns to a more stable state. A provisional cline was established based on the chemical and physical properties of the water column between 30 and 40 m within the sink. This cline is likely reestablishing itself after the flushing event. The abiotic factors that most likely contribute to the ordination pattern of bacterial communities observed were temperature, depth and dissolved oxygen (Table 2.3).

On the last sample day in August in 2011, the 10 m communities share less than 20% similarity to other depths corresponding to the cline between 10 m and 20 m (Figure 2.11). Similarly, the 40 m community fingerprints cluster independently while the 20 and 30 m samples cluster together at 40% similarity. These groupings correlate to the 3 provisional zones established by the clines. The abiotic factors largely contributing to the ordination pattern of the bacterial communities are sulfide, dissolved oxygen, temperature and oxidation-reduction potential (Table 2.3). These observations suggest that the clines that were disrupted by the turnover event in February 2011, and not quite reestablished in June 2011, were clearly reestablished by August 2011.

Clustering all of the community fingerprints together over the entire length of the study including all depths highlighted the fact that immediately after the turnover event of February 2011, communities at all depths were more similar to each other than to those of other dates and depths (Figure 2.12). The relative homogeneity of the microbial communities observed in the February 2011 samples was accompanied by relatively homogenous physical and chemical parameters between the depths not seen on other collection dates of this study. It appears that the turnover event brought colder and subsequently denser surface water into the sinkhole causing an increase in similarity of the bacterial communities which corresponded to the increase in similarity of the physical and chemical properties of the water column at the different depths.

Since it was observed that the 40 m depth geochemistry was relatively stable in the present study and that of Garman et al. (2011), 40 m community fingerprints the present study were clustered to see if seasonal changes could be observed (Figure 2.13). It was found that the similarity of the 40 m communities prior to the date of the turnover event

was greater than that of the 40 m communities after the turnover event and that the topography of the dendogram illustrations the turnover event.

Analysis of the *dsr* gene responsible for dissimilatory sulfite reduction within the sink provides insight to the sulfur reducing prokaryotes that inhabit the different depths of the sink. Results indicate that the reductive *dsr* gene is only found in regions of low dissolved oxygen, indicating that bacteria containing the reductive dsr gene are not found in more highly oxygenated water. The presence of the *dsr* gene only at areas of low dissolved oxygen concentration highlight the dynamic seasonal nature of the sulfur reducing prokaryotes utilizing the dissimilatory sulfate reduction pathway (Figure 2.14). During days when oxygen penetrated into the sink, the *dsr* gene was undetectable by PCR. This absence may be the result of oxygen toxicity of dissimilatory sulfite reducing prokaryotes, out competition of dissimilatory sulfite reducing prokaryotes or simply physical displacement of them. The absence of the *dsr* gene was usually accompanied by a lag phase which even in anoxic conditions time needed to pass before the *dsr* communities reestablished themselves (Figure 2.14). Sulfur metabolite concentrations generally coincided with the presence or absence of the *dsr* gene. While the DGGE fingerprints were not as robust as the 16s rRNA fingerprints, cluster analysis of all dates and depths showed some seasonal similarity (Figure 2.16). *dsr*-containing communities from 2009 clustered together into a single node, while *dsr*-containing communities from dates after the turnover event clustered together into a single node with the exception of one replicate. This suggests that the prokaryotic community using the dissimilatory sulfite reducing pathway after the turnover event was not the same community that was found before the event.

Other marine pits and basins share some similarities with Jewfish sink with respect to water chemistry and microbiology. Many of these features exhibit water stratified with oxygen and sulfur gradients. The Santa Barbara Basin, although not a karst feature, has a pit-like bathymetry that differentiates the biogeochemistry within the basin from the surrounding marine waters. The deepest part of the basin shares an anoxic and sulfide profile similar to Jewfish sink. Dissolved oxygen decreases with depth, more so than surrounding marine waters, and is accompanied by an increase in sulfide concentration (Kuwabara, Van Geen, McCorkle, & Bernhard, 1999). Another marine pit, the Cariaco Trench, contains anoxic bottom waters that are stagnant like Jewfish sink. These waters have been shown to support microbial growth largely due to the rapid rate of sulfate reduction near oxic-anoxic transition zones (Fry, 1991 #1887). Neither of these systems have been recorded as having a turnover event and appear to have a stable microbial consortia with respect to Jewfish sink.

Jewfish sink can be characterized by having stable bottom waters that support a microbial community that remains relatively similar throughout the seasons. The upper portions of the sink (depths ≤ 30 m) vary and fluctuate as a result of the seasonal hydrology of the system. Clines establish themselves within the sink and establish zones that are populated by distinct bacterial communities. Occasional turnover events disrupt the stable bottom waters and here are shown to affect the microbial communities. Two studies that spanned a total of 6 years only recorded 2 turnover events. The events do not appear to be seasonal or predictable occurrences and are most likely due to multiple factors or insufficient sampling frequency. The disrupted microbial communities take time to reestablish themselves after a turnover event and

were not observed to attain the same community composition prior to the event. The clines did reestablish themselves seasonally and after a turnover event the cline between 30 and 40 m established itself approximately 4 months later. Prokaryotes having the dissimilatory sulfite reductase gene *dsr* are present in the sink when oxygen concentrations are low and are absent or undetectable in the water column when oxygen concentrations are high (≥1 mg/L). DGGE profiles for the *dsr* communities are not as robust as for the 16s rRNA communities, but do allow for similarity between communities to be observed. The turnover event at Jewfish sink established two distinct dissimilatory sulfite reducing communities at depth representing species dwelling within the sink before the event and species dwelling in the sink after the event. A proposed model for the seasonal biogeocomplexity found at Jewfish sink can be found in Figure 2.17. Unlike blue or black holes, no distinct microbial layer was observed and Datasonde recordings did not indicate a distinct thermocline representative of the phototrophic sulfur metabolism responsible for the thermoclines in blue and black holes although some temperature anomalies in Jewfish sink were noted. This is likely due to the small (D = 6m) entrance to Jewfish sink and the limited light that penetrates the sink. Particulate matter was not observed using the Van Dorn bottle sampling method utilized here, but likely was present in the sink during the time frame of this study as described in Garman et al. (2011).

References:

Clarke, K.R., & Gorley, R.N. (2006). PRIMER v6: User Manual/Tutorial. *PRIMER-E*.

DeLong, E. F., 1992. Archaea in coastal marine environments. Proceedings of the National Academy of Sciences of the United States of America 89(12):5685-9.

El-Dessouky, H. T. & H. M. Ettouney, 2002. Appendix A - Thermodynamic Properties. In El-Dessouky, H. T. & H. M. Ettouney (eds) Fundamentals of Salt Water Desalination. Elsevier Science B.V., Amsterdam, 525-563.

Ferris, M. J., G. Muyzer & D. M. Ward, 1996. Denaturing gradient gel electrophoresis profiles of 16S rRNA-defined populations inhabiting a hot spring microbial mat community. Applied and environmental microbiology 62(2):340-6.

Ford, D. & P. W. Williams, 2007. Karst Hydrogeology and Geomorphology. John Wiley & Sons, Chichester, England.

Garman, K. M. & J. R. Garey, 2005. The transition of a freshwater karst aquifer to an anoxic marine system. Estuaries 28(5):686-693.

Garman, K. M., H. Rubelmann, D. J. Karlen, T. H. Wu & J. R. Garey, 2011. Comparison of an inactive submarine spring with an active nearshore anchialine spring in Florida. Hydrobiologia 677(1):65-87 doi:10.1007/s10750-011-0740-2.

Geets, J., B. Borremans, L. Diels, D. Springael, J. Vangronsveld, D. van der Lelie & K. Vanbroekhoven, 2006. DsrB gene-based DGGE for community and diversity surveys of sulfate-reducing bacteria. Journal of microbiological methods 66(2):194-205 doi:10.1016/j.mimet.2005.11.002.

Herbert, R. A., A. Gall, T. Maoka, R. J. Cogdell, B. Robert, S. Takaichi & S. Schwabe, 2008. Phototrophic purple sulfur bacteria as heat engines in the South Andros Black Hole. Photosynth Res 95(2-3):261-268 doi:DOI 10.1007/s11120-007-9246-1.

Kuwabara, J. S., A. Van Geen, D. C. McCorkle & J. M. Bernhard, 1999. Dissolved sulfide distributions in the water column and sediment pore waters of the Santa Barbara Basin. Geochim Cosmochim Acta 63(15):2199-2209.

Millero, F. J. & A. Poisson, 1981. International one-atmosphere equation of state of seawater. Deep-Sea Research 28:625-629.

Mylroie, J. E., J. L. Carew & A. I. Moore, 1995. Blue Holes - Definition and Genesis. Carbonate Evaporite 10(2):225-233.

Schwabe, S. & R. A. Herbert, 2004. Black Holes of the Bahamas: what they are and why they are black. Quatern Int 121:3-11 doi:DOI 10.1016/j.quaint.2004.01.019.

Simon, J. & P. M. H. Kroneck, 2013. Microbial Sulfite Respiration. In Poole, R. K. (ed) Advances in Microbial Physiology, Vol 62. Advances in Microbial Physiology, vol 62. Academic Press Ltd-Elsevier Science Ltd, London, 45-117.

Wagner, M., A. J. Roger, J. L. Flax, G. A. Brusseau & D. A. Stahl, 1998. Phylogeny of dissimilatory sulfite reductases supports an early origin of sulfate respiration. Journal of bacteriology 180(11):2975-82.

Table 2.1. Primers used in amplification of the *dsr* gene. An equimolar mixture of 10 forward primers (1 – 10F) and 10 reverse primers (1 – 10R) was used in the polymerase chain reaction of the *dsr* gene from environmental DNA. The primers were designed from an alignment of all *dsr* genes of Bacteria and Archaea retrieved from the Integrated Microbial Genomes database.

Name	Sequence
1F	5' - ACSCACTGGAAGCACG - 3'
2F	5' - ACCCAYTGGAAACAC -3'
3F	5' - GGCCACTGGAARCACG - 3'
4F	5' - ACCCATTGGAAACATG - 3'
5F	5' - ACTCACTGGAARCACG - 3'
6F	5' - GGGCACTGGAAACACG - 3'
7F	5' - GSTYACTGGAAACACG - 3'
8F	5' - ACCAATCGGTAATGGT - 3'
9F	5' - AAGGGGCCDTGGCCVAG - 3'
10F	5' - CVTGGGSBMCHRSHGYH - 3'
1R	5' - GTGTAGCAGTTACCGCA - 3'
2R	5' - GTGTAACAGTTTCCACA - 3'
3R	5' - GTGTAACAGTTACCGCA - 3'
4R	5' - GTGTAGCAGTTGCCGCA - 3'
5R	5' - GTGTAGCAGTTTCCGCA - 3'
6R	5' - GTGTAGCAGTTACCACA - 3'
7R	5' - GTGTAACAGTTACCACA - 3'
8R	5' - GTATAGCARTTGCCGCA - 3'
9R	5' - TCYTTACAMCKRSCRCA - 3'
10R	5' - CTCAGGCATCTACCACA - 3'

Table 2.2. Sulfur metabolite concentrations at all dates and depths within Jewfish Sink. The mean of each concentration is given with standard deviation.

Date	Depth	Sulfide (mg/L)	Sulfite (mg/L)	Thiosulfate (mg/L)
9/17/2009	10 m	0 ± 0	0 ± 0	0 ± 0
	20 m	0.7 ± 0.2	4.5 ± 0.5	5.3 ± 0.3
	30 m	4 ± 0	13.3 ± 1.2	11 ± 0
	40 m	4 ± 0	15.7 ± 0.6	15.2 ± 0.8
12/13/2009	10 m	0 ± 0	0 ± 0	0 ± 0
	20 m	0 ± 0	0 ± 0	0 ± 0
	30 m	0 ± 0	0 ± 0	0 ± 0
	40 m	1.5 ± 2.1	12 ± 8.5	6.3 ± 6.5
1/29/2010	10 m	0 ± 0	0 ± 0	0 ± 0
	20 m	0 ± 0	0 ± 0	0 ± 0
	30 m	0 ± 0	0 ± 0	0 ± 0
	40 m	4 ± 0	12.7 ± 2.3	15.2 ± 8.8
4/23/2010	10 m	0 ± 0	0 ± 0	0 ± 0
	20 m	0 ± 0	0.7 ± 1.2	0 ± 0
	30 m	0 ± 0	0 ± 0	0 ± 0
	40 m	7 ± 0	20 ± 0	8.25 ± 1.3
6/9/2010	10 m	0 ± 0	0 ± 0	0 ± 0
	20 m	0.03 ± 0.06	0.8 ± 1.3	0 ± 0
	30 m	0 ± 0	0.8 ± 1.3	0 ± 0
	40 m	3.3 ± 0.6	15.3 ± 2.3	25.8 ± 20.9
10/22/2010	10 m	0 ± 0	0 ± 0	0 ± 0
	20 m	0 ± 0	0 ± 0	0 ± 0
	30 m	0 ± 0	0 ± 0	0 ± 0
	40 m	0.02 ± 0.006	4.3 ± 0.3	0 ± 0
2/19/2011	10 m	0 ± 0	0 ± 0	0 ± 0
	20 m	0 ± 0	0 ± 0	0 ± 0
	30 m	0 ± 0	0 ± 0	0 ± 0
	40 m	0 ± 0	0 ± 0	0 ± 0
6/18/2011	10 m	0 ± 0	0 ± 0	0 ± 0
	20 m	0 ± 0	0 ± 0	0 ± 0
	30 m	0 ± 0	0 ± 0	0 ± 0
	40 m	0 ± 0	2.7 ± 2.5	2 ± 3.5
8/2/2011	10 m	0 ± 0	0 ± 0	0 ± 0
	20 m	0 ± 0	0 ± 0	0 ± 0
	30 m	0 ± 0	0 ± 0	0 ± 0
	40 m	7.7 ± 4.0	20 ± 0	32.5 ± 18.9

Table 2.3. 16s rRNA DGGE best subset of environmental variables analysis (BIOENV) for each sample date. Correlation values and the abiotic variables that best explain the ordination pattern found within the 16s DGGE fingerprints at any given date.

	Correlation	Variables
9/17/2009	0.840	salinity
	0.840	pH, salinity
	0.827	dissolved oxygen, salinity
12/13/2009	0.891	depth, sulfide, oxidation-reduction potential
	0.891	depth, sulfite, oxidation-reduction potential
	0.891	depth, thiosulfate, oxidation-reduction potential
1/29/2010	0.863	temperature
	0.851	pH, temperature
	0.819	dissolved oxygen, temperature
4/23/2010	0.586	sulfite, pH
	0.583	sulfide, thiosulfate, pH
	0.579	sulfide, pH
6/9/2010	0.613	sulfide, dissolved oxygen, pH
	0.613	sulfite, dissolved oxygen, pH
	0.613	thiosulfate, dissolved oxygen, pH
10/22/2010	0.869	sulfide, salinity
	0.869	sulfite, salinity
	0.858	sulfide, sulfite, salinity
2/19/2011	0.781	depth, salinity
	0.763	salinity
	0.734	temperature, salinity
6/18/2011	0.402	temperature
	0.377	depth, temperature
	0.323	dissolved oxygen, temperature
8/2/2011	0.626	sulfide, dissolved oxygen, temperature
	0.619	sulfide, dissolved oxygen
	0.619	sulfide, dissolved oxygen, oxidation-reduction potential

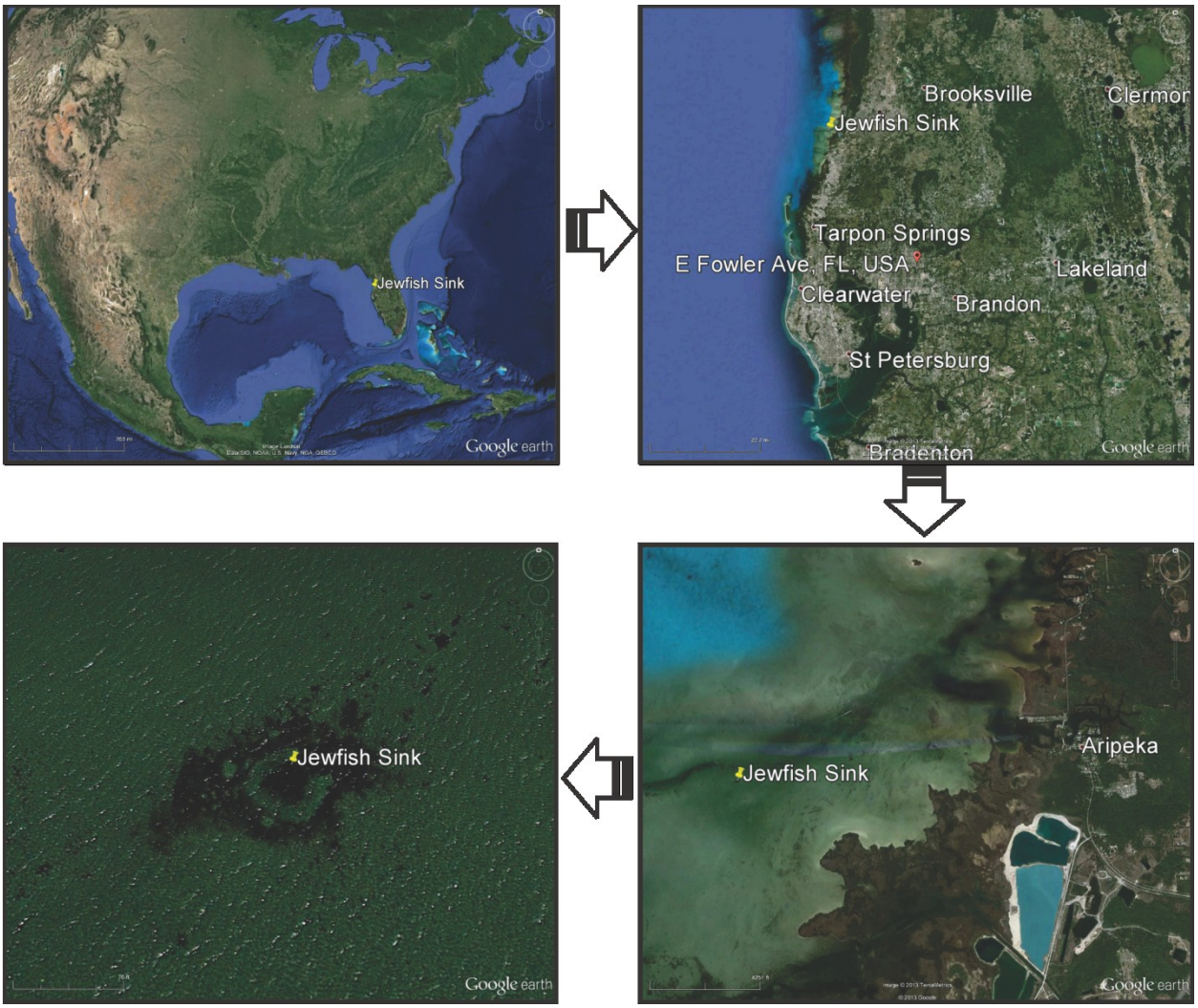

Figure 2.1. Relative location of Jewfish Sink to the coastline of Florida. Jewfish Sink is located about 39 miles northwest of the University of South Florida, roughly 1 km offshore from the town of Aripeka. The entrance to the sink, 6 m in diameter, is visible through satellite imagery.

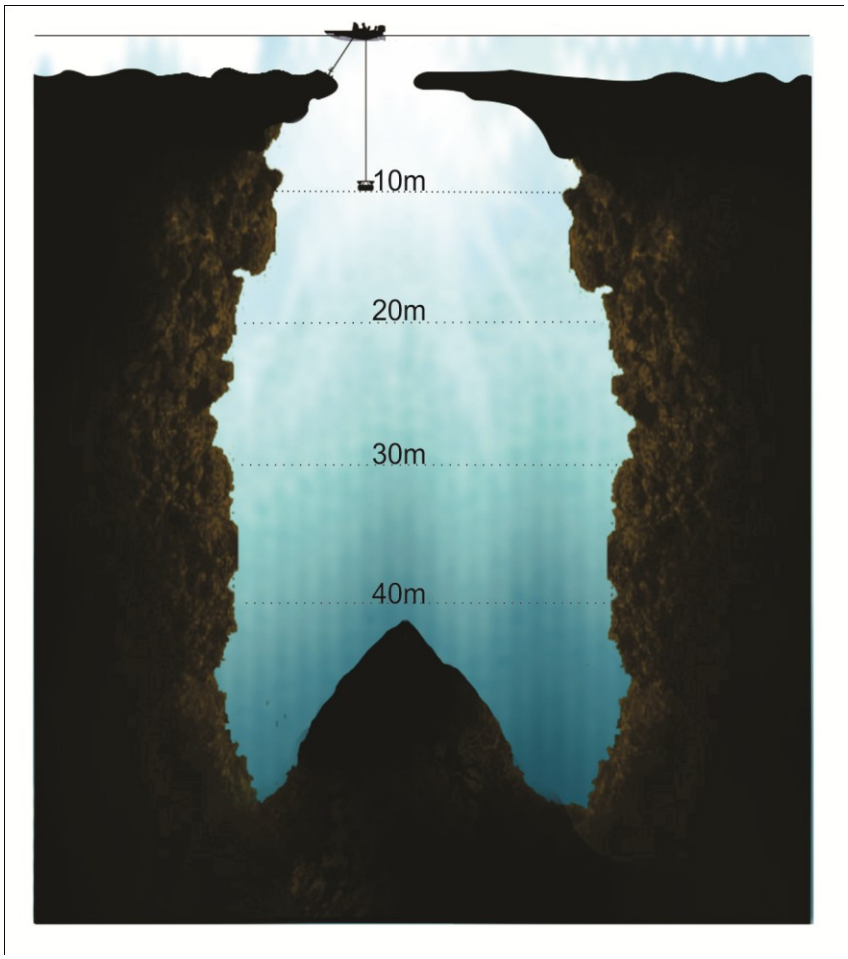

Figure 2.2. Bathymetry of Jewfish Sink with diagram of sampling strategy. A van dorn bottle was lowered to the depths of 10 m, 20 m, 30 m and 40 m 5 times each in order to retrieve 1 L of water from the water column within the sink.

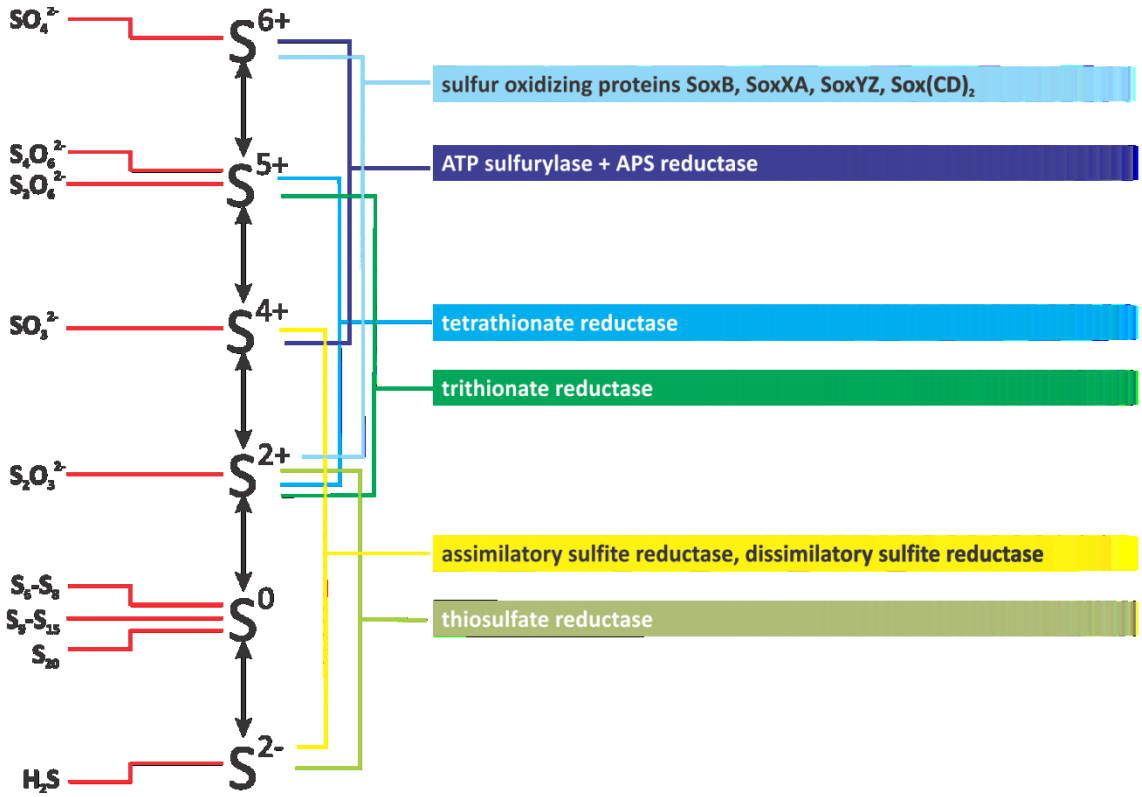

Figure 2.3. Different oxidation states of sulfur with examples of polyatomic molecules associated with each state. Select enzymes associated with conversion of sulfur between states are highlighted.

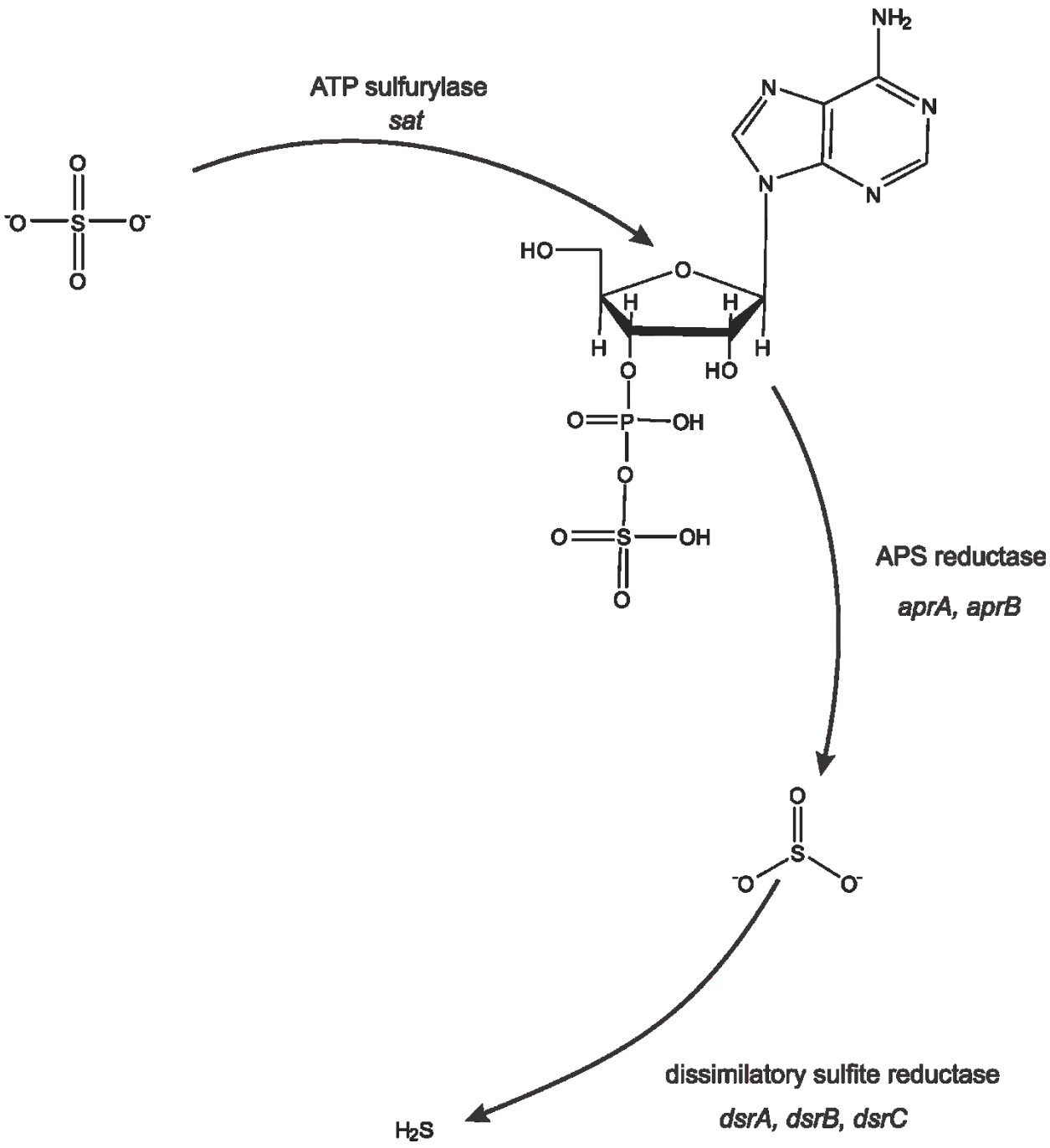

Figure 2.4. Prokaryotic dissimilatory sulfate reduction. Enzyme names are accompanied by the genes that are associated with them.

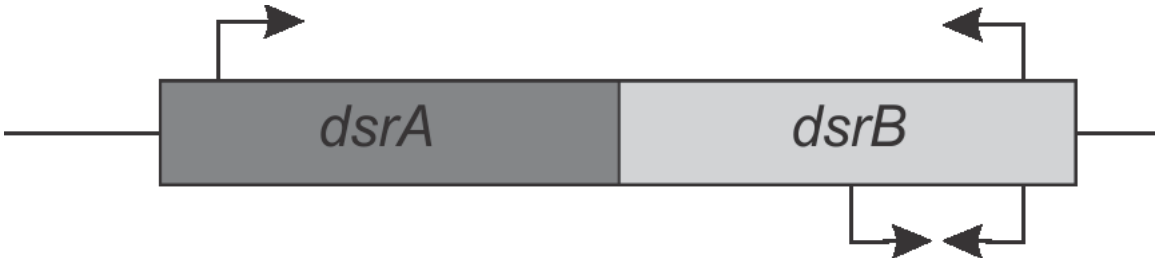

Figure 2.5. *dsr* PCR and DGGE strategy. The genes encoding the A and B subunits of the dissimilatory sulfite reductase are located adjacent to each other on a single operon. The preliminary PCR reaction utilized primers that amplified a ≈ 1900 bp section of the *dsrA* and *dsrB* genes. From the purified ≈ 1900 bp PCR product, a ≈ 300 bp product of *dsrB* was targeted for DGGE using primers DSRp2060F and DSR4R DGGE.

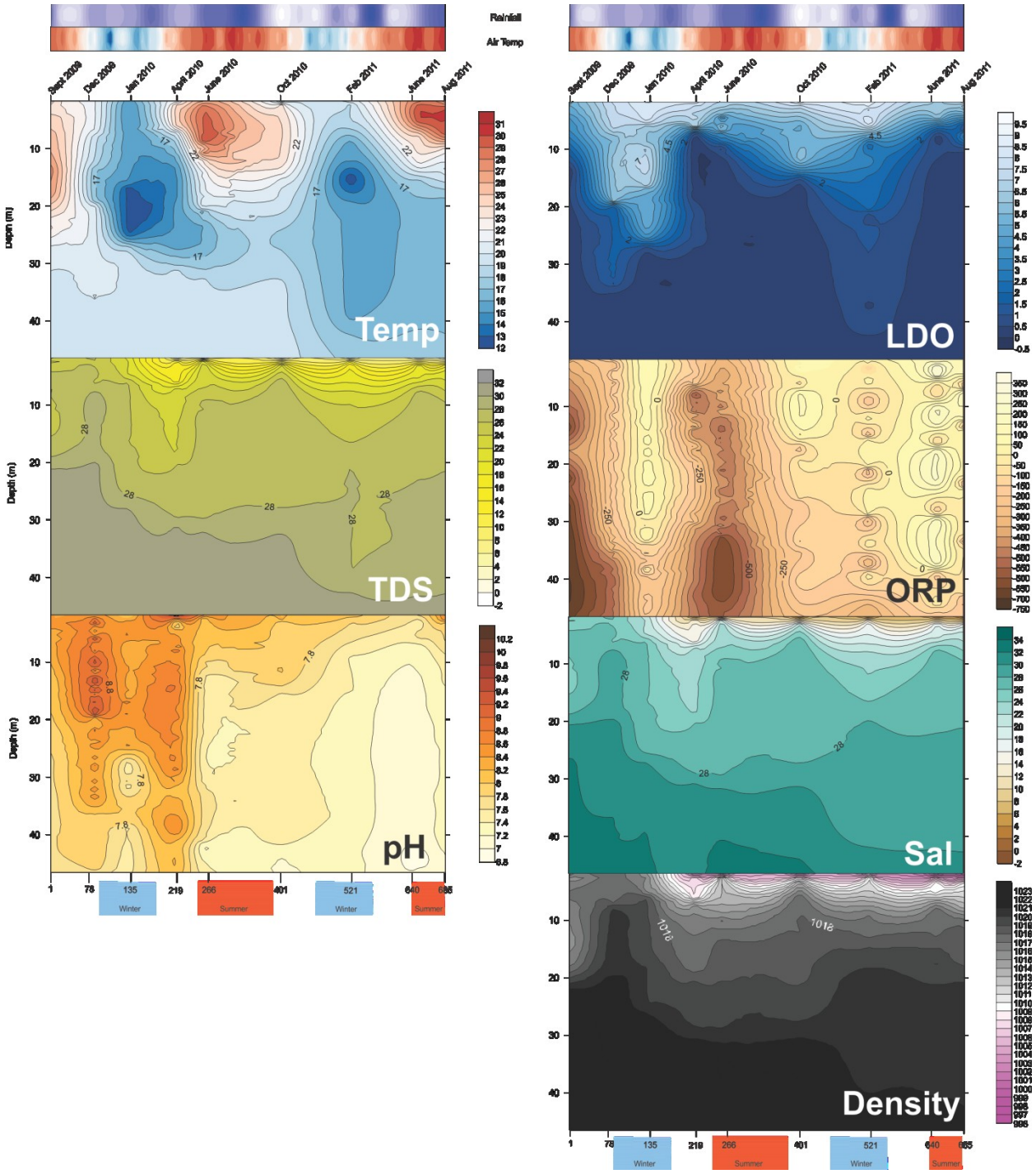

Figure 2.6. Geochemical profile obtained from the Datasonde of Jewfish Sink over 685 days. Temperature (Temp), Total Dissolved Solids (TDS), pH, Liquid Dissolved Oxygen (LDO), Oxidation-Reduction Potential (ORP), Salinity (Sal) and calculated Density are shown in individual panels. Values between sample dates were interpolated using the kriging method. Uninterpolated data can be seen in figures A1-A9 of the appendix. Rainfall measurements and air temperature heatmaps are displayed overhead of the panels. Temperature is measured in degrees Celsius. TDS is measured in grams per liter. LDO is measured in milligrams per liter. ORP is measured in millivolts. Salinity is measured in parts per thousands. Density is displayed in kg/m^3. The depth within the water column of the sink is displayed on the y-axis. The sample day within the timeline of the study is displayed on the base of the figure along the x-axis with corresponding calendar date labeled on the top of the figure. The corresponding winter and summer seasons are highlighted in blue and red respectively.

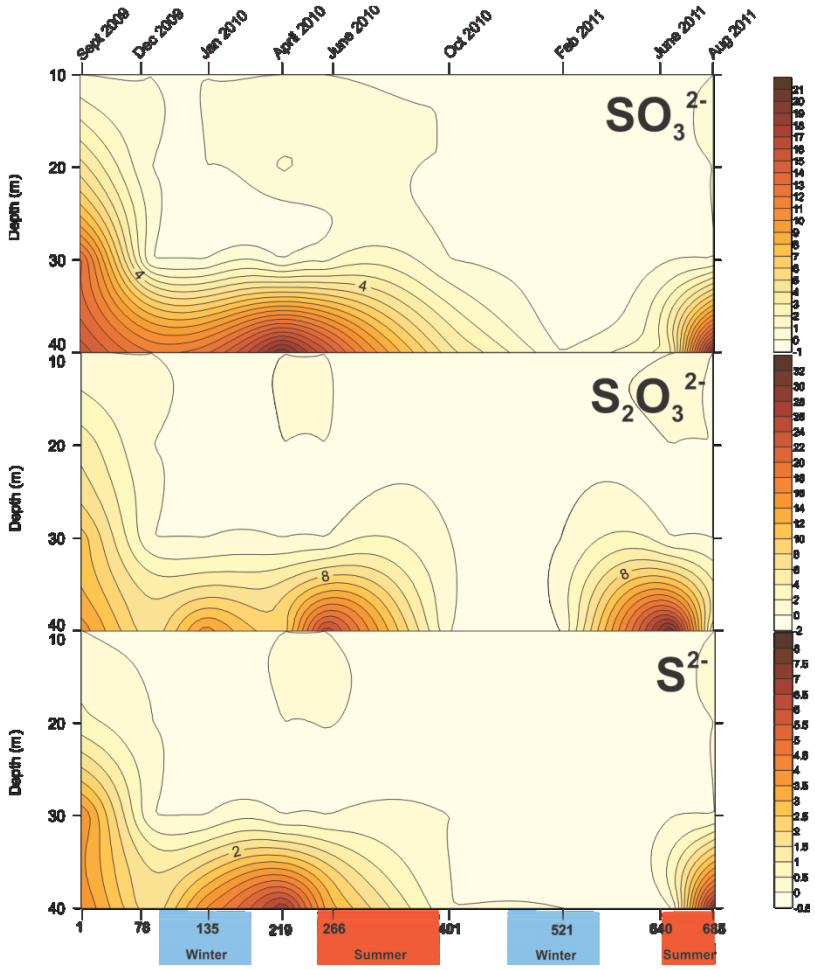

Figure 2.7. Sulfite, thiosulfate and sulfide profiles of Jewfish Sink over 685 days. The depth within the water column of the sink is displayed on the y-axis. The sample day within the timeline of the study is displayed on the base of the figure along the x-axis with corresponding calendar date labeled on the top of the figure. The corresponding winter and summer seasons are highlighted in blue and red respectively. All values shown are in milligrams per liter.

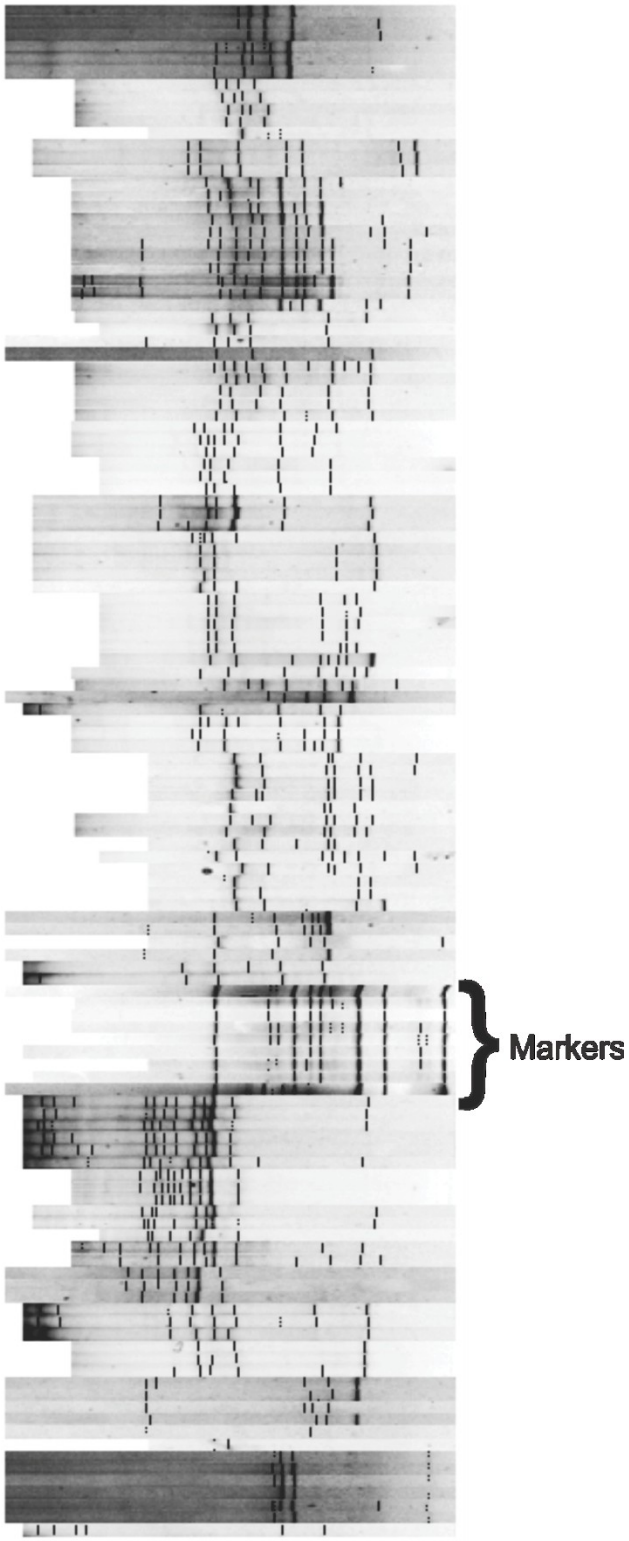

Figure 2.8. Normalized gel photo of 16s DGGE results for each date and depth with markers labeled. 100 categories along the x-axis were established and given ranges (eg: 0-1, 1-2, etc.). Each band marked with a black line was considered present for a given range. Lanes were sorted based on similarity. Each marker lane was from a gel run on a different date containing fingerprints of a specific sample day.

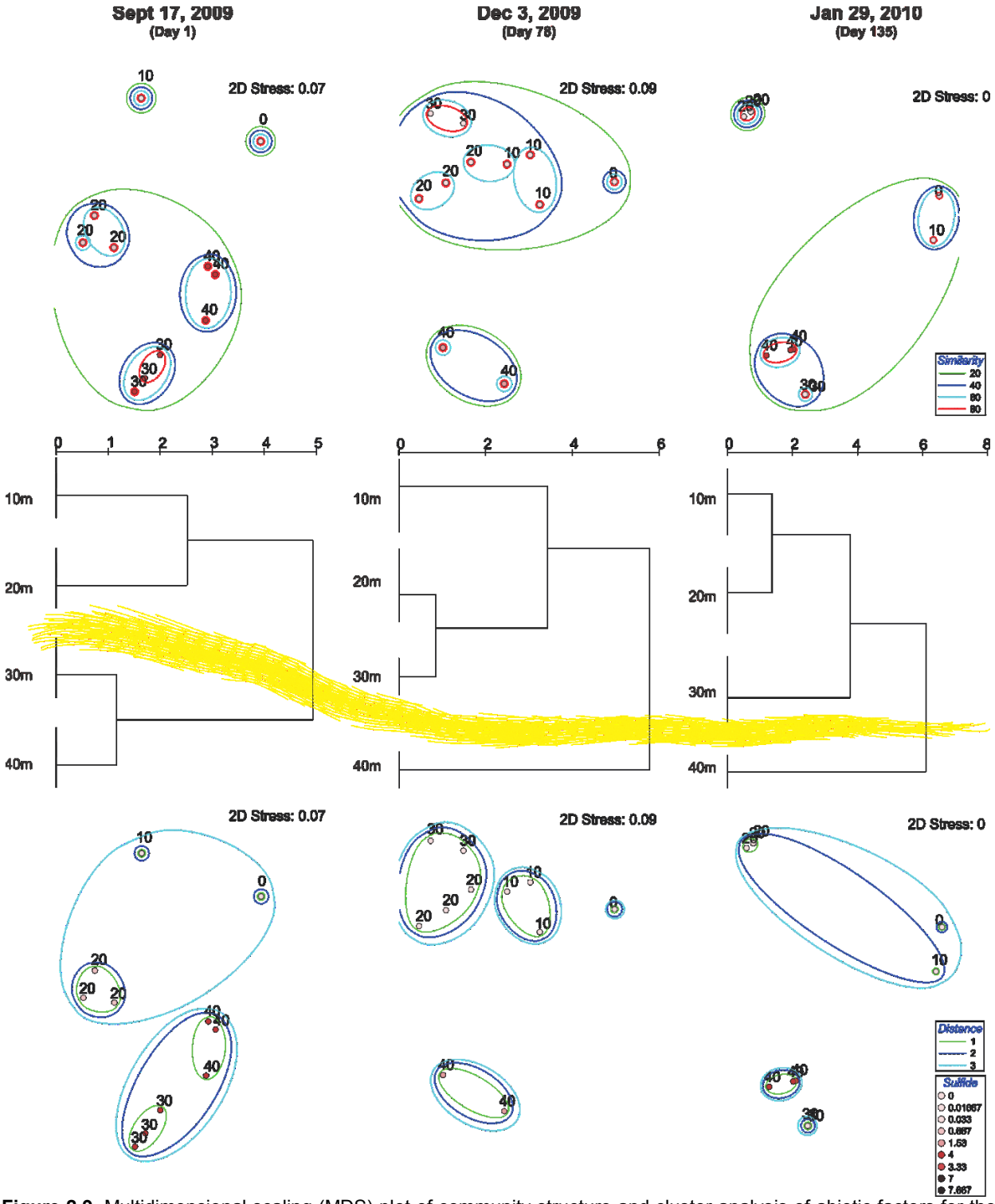

Figure 2.9. Multidimensional scaling (MDS) plot of community structure and cluster analysis of abiotic factors for the first three sample dates. Top panel: sample depths arranged in an MDS ordination according to fingerprint similarity with clusters showing the percent similarity between individual community fingerprints. Middle panel: dendograms of geochemical measurements for each depth shown with the Euclidean distance between samples labeled. Provisional clines are highlighted, where the geochemistry between two depths has a Euclidean distance ≥ 4. Bottom panel: sample depths arranged in an MDS ordination according to fingerprint similarity with clustering overlays shown as Euclidean distance determined by the abiotic factors measured at each site.

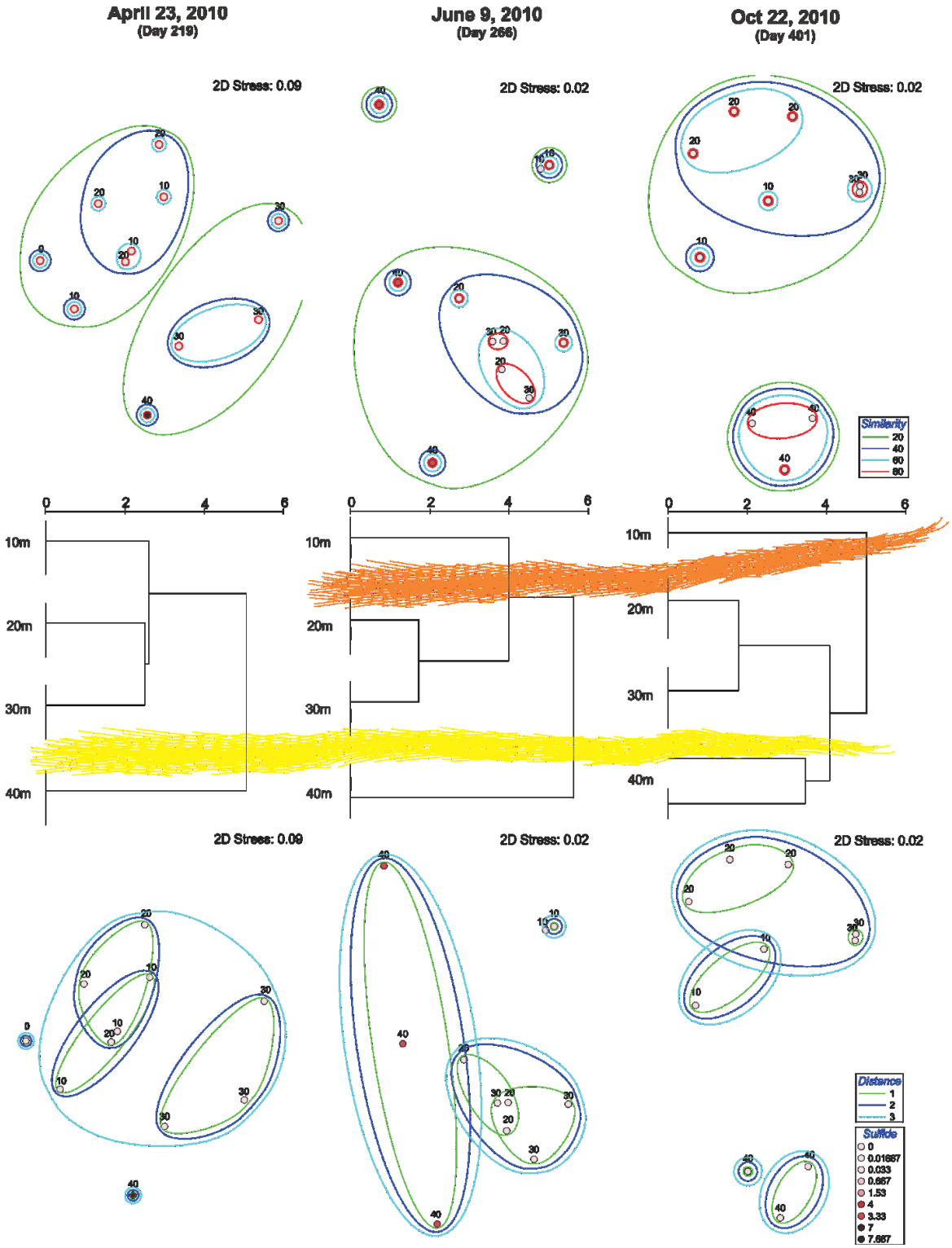

Figure 2.10. Multidimensional scaling (MDS) plot of community structure and cluster analysis of abiotic factors for the second three sample dates. Top panel: sample depths arranged in an MDS ordination according to fingerprint similarity with clusters showing the percent similarity between individual community fingerprints. Middle panel: dendograms of geochemical measurements for each depth shown with the Euclidean distance between samples labeled. Provisional clines are highlighted, where the geochemistry between two depths has a Euclidean distance ≥ 4. Bottom panel: sample depths arranged in an MDS ordination according to fingerprint similarity with clustering overlays shown as Euclidean distance determined by the abiotic factors measured at each site.

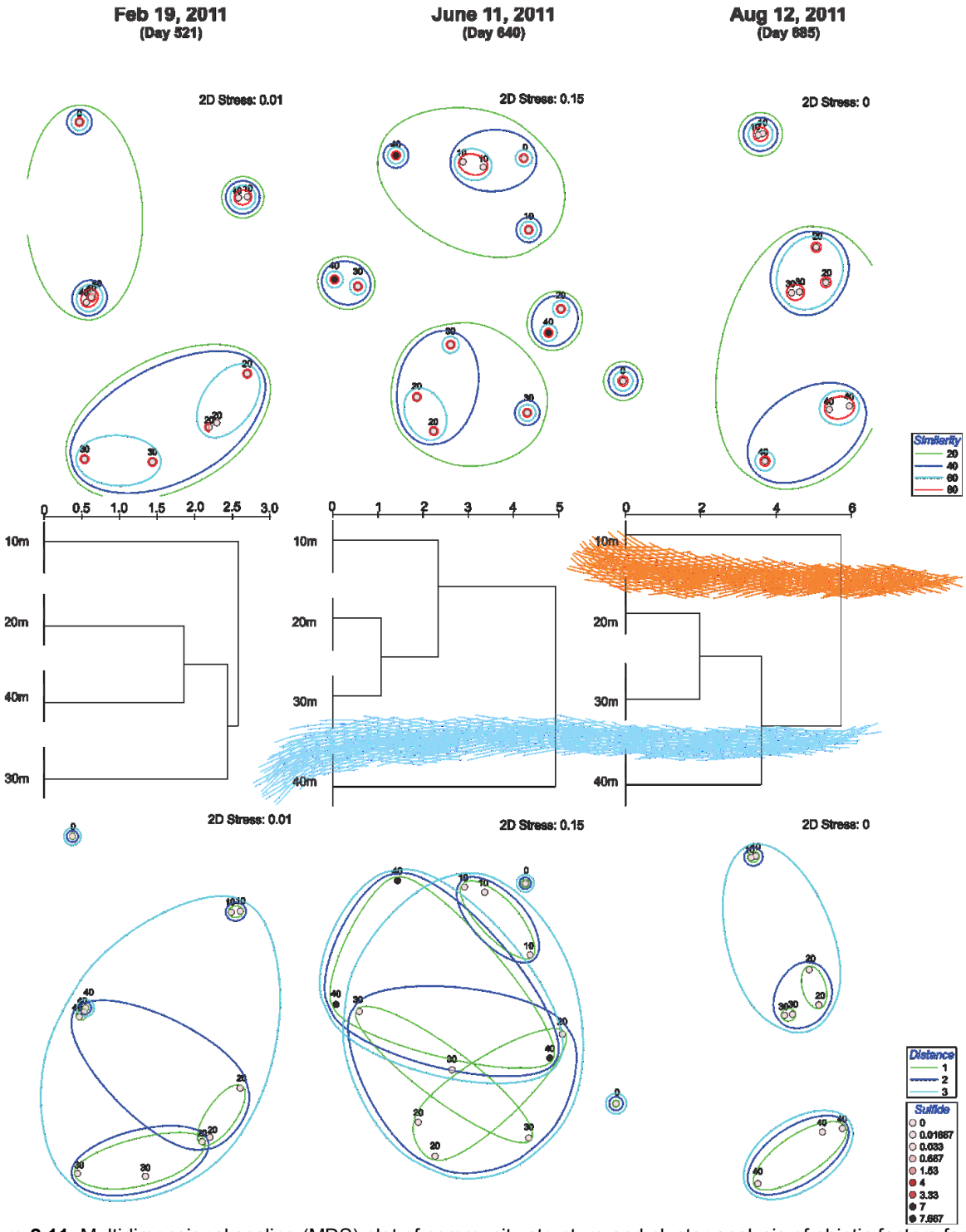

Figure 2.11. Multidimensional scaling (MDS) plot of community structure and cluster analysis of abiotic factors for the last three sample dates. Top panel: sample depths arranged in an MDS ordination according to fingerprint similarity with clusters showing the percent similarity between individual community fingerprints. Middle panel: dendograms of geochemical measurements for each depth shown with the Euclidean distance between samples labeled. Provisional clines are highlighted, where the geochemistry between two depths has a Euclidean distance ≥ 4. Bottom panel: sample depths arranged in an MDS ordination according to fingerprint similarity with clustering overlays shown as Euclidean distance determined by the abiotic factors measured at each site.

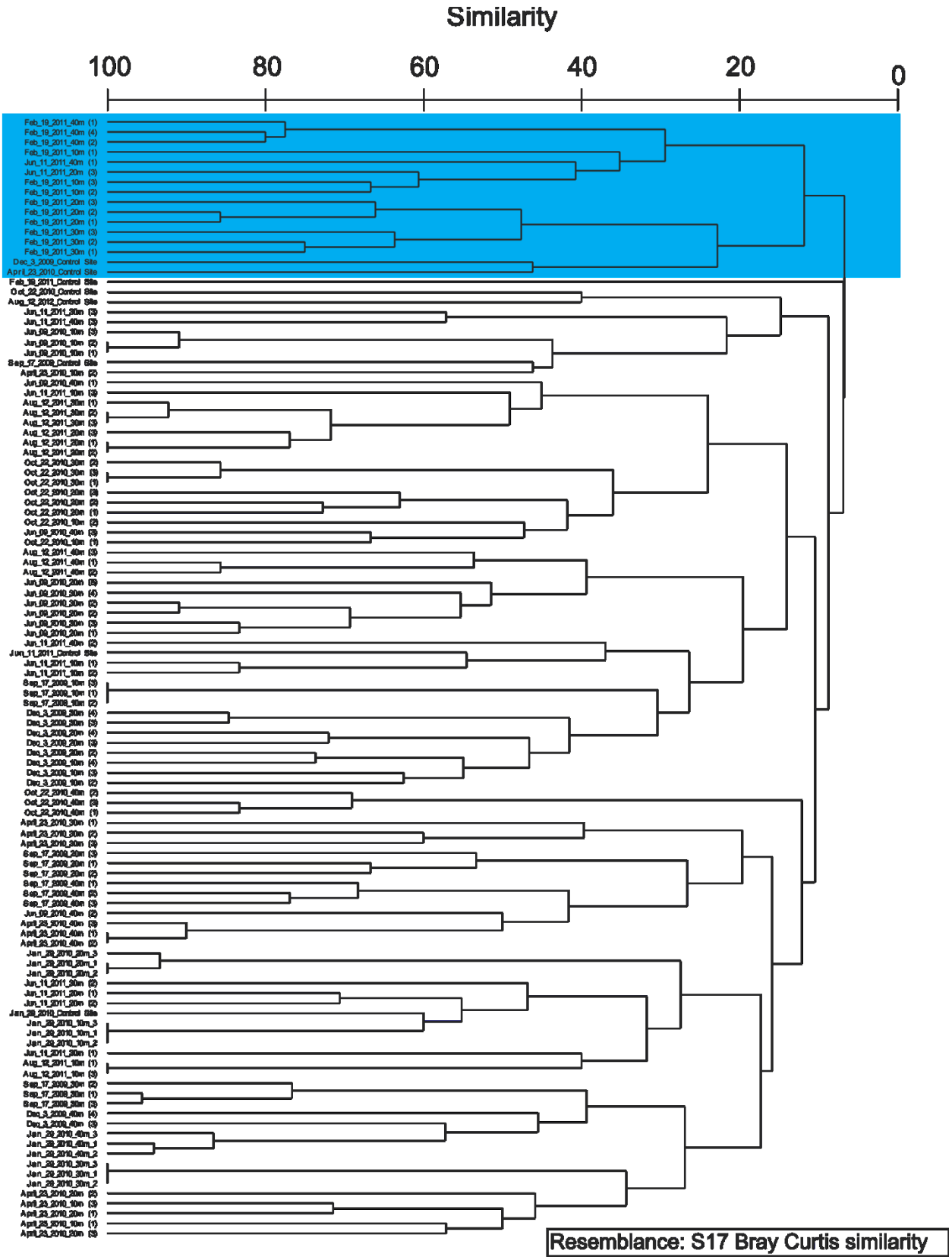

Figure 2.12. Cluster analysis of 16s DGGE fingerprints at all depths and all dates. The node highlighted in blue contains all community fingerprints from February 19, 2011.

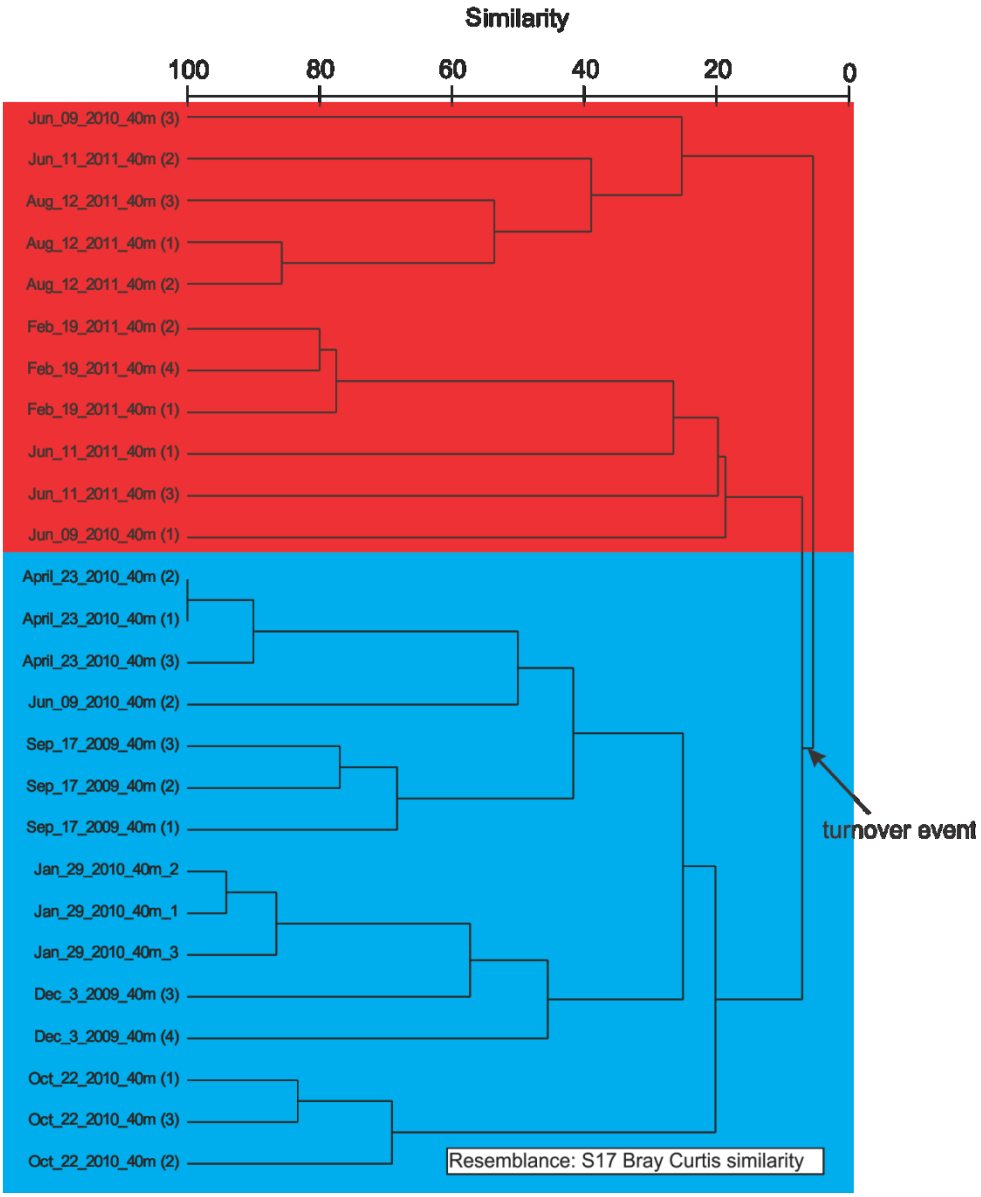

Figure 2.13. Cluster analysis of 16s DGGE fingerprints at 40 meter sites showing major groupings pre- and post turnover. The node designated in blue contains 40 meter fingerprints sharing at least 20% similarity which all fall before the turnover event at February 19, 2011. The red nodes contain dates falling at the turnover event or after, with the exception of the June 9, 2010 date which contained 3 variable fingerprints for the 40 meter replicates.

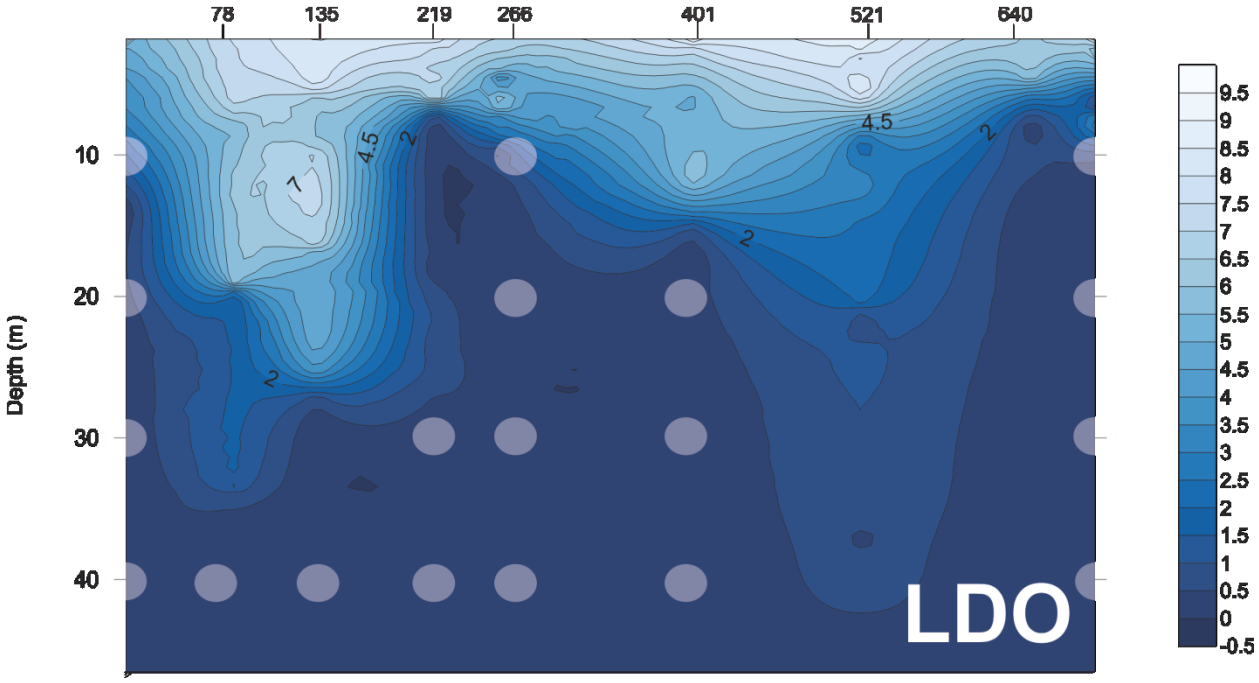

Figure 2.14. *dsr* presence and absence at Jewfish Sink superimposed on LDO concentrations. White circles represent the presence of the *dsr* gene as determined by PCR. Sample dates are designated at the top along the x-axis. Days within the study begin at day 1 and continue through to day 685. Depth is displayed along the y-axis. Liquid dissolved oxygen is displayed as a gradient in mg/L.

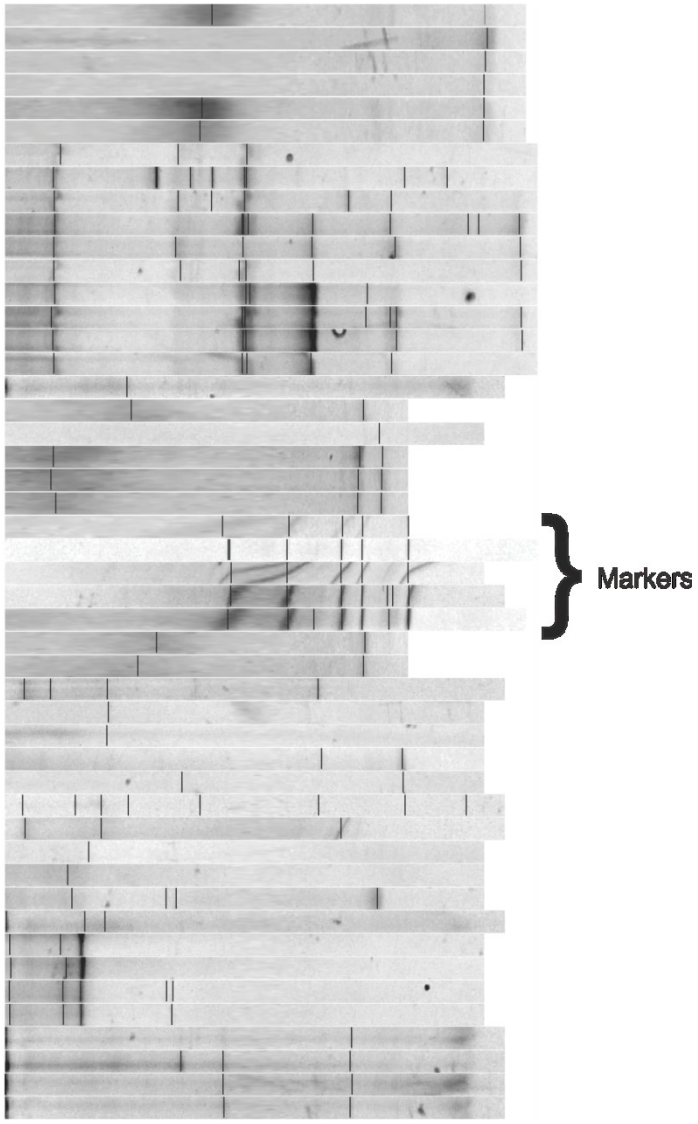

Figure 2.15. Normalized gel photo of *dsr* DGGE results for each date and depth with markers labeled. 100 categories along the x-axis were established and given ranges (eg: 0-1, 1-2, etc.). Each band marked with a black line was considered present for a given range. Lanes were sorted based on similarity. Each marker lane was from a gel run on a different date containing fingerprints of a specific sample day.

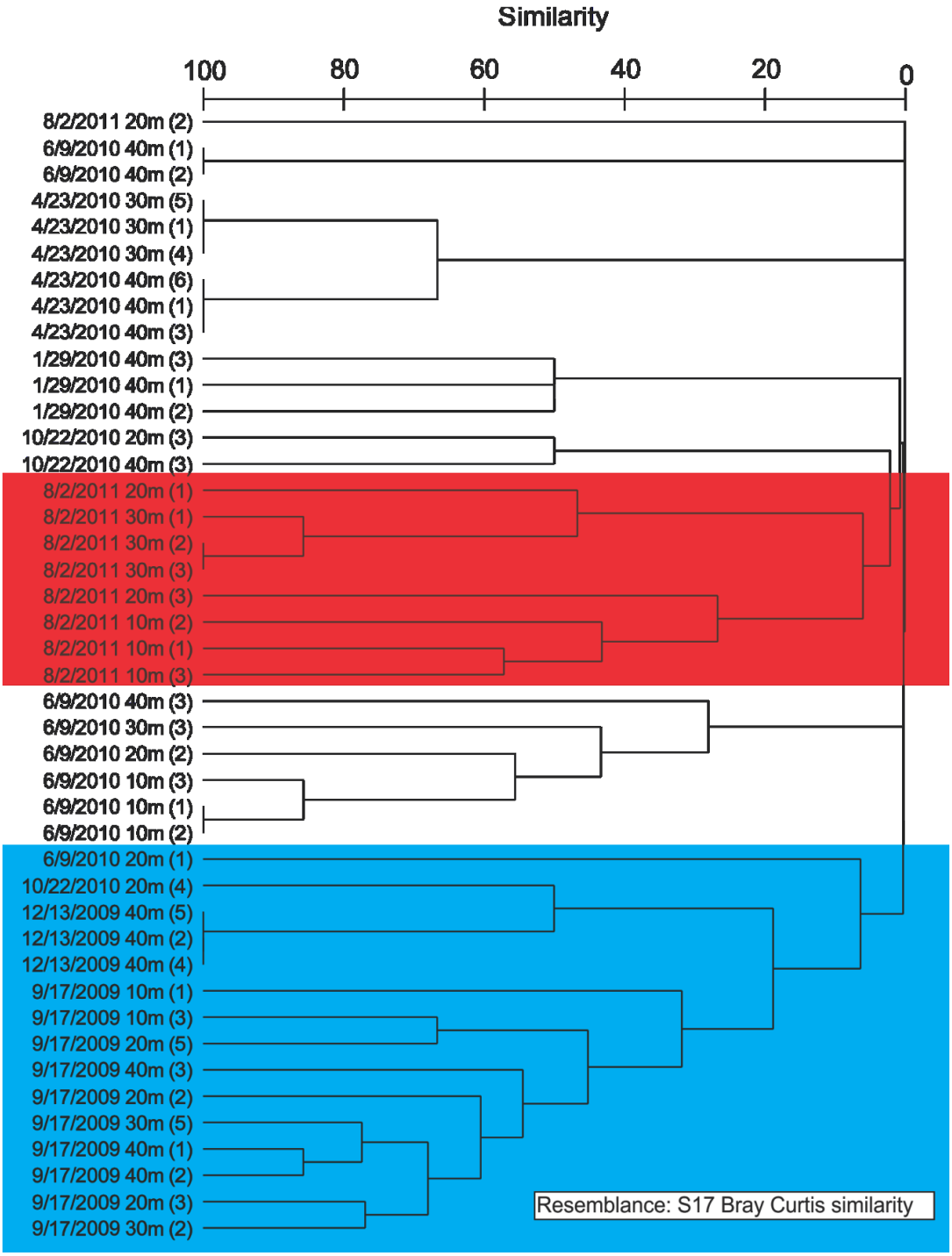

Figure 2.16. Cluster analysis as determined by *dsr* DGGE fingerprint similarity. The node highlighted in blue contains all fingerprints from sample dates during 2009, prior to the turnover event. The *dsr* gene was not detected during February, 2011 at the observed turnover event and therefore produced no fingerprints. However, fingerprints of the *dsr* communities after the event clustered together in the node highlighted in red.

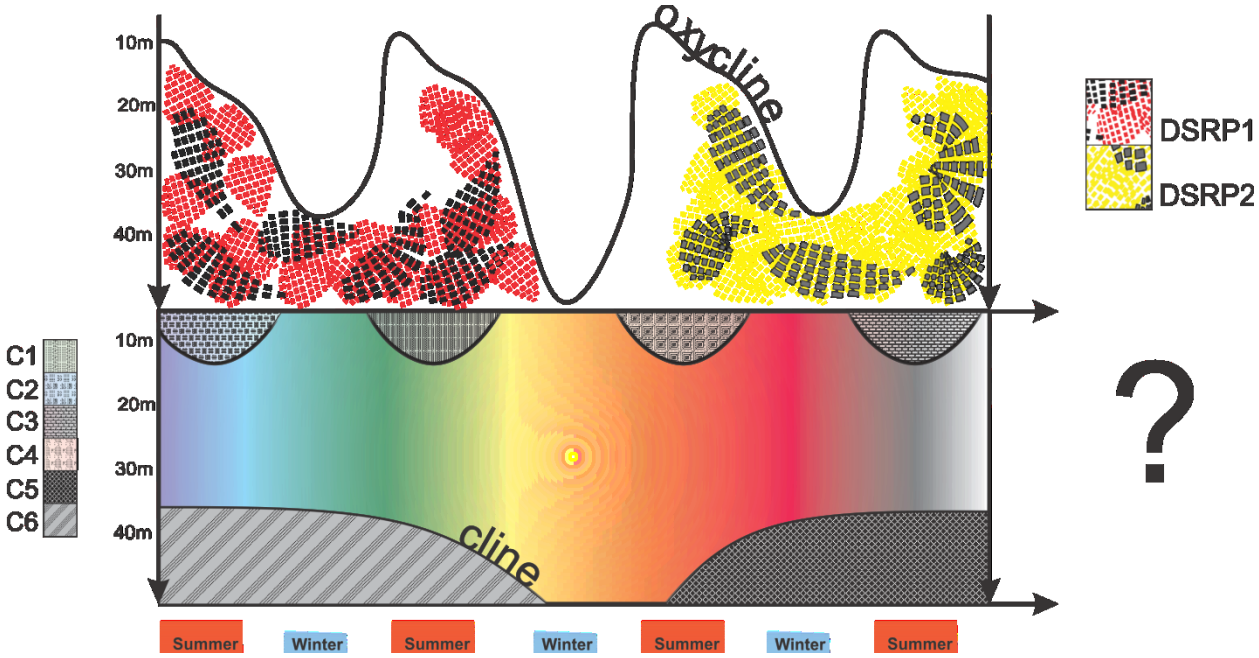

Figure 2.17. Provisional model representing the biogeocomplexity of Jewfish sink over multiple seasons. The top panel highlights the change in the oxycline over the seasons with an occasional turnover event during winter. Two distinct dissimilatory sulfite reducing prokaryote communities (DSRP1 and DSRP2) are seen and are separated by the descent of the oxycline to the lowest depths of the sink. A lag phase can be seen where the communities do not establish themselves immediately after oxygen levels begin to rise. The bottom panel represents the clines observed as a result of the physical and chemical data analyzed. Bacterial communities (C1 – C6) are represented by specific patterns, showing the distinct community composition created by the seasonal clines. Color gradation throughout the sink highlights the observed similarity among communities where clines have created zones within the water column with similar chemical and physical properties.

CHAPTER THREE: THE BIOGEOCOMPLEXITY OF SEDIMENT COMMUNITIES NEAR AN ARSENIC-RICH SHALLOW MARINE HYDROTHERMAL VENT

This chapter is currently in review for publication as: Rubelmann H, Karlen DJ, and Garey JR. (2014). *The biogeocomplexity of sediment communities near an arsenic-rich shallow marine hydrothermal vent*. My part of this project included processing of the sediment samples (extraction, cloning, sequencing) for prokaryotic communities. I also had the lead role in carrying out the analysis, making all of the figures, and writing the manuscript.

Abstract:

The biocomplexity of the sediment communities along a 120 m transect near a shallow marine hydrothermal vent at Tutum Bay, Papua New Guinea was thoroughly examined. A count of macro- and meiofaunal organisms was combined with bacterial and eukaryotic SSU rRNA gene surveys to assess biodiversity. Each site along the transect had distinct microbial communities. Near-vent sites were more similar to each other than sites further from the vent. Some species, such as those belonging to *Ignavibacterium, Caldilinea,* and *Capitella* were only found near-vent. Biodiversity generally increased with distance from the vent. The community composition responded to the presence of hydrothermal fluids with a clear correlation between temperature and thermophilic organisms. Primary production appeared to be a mix of chemo- and phototrophy. Food web and association analyses suggest many potential interactions between organisms occur at certain sites, and that species distributions and interactions occur in the context of complex spatial relationships related to the geochemistry of the hydrothermal vent fluids. While Tutum Bay is heavily influenced by arsenic, no specific

correlation between organisms that metabolize arsenic and the concentration of different oxidation states of arsenic ions was observed, perhaps because very little of the arsenic present was bioavailable. An observed even distribution of arsenic reducers along the transect could be due to background arsenic metabolism. This study represents the first to encompass biocomplexity on such a broad phylogenetic range and across such a wide area at a marine shallow-water hydrothermal vent.

Introduction:

Deep-sea hydrothermal systems are light restricted and rely on chemosynthesis for this energy input, using organic detritus as the carbon source in the synthesis of biomolecules. Oxidation reactions of reduced chemical species (H_2S, H_2, CH_4, etc.) provide electron donors necessary for chemotrophic growth. In seawater, where sulfur species are readily available, the oxidation of reduced sulfur provides energy to synthesize organic carbon, highlighting the importance of the sulfur cycle in sustaining these communities (Jannasch, 1995).

In contrast, shallow-sea hydrothermal systems are not as light limited and are not characterized by an abundance of vent-specific taxa. Here, chemosynthesis runs parallel to photosynthesis as a means of primary production. Many shallow-sea hydrothermal vent systems are characterized by bacterial mats, similar to deep-sea vents, and chemosynthesis occurs near the vent itself and in the superficial layer of water above the vents (Tarasov *et al.*, 2005). Diatoms, cyanobacterial mats, and other algae aid in this primary production.

The shallow-sea hydrothermal system of Tutum Bay, Ambitle Isle, Papua New Guinea serves as a natural laboratory to study the biocomplexity of prokaryotic and

eukaryotic species sustaining a novel ecology. Being arsenic- and iron-rich, the metabolic repertoire and subsequent biodiversity of species found at the site differs from other commonly studied shallow hydrothermal-sea vent systems. As an arsenic rich system, the potentially toxic qualities of arsenic represent a hurdle for sustaining communities at Tutum Bay's hydrothermal systems. Not only is arsenate a structural analogue of phosphate that can inhibit oxidative phosphorylation, but arsenite binds to sulfhydryl groups and vicinal thiols of many proteins, disrupting the function of numerous proteins. Arsenic has 4 oxidation states: As (-III), As (0), As (III) and As (V) – the latter two being most prevalent in nature (Oremland and Stolz, 2003). Arsenate readily adsorbs onto aluminum and iron hydroxides, forming inorganic compounds that reduce their bioavailability. Arsenite does this less readily, leaving it mobile, with more potential for toxicity in hydrological systems. Further complicating arsenic mobility, Fe (III) reducing bacteria are able to reduce ferric oxyhydroxides, and subsequently release arsenate back into the hydrological system (Konhauser, 2007).

Both prokaryotes and eukaryotes have developed methods to deal with the toxic nature of arsenic. The discovery that microorganisms synthesized and excreted trimethylarsine suggested that other methylated forms of arsenic exist. Further studies showed that some animals can convert inorganic forms of arsenic into both methyl arsenic and dimethyl arsenic (Doak and Freedman, 1970) which are excreted in the urine (Thomas *et al*., 2007). In addition to methylation, prokaryotes have evolved enzymes that allow both the oxidation and reduction of arsenic. Dissimilatory arsenate-respiring prokaryotes reduce arsenic (V) to arsenic (III) when other more favorable terminal electron acceptors are not present and couple the reaction to the oxidation of

organic compounds. Heterotrophic arsenite oxidizers convert As (III) found on the cell membrane to less toxic As (V). This process is seen as a defense mechanism against the more toxic arsenite, which easily enters the cell. Lastly, chemoautotrophic arsenite oxidizers reduce oxygen or nitrate during the oxidation of arsenite and use the energy to fix CO_2 (Oremland and Stolz, 2003).

Extensive chemical analysis has been performed along transects at Tutum Bay, specifically at hydrothermal Vent 4 (Akerman *et al.*, 2011; Price and Pichler, 2005). Mechanisms have been proposed for the biogeochemical cycling of arsenic and other inorganic metabolites based on Gibbs free energy calculations at this vent (Akerman *et al.*, 2011), and the distribution and speciation of arsenic has been well characterized with particular attention to the element's bioavailability (Price and Pichler, 2005). Our study focuses on the biocomplexity along a specific transect, V4-B, (Figure 3.1) with attention to the phylogenetic biodiversity and functional repertoire present in pore water samples at particular sites along the transect. Bacterial 16S rRNA genes and eukaryote 18S rRNA gene were sequenced from clone libraries and distributed into functional guilds and trophic groups. These data were combined with morphological data scored from the same sites. These ecological patches were linked to the physical parameters previously described and particular attention was given to the evidence of arsenic and iron metabolizing organisms throughout the transect. This may represent the first study broadly assessing the biocomplexity of bacteria and eukaryotes from both DNA and morphological assessments.

Materials and methods:

Sampling site and collection:

The Tutum Bay site has been described (Akerman *et al.*, 2011; Pichler and Dix, 1996; *Pichler et al.*, 2006; Price and Pichler, 2005). The transect for this study is shown in Figure 3.1. Sediment samples for macrofaunal and meiofaunal analyses were collected in replicates of 5 as described by Karlen *et al.* (2010). Samples were sieved through a 500 µm mesh screen to collect macrofauna and then onto a 50 µm screen to collect meiofauna. Core samples for bacterial DNA were collected at the 10 cm horizon of sediment cores. Five samples for eukaryote DNA analyses were collected at each site along the transect with a 60 ml syringe corer to a depth of 5 cm and the replicates pooled. Sediment was passed through a 4 mm sieve to eliminate large macrofauna. Samples for sequencing eukaryote DNA were collected at sites 0 m, 7.5 m, 12 m, 20 m, 30 m, 60 m, 90 m, 120 m, 180 m, 250 m and 300 m from the vent and frozen until used.

Porewater analysis:

Porewater analysis has been described in detail in Price *et.al.* (2007) and again by Akerman *et. al.* (2011). The geochemical data used in the analyses here is from Table 1 of Akerman *et. al.* (2011). Briefly, porewater was collected at 10cm sediment depth by research divers. Samples were brought on-board a research vessel and immediately measured for sensitive parameters. Arsenic species required preservation described in Price *et.al.* (2007) after which final measurements were taken in a lab.

Macrofaunal and meiofaunal identification:

Macrofaunal samples were rinsed onto a 500 µm mesh sieve and identified to the lowest practical taxonomic level (Karlen *et al.,* 2010). Each specimen was archived and voucher specimens were photographed.

Meiofaunal samples were decanted from sieved sediment onto a 50 µm mesh plankton net placed in a funnel. The remaining sediment was resuspended, and meiofauna again decanted onto the plankton net. This process was repeated 5 times and the meiofaunal specimens sorted to the lowest practical taxonomic level. The specimens were archived and photographed.

Eukaryote and bacterial sequencing and identification:

Sediment DNA was extracted from 0.5 g sediment using a MoBio UltraClean Soil DNA extraction kit (Mo Bio Laboratories, Carlsbad, CA, USA). PCR was performed using ID Labs IDProof™ Polymerase Enzyme (ID Labs, London, ON, Canada) optimized for 50 µL reactions. Primers used for the 18s rRNA gene PCR were 18S4 (5'-CCGGAATTCAAGCTTGCTTGCTTGTCTCAAAGATTAAGCC-3') and 18S5 (5'-CCGGAATTCAAGCTTACCATACTCCCCCCGGAACC-3') (Mackey *et al.*, 1996). Primers used for the 16s rRNA gene PCR were 27F (5' - AGAGTTTGATCCTGGCTCAG - 3') and 1492R (5' - GGTTACCTTCTTACGACTT - 3') (DeLong, 1992). The 18s PCR consisted of an initial 2 min 95 °C denaturation, 45 cycles of 15 sec at 95 °C, 1 min at 50 °C, 1 min at 72 °C, followed by a 72 °C extension for 7 min. The protocol for 16s PCR differed in that 40 cycles with a 45 °C annealing temperature and a 2 min extension step was used.

Cloning was done with a PCR4-TOPO-TA Cloning Kit (Invitrogen, Carlsbad, CA, USA). Clones were isolated into 96-well culture plates, cultured and DNA extracted using the Eppendorf Perfectprep Plasmid 96 Vac miniprep kit (Eppendorf, Hamburg, Germany). The resulting plasmid DNAs were sequenced by Polymorphic DNA Technologies, Inc. (Alameda, CA, USA). Sequences were filtered for quality (Wu *et al*., 2009) and submitted to Genbank (accession numbers JN837712.1 - JN839729, JQ241793 – JQ244768).

Sequences were clustered into Operational Taxonomic Units (OTUs) using SEQUENCHER (Gene Codes, Ann Arbor, MI, USA). Eukaryote OTUs were established according to a 99% identity (Wu *et al*., 2009). Prokaryotic OTUs were established using 97% identity. OTUs and singletons were identified to the nearest identifiable match using NCBI's database and BLAST algorithm (uncultured organism matches were not considered). This identification was used to provisionally identify the genus of each OTU in further analyses (Wu *et al.*, 2011).

Classification of functional guilds and trophic groups:

Potential metabolic capabilities of each provisional bacterial genus were assessed from the literature. In some cases, a genus would fall into more than one functional guild (e.g.: sulfur reducing, iron reducing and arsenic oxidizing), and scored more than once. Facultative aerobes or anaerobes were similarly considered in both categories. Eukaryotic organisms were classified into trophic groups based on feeding habits or metabolic capabilities. If organisms fell into more than one group, they were also considered in both categories.

Biodiversity calculations, association analyses and networks:

Primer-E (Clarke and Gorley, 2006) was used to calculate Shannon diversity at each site. Cluster analysis was also performed in Primer-E for abiotic factors, macro- and meiofauna, and at the phylum level, genus level and sequence level for bacteria and eukaryotes across all sites. The abundance data were square root transformed and clustered by Bray-Curtis similarity. Abiotic data were normalized and clustered according to Euclidean distance. Association analyses were performed on species found at more than one site together and dendograms were made using the Primer-E software.

Phylogenetic networks were created using the clustered OTUs and singletons for both prokaryotes and eukaryotes with the Cytoscape software package (Shannon *et al.*, 2003). A functional guild network of prokaryotes and a trophic food web were also created using the Cytoscape software.

The Surfer software package (Golden Software Inc., Golden, CO, USA) was used to interpolate a gradient of abiotic factors using an x,y coordinate system corresponding to the transect V4-B according to chemical analyses done at each site.

Results:

Abiotic factors:

Abiotic factors across the transect (Figure 3.2) show a distribution characteristic of the hydrothermal venting found at the site. Sites from 0 – 12 m are heavily influenced by hydrothermal fluids, while sites further out are more closely related to that of normal sea water. Although diffuse venting is present and may be seen in the pH and oxidation-reduction potential differences found from site to site and a small temperature rise at 60

m, the abiotic factors generally formed a gradient along the transect towards that of normal seawater away from the vent. Arsenic concentrations remained higher than normal seawater at all sites.

The temperature ranged from 99 °C at the vent to 29 °C 300 m from the vent. Arsenic (V) and Iron (II) (Figure 3.2, B and H) show an inverse correlation at near-vent sites, with Arsenic (V) concentrations peaking at 7.5 m and Iron (II) concentrations below detection levels. Arsenic (III) has the highest concentration at the vent (944 μg L^{-1}) which gradually diminishes away from the vent. Lastly, the concentration of sulfate increases with increased distance from the vent.

Biotic and abiotic interactions:

Similarity clustering of biotic and abiotic factors in Primer-E (Figure 3.3) shows a general trend visualized in Figures 3.2, 3.4 and 3.7. Near-vent sites cluster together more closely than sites distant from the vent. While not all data was available for each factor at every site, 90m and 120m exclusively cluster together, showing the same dendogram topology for all biotic data. With the exception of eukaryotic sequence data, contiguous sites appear more similar in biota than noncontiguous sites. The abiotic data shows the incongruity of the 7.5m site with the rest of the near-vent sites, which can also be seen in Figure 3.2 primarily due to Arsenic (V) and Iron (II) concentrations.

Bacterial diversity:

Bacterial species found along the transect are represented in Figure 3.4. The patch assemblages found at 7.5 m and 12 m are easily distinguishable from the sites found further away from the vent. The phylum *Chlorobi* is found only at the two near-vent sites and *Proteobacteria* diversity is greatly reduced compared to the 20 meter to

120 meter sites. *Actinobacteria* was the most abundant phylum found at 7.5 m from the vent (68 individuals representing 37 species) with *Proteobacteria* following with 64 individuals representing 49 species. At 12 m from the vent, *Chlorobi*, predominantly found as the genus *Ignavibacterium*, and *Chloroflexi* are more abundant than anywhere else along the transect. The diversity and relative abundance of *Proteobacteria* dominates the 20 meter to 120 meter sites, with *Gammaproteobacteria* having the highest abundance (348 individuals) followed by *Deltaproteobacteria* (287 individuals). Distribution lines show species similarity between sites, showing the greatest sharing of species at sites away from the vent (20m – 120m). Only one OTU was found at all sites (black distribution line) and matched most closely to *Acidomicrobium ferrooxidans* (87% similarity). Figure 3.5 shows the distribution of the most common genera along the transect. *Ingavibacterium* and *Caldilinea* are exclusively found at the near-vent sites, while *Steroidobacter*, *Thiohalomonas*, *Pelagibius*, and *Thiohalospira* are exclusive to the 20 m to 120 m sites. Many genera are represented throughout the whole transect but tend to be in low abundance at the 12 m site.

Eukaryotic diversity:

Eukaryotic organisms, both sequenced from environmental DNA and scored by morphological identification, show an abundance of nematodes and arthropods throughout the transect (Figure 3.7). The vent site has the highest abundance of annelids, primarily due to the abundance of one species of *Capitella*. *Playthelminthes*, fungi, and heterokonts are found throughout, with fungi and heterokonts showing extreme heterogeneity from site to site.

The dominant eukaryotic genera from sequence data shows many vent specific (0 m) species: *Capitella*, *Linuche*, *Schlerochilius*, *Cladophora*, *Neochromadora*, *Oblongichytrium*, and *Thoracostomopsidae* (Figure 3.8). Other genera such as *Pauliella*, *Penicillium* and *Stauroneis* are found at all sites among the transect.

Functional analyses:

The functions of bacteria along the transect show several trends (Figure 3.6). Thermophilic bacteria are found at near-vent sites in high abundance and decrease at 20 m and outward. The abundance and diversity of mesophiles peaks at 20 and 30 m and generally are higher away from the vent. Nitrogen, sulfur, and arsenic metabolizers are abundant at near-vent sites, although not as diverse as at sites 20 m outwards. Iron metabolizers, while present throughout the transect, show the lowest abundance and diversity at the 12 meter site.

Association analysis:

An association analysis between the bacterial sequences, eukaryotic sequences and the morphologically scored organisms found along the transect can be seen in Figure 3.9. There were a total of 130 OTUs that were found at more than one site together. These OTUs can be seen clustered into a similarity dendogram next to a heat map representing their relative distribution along the transect. Six clades formed with correlation values > 0.5.

Discussion:

The geochemistry of the shallow hydrothermal system at Vent 4-B in Tutum Bay appears to strongly influence the biodiversity found throughout the transect. Animal and microbial communities appear to be influenced by abiotic factors as seen in a distinct

near-vent community consisting of sites less than 20 m from the vent (Figure 3.3, 3.4, 3.7). Other communities as far as 300 m from the vent (Figure 3.2) still show hydrothermal influences. While these communities are unique at every site, some similarity is evident. Network distribution lines linking species found at more than one site show clear similarity between sites further from the vent (≥20m) while species found both near-vent and further from vent are limited in number. The bacterial communities near the vent (7.5m and 12m) reveal increased heterogeneity compared to sites further from the vent. This is also indicated by abiotic factors suggesting that there are more microhabitats near Vent 4-B than revealed within this study.

Bacterial diversity:

The bacterial community (Shannon's diversity index = 4.76) at 7.5 m is dominated by thermophilic *Actinobacteria* and *Proteobacteria* (Figure 3.4). Members of *Acidimicrobiacea* (including the genus *Aciditerrimonas*) within *Actinobacteria* have the highest relative abundance within the community at 7.5 m. These bacteria are commonly found in areas of extreme acidity and high sulfur concentration. They are either mesophilic or moderately thermophilic and capable of iron oxidation (Itoh *et al.*, 2011). The 7.5 m site is slightly acidic (Figure 3.2) with sulfide concentrations roughly 3 ppm (Figure 3.10).The 12 meter site has the lowest bacterial diversity of all sites (Shannon's diversity index = 4.07), where members of *Actinobacteria* decrease significantly. *Chlorobi* and *Chloroflexi,* particularly the genus *Ignavibacterium,* become dominant. Members of *Ignavibacterium*, while belonging to the genus *Chlorobi*, are obligate chemoheterotrophs, grow anaerobically, and are moderate thermophiles (Iino *et al.*, 2010). At both near-vent sites, members of the genus *Caldilinea* are relatively

abundant, similar to sediments of the nearby transect 4-A (Meyer-Dombard *et al.*, 2012). Type species for *Caldilinea* were isolated from a deep-hot aquifer in France and from a hot-spring in Japan. While *Caldilinea* belongs to *Chloroflexi* (green non-sulfur bacteria), neither type species can grow under phototrophic conditions (Gregoire *et al*., 2011; Sekiguchi *et al*., 2003). The biodiversity of bacteria 20-120 m from the vent is greater than near-vent (Shannon's diversity index = 4.78 – 5.23). *Proteobacteria* dominate while members of *Chlorobi* are absent. The *Actinobacteria* family *Acidimicrobiacea,* and *Proteobacteria* genera *Desulfacinum* and *Thioalkalivibrio* are found in greatest relative abundance. A type species of the genus *Desulfacinum* was isolated from a shallow-water hydrothermal vent in Greece (Sievert and Kuever, 2000). It is thermophilic, anaerobic, mixotrophic and can reduce sulfate (Rees *et al*., 1995). *Thioalkalivibrio* species are tolerant to hypersaline and alkaline environments. Their metabolic capabilities include sulfur oxidation and reduction, denitrification, and thiocyanate metabolism (Muyzer *et al*., 2011). They tend to be mesophilic, explaining why they are found in greatest relative abundance away from the vent.

Functional guilds:

Classifying bacterial genera into functional guilds reveals trends linking abiotic factors to biodiversity (Figure 3.10). The temperature of the pore water remains high until after 12 m where it sharply decreases. A small rise in temperature around 60 m can be attributed to observed diffuse venting. The relative abundance of thermophiles also follows this trend with a minor peak at 60 m that matches a local rise in temperature. The relative abundance of mesophiles follows an inverse trend, increasing as the temperature decreases. Oxidation-reduction potential increases with distance

from the vent and corresponds to an increase in relative abundance of aerobically-respiring organisms. An exception at 7.5 m was observed, where the relative abundance of aerobic organisms was higher than at 12 m, perhaps because facultative organisms were scored into both guilds. A low relative abundance of nitrogen oxidizers was found, while nitrogen reducers increased with distance from the vent (Figure 3.10). Nitrite concentrations were low (< 1 ppm) at all sites and nitrate concentrations generally increased with distance from the vent following a trend similar to nitrogen-reducing bacteria. The relative abundance of sulfur-reducing bacteria varied greatly while sulfur-oxidizing bacteria increased further from the vent (Figure 3.10). While sulfur-reducing bacteria did not correspond to concentrations of either sulfide or sulfate, sulfur-oxidizers appeared to increase as the concentration of sulfate increased at least for the first 60 m of the transect. Arsenic (III) and arsenic (V) species, primarily found as arsenite and arsenate, respectively, did not follow a clear trend along the transect. Arsenic (V) was found at higher concentration than arsenic (III) at the 7.5 meter site while arsenic (III) was highest at the 12 meter site (Figure 3.10). Arsenic-reducing bacteria were more abundant than arsenic-oxidizing bacteria, which were nearly absent along the transect. There did not appear to be a relationship with arsenic (III) or arsenic (V) to arsenic-oxidizing or arsenic-reducing bacteria. Previous studies have measured the amount of bioavailable arsenic along the 4B transect (Price and Pichler, 2005). The amount of bioavailable arsenic represented only a small amount of the total arsenic present in the samples from the previous study, suggesting limited availability of arsenic to local biota. Iron reduction, which introduces arsenate back into the system through the reduction of iron (III) oxyhydroxides, was similarly examined. The relative

abundance of iron reducers and oxidizers increases and decreases together along the transect, generally corresponding to the amount of Iron (II) in the system (Fig 10). No data was available for Iron (III).

Arsenic cycling at Tutum Bay:

A schematic of arsenic cycling at Tutum Bay may be seen in Figure 3.12. It reflects the finding that most arsenic at Tutum Bay is adsorbed onto iron oxyhydroxides. Biological data from this study are depicted as blue arrows and suggest a mechanism by which biota may interact with arsenic compounds at Tutum Bay. The largest arrow (black) points to the abiotic process of As (V) adsorbing onto iron (III) oxyhydroxides. The reverse process can happen both abiotically (smaller black arrows) and biotically (blue arrows). This is facilitated by iron-reducing bacteria, which reduce ferric oxyhydroxides, remobilizing arsenate. Orpiment (As_2S_3) formation can occur during the mineralization of sulfide in the presence of arsenite. This is usually indirectly related to the presence of sulfur-reducing bacteria. Members of the genus *Desulfotomaculum* (found at Tutum Bay) have been shown to reduce both As (V) and S (VI) to produce orpiment (Newman *et al.*, 1997). The methylation of arsenic species by a range of organisms is shown as blue arrows. Although we found biological support for this model, neither aluminum oxyhydroxides nor orpiment were assayed at Tutum Bay. Microbes known to produce DMA and MMA were detected, but these compounds were not found in Tutum Bay porewater samples (Price and Pichler, 2005). It is possible that volatile forms of arsenic or other forms of organic arsenic were produced or that organisms we identified capable of forming DMA and MMA were inactive.

Eukaryote diversity:

Macrofauna and meiofauna were identified by microscopy and microbial eukaryotes identified by sequencing 18S rRNA genes isolated from sediment. Eukaryotic diversity along the transect varies greatly (Shannon's diversity index = 2.7 – 4.47) with the highest diversity furthest from the vent (120 meter site) (Figure 3.7). At the 0 meter site (Shannon's diversity index = 3.47), members of the genera *Capitella* and *Viscosia* have the highest relative abundance (Figure 3.8). *Capitella* species are opportunistic polychaete annelids present in unstable habitats. Certain capitellids inhabit shallow-hydrothermal areas in Greece and have adapted to survive sulfidic, low organic environments (Gamenick, 1998). *Viscosia,* an r-strategist nematode, exploits low diversity niches (Semprucci *et al.*, 2013) and are often found in disturbed environments. The genus *Cladosporium*, a cosmopolitan fungus, has the third highest relative abundance at the 0 meter site. Members of the genus are typically plant pathogens, but also decompose decaying organic material (Bensch *et al.*, 2012). The molecular data showed that 30 m from the vent (Shannon's diversity index = 4.22), the fungus *Sarocladium* had the highest relative abundance followed by the diatom, *Lemnicola* (Figure 3.8). *Sarocladium* dominates the sequence data at 30, 60 and 120 m. *Sarocladium* is a fungus found in soda lakes and closely related to the genus *Acremonium* which is found in marine environments (Grum-Grzhimaylo *et al.*, 2013). Our most prevalent *Sarocladium* 18S gene sequence is a 100% match to *Sarocladium kiliense* (HQ232198) and a 96% match to *Acremonium brevis* (HQ232183.1). Eukaryote diversity was lowest 60 m from the vent (Shannon's diversity index = 2.7). Sequencing data at 90 m shows that nematodes of the genus *Chromadorita* were in

highest relative abundance, followed by the diatom *Navicula*. Data from the hand-sorted meiofauna and macrofauna did not always agree with the molecular data. For example, only a few nematode sequences were found at the 30 meter site while the bulk of hand-sorted specimens from the 30 meter site were nematodes. This is because hand-sorting of macrofauna and meiofauna excludes organisms such as filamentous fungi and heterokonts, abundant in the molecular analysis but absent from the hand-sorted data set.

Trophic interactions:

Where trophic information was available, each genus of bacteria and eukaryote were categorized by feeding habits. A food web was created for each site (Figure 3.12).The diversity of bacterial and eukaryotic primary producers fluctuates across the transect. Consumers mainly consisted of parasitic species of fungus, although predatory species of nematodes were found. Detritivores and decomposers represented the most diverse trophic groups with heterotrophic bacteria slightly more diverse than saprovoric eukaryotes. We were unable to classify some genera into trophic groups because of limited available information.

Association analysis:

An association analysis was carried out with combined bacterial and eukaryotic species found at more than one site together (Figure 3.9). Six nodes with correlation values of 0.5 or greater represent taxa that share a common distribution pattern across the transect. Node 1 contains species found mostly at both the 30 meter and 90 meter sites. Node 2 contains the least number of taxa which are found mainly at the 30 meter and 120 meter site. Node 3 represents taxa found both at 30 m and 60 m while node 4

represents taxa found both at 60 m and 90 m. Node 5 is the largest and contains taxa found mainly at the 90 and 120 m sites. The association analysis shows that taxa found both near and far vent are relatively sparse and the most similar distribution patterns are either near-vent (node 3) or away from vent (node 5). These associations demonstrate that there are likely many interactions among phylogenetically diverse organisms at these sites, possibly including predator-prey relationships, commensalism, parasitism, and symbiotic relationships. Some of these interactions are shown in the food webs (Figure 3.11).

Comparison to other studies:

Similarities exist between the Tutum Bay communities and those of vent areas from other studies, but most studies do not sample as far from the vent as ours. One example of similar findings involves the *Capitella* genus described above. In addition, Sievert *et al*. (1999) found a high relative abundance of dissimilatory iron-reducing bacteria in the transition zone of a shallow-water hydrothermal vent near Milos Island, Greece. At the Tutum Bay transect, an increased relative abundance of dissimilatory iron-reducing bacteria is also seen in the transition zone from near-vent to far-vent (Figure 3.10). DNA analysis at the transect of Milos Island revealed the first report of *Acidobacterium* at a hydrothermal site (Sievert *et al*., 2000). At Tutum Bay, DNA analyses found *Acidobacterium* at near-vent sites but also throughout the transect. In a shallow-water hydrothermal system in Japan, sulfur-oxidizing *Chlorobi* appeared to dominate the near-vent microbial mats (Hirayama *et al*., 2007). While the *Chlorobi* species found in Japan are photoautotrophic, our study finds all but 1 of 106 sequences at Tutum Bay belong to the genus *Ignavibacterium* which grows heterotrophically. A

recent shallow-water pyrosquencing study in the Okinawa Trough found bacterial communities dominated by sulfur-metabolizing organisms. They found members of the genus *Nautilia* and *Thiomicrospira* as the major component of the two hydrothermal vents sampled (Zhang *et al*., 2012). Neither genus was found in our study. Members of *Thiohalomonas* and *Thioprofundum* were the most abundant representatives of sulfur oxidizers at our Tutum Bay transect. Our study yielded 1930 bacterial 16s rRNA gene sequences across the Tutum Bay transect, but only 158 represented sulfur oxidizers with the majority (n=85) found at the 90 and 120 m sites, suggesting that sulfur oxidation is not a major metabolic process in Tutum Bay. The samples in the Taiwan study were taken from the water column of a vent heavily colored with sulfur precipitants, while our samples were from sediment pore water.

Conclusions:

This study is the first to assess biocomplexity across a broad phylogenetic range including bacteria, microbial eukaryotes, meiofauna and macrofauna from a shallow-water hydrothermal vent. Biodiversity generally increased with distance from the vent, with an exception where diffuse venting was found. Hydrothermal influences were found across the entire 120 m transect, suggesting that hydrothermal vents can influence a larger region than previously thought. The biodiversity of the communities responded to the presence of hydrothermal fluids with a clear correlation between temperature and thermophilic organisms. No specific correlation between organisms that metabolize arsenic and the concentration of different oxidation states of arsenic ions was observed, perhaps because very little of the arsenic present was bioavailable. The even distribution of arsenic reducers may represent background arsenic metabolism. Primary

production throughout the transect appeared to be a mix of chemo- and phototrophy. Food web and association analyses of organisms at the site, together with the varied geochemical environment across the transect suggest many potential interactions between phylogenetically diverse organisms occur at certain sites, and that species distributions and interactions occur in the context of complex spatial relationships.

References:

Akerman, N. H., R. E. Price, T. Pichler & J. P. Amend, 2011. Energy sources for chemolithotrophs in an arsenic- and iron-rich shallow-sea hydrothermal system. Geobiology 9(5):436-45 doi:10.1111/j.1472-4669.2011.00291.x.

Bensch, K., U. Braun, J. Z. Groenewald & P. W. Crous, 2012. The genus Cladosporium. Studies in mycology 72(1):1-401 doi:10.3114/sim0003.

Clarke, K. R. & R. N. Gorley, 2006. PRIMER v6: User Manual/Tutorial. PRIMER-E.

DeLong, E. F., 1992. Archaea in coastal marine environments. Proceedings of the National Academy of Sciences of the United States of America 89(12):5685-9.

Doak, G. O. & L. D. Freedman, 1970. Organometallic compounds of arsenic, antimony, and bismuth. Wiley-Interscience, New York.

Gamenick, I., Abbiati, M., and O. Giere, 1998. Field distribution and sulphide tolerance of *Capitella capitata* (Annelida: Polychaeta) around shallow water hydrothermal vents off Milos (Aegean Sea). A new sibling species? Marine Biology(130):447-453.

Gregoire, P., M. Bohli, J. L. Cayol, M. Joseph, S. Guasco, K. Dubourg, J. Cambar, V. Michotey, P. Bonin, M. L. Fardeau & B. Ollivier, 2011. *Caldilinea tarbellica* sp. nov., a filamentous, thermophilic, anaerobic bacterium isolated from a deep hot aquifer in the Aquitaine Basin. International journal of systematic and evolutionary microbiology 61(Pt 6):1436-41 doi:10.1099/ijs.0.025676-0.

Grum-Grzhimaylo, A. A., M. L. Georgieva, A. J. Debets & E. N. Bilanenko, 2013. Are alkalitolerant fungi of the Emericellopsis lineage (Bionectriaceae) of marine origin? IMA fungus 4(2):213-28 doi:10.5598/imafungus.2013.04.02.07.

Hirayama, H., M. Sunamura, K. Takai, T. Nunoura, T. Noguchi, H. Oida, Y. Furushima, H. Yamamoto, T. Oomori & K. Horikoshi, 2007. Culture-dependent and -independent characterization of microbial communities associated with a shallow submarine hydrothermal system occurring within a coral reef off Taketomi Island, Japan. Applied and environmental microbiology 73(23):7642-56 doi:10.1128/AEM.01258-07.

Iino, T., K. Mori, Y. Uchino, T. Nakagawa, S. Harayama & K. Suzuki, 2010. *Ignavibacterium album* gen. nov., sp. nov., a moderately thermophilic anaerobic bacterium isolated from microbial mats at a terrestrial hot spring and proposal of *Ignavibacteria classis* nov., for a novel lineage at the periphery of green sulfur bacteria. International journal of systematic and evolutionary microbiology 60(Pt 6):1376-82 doi:10.1099/ijs.0.012484-0.

Itoh, T., K. Yamanoi, T. Kudo, M. Ohkuma & T. Takashina, 2011. *Aciditerrimonas ferrireducens* gen. nov., sp. nov., an iron-reducing thermoacidophilic actinobacterium isolated from a solfataric field. International journal of systematic and evolutionary microbiology 61(Pt 6):1281-5 doi:10.1099/ijs.0.023044-0.

Jannasch, H. W., 1995. Seafloor Hydrothermal Systems. In Susan E. Humphris, R. A. Z., Lauren S. Mullineaux, Richard E. Thomas (ed) Seafloor Hydrothermal Systems. vol 91. American Geophysical Union, Washington, DC.

Karlen, D. J., R. E. Price, T. Pichler & J. R. Garey, 2010. Changes in Benthic Macrofauna Associated with a Shallow-Water Hydrothermal Vent Gradient in Papua New Guinea. Pacific Science 64(3):391-404.

Konhauser, K., 2007. Introduction to geomicrobiology. Blackwell Pub., Malden, MA.

Mackey, L. Y., B. Winnepenninckx, R. De Wachter, T. Backeljau, P. Emschermann & J. R. Garey, 1996. 18S rRNA suggests that Entoprocta are protostomes, unrelated to Ectoprocta. Journal of molecular evolution 42(5):552-9.

Meyer-Dombard, D. R., R. E. Price, T. Pichler & J. P. Amend, 2012. Prokaryotic Populations in Arsenic-Rich Shallow-Sea Hydrothermal Sediments of Ambitle Island, Papua New Guinea. Geomicrobiology Journal 29(1):1-17 doi:Doi 10.1080/01490451.2010.520073.

Muyzer, G., D. Y. Sorokin, K. Mavromatis, A. Lapidus, B. Foster, H. Sun, N. Ivanova, A. Pati, P. D'Haeseleer, T. Woyke & N. C. Kyrpides, 2011. Complete genome sequence of *Thioalkalivibrio* sp. K90mix. Stand Genomic Sci 5(3):341-55 doi:10.4056/sigs.2315092.

Newman, D. K., T. J. Beveridge & F. Morel, 1997. Precipitation of Arsenic Trisulfide by Desulfotomaculum auripigmentum. Applied and environmental microbiology 63(5):2022-8.

Oremland, R. S. & J. F. Stolz, 2003. The ecology of arsenic. Science 300(5621):939-944 doi:DOI 10.1126/science.1081903.

Pichler, T. & G. R. Dix, 1996. Hydrothermal venting within a coral reef ecosystem, Ambitle island, Papua New Guinea. Geology 24(5):435-438 doi:Doi 10.1130/0091-7613(1996)024<0435:Hvwacr>2.3.Co;2.

Pichler, T., J. P. Amend, J. R. Garey, P. Hallock, N. P. Hsia, D. Karlen, D. R. Meyer-Dombard, B. J. McCloskey & R. E. Price, 2006. A Natural Laboratory to Study Arsenic Geobiocomplexity. Eos, Transactions American Geophysical Union 87(23):221-225.

Price, R. E. & T. Pichler, 2005. Distribution, speciation and bioavailability of arsenic in a shallow-water submarine hydrothermal system, Tutum Bay, Ambitle Island, PNG. Chemical Geology 224(1-3):122-135 doi:DOI 10.1016/j.chemgeo.2005.07.017.

Rees, G. N., G. S. Grassia, A. J. Sheehy, P. P. Dwivedi & B. K. C. Patel, 1995. *Desulfacinum infernurn* gem nov., sp. nov., a Thermophilic Sulfate-Reducing Bacterium from a Petroleum Reservoir. International Journal of Systematic Bacteriology 45(1):85-89.

Sekiguchi, Y., T. Yamada, S. Hanada, A. Ohashi, H. Harada & Y. Kamagata, 2003. *Anaerolinea thermophila* gen. nov., sp. nov. and *Caldilinea aerophila* gen. nov., sp. nov., novel filamentous thermophiles that represent a previously uncultured lineage of the domain Bacteria at the subphylum level. International journal of systematic and evolutionary microbiology 53(Pt 6):1843-51.

Semprucci, F., M. Moreno, S. Sbrocca, M. Rocchi, G. Albertelli & M. Balsamo, 2013. The nematode assemblage as a tool for the assessment of marine ecological quality status: a case-study in the Central Adriatic Sea. Mediterranean Marine Science 14(1):48-57.

Shannon, P., A. Markiel, O. Ozier, N. S. Baliga, J. T. Wang, D. Ramage, N. Amin, B. Schwikowski & T. Ideker, 2003. Cytoscape: a software environment for integrated models of biomolecular interaction networks. Genome research 13(11):2498-504 doi:10.1101/gr.1239303.

Sievert, S. M., T. Brinkhoff, G. Muyzer, W. Ziebis & J. Kuever, 1999. Spatial heterogeneity of bacterial populations along an environmental gradient at a shallow submarine hydrothermal vent near Milos Island (Greece). Applied and environmental microbiology 65(9):3834-42.

Sievert, S. M. & J. Kuever, 2000. *Desulfacinum hydrothermale* sp. nov., a thermophilic, sulfate-reducing bacterium from geothermally heated sediments near Milos Island (Greece). International journal of systematic and evolutionary microbiology 50 Pt 3:1239-46.

Sievert, S. M., J. Kuever & G. Muyzer, 2000. Identification of 16S ribosomal DNA-defined bacterial populations at a shallow submarine hydrothermal vent near Milos Island (Greece). Applied and environmental microbiology 66(7):3102-9.

Tarasov, V. G., A. V. Gebruk, A. N. Mironov & L. I. Moskalev, 2005. Deep-sea and shallow-water hydrothermal vent communities: Two different phenomena? Chemical Geology 224:5-39.

Thomas, D. J., J. Li, S. B. Waters, W. Xing, B. M. Adair, Z. Drobna, V. Devesa & M. Styblo, 2007. Arsenic (+3 Oxidation State) Methyltransferase and the Methylation of Arsenicals. Experimental Biology and Medicine 232(1):3-13.

Wu, T., E. Ayres, G. Li, R. D. Bardgett, D. H. Wall & J. R. Garey, 2009. Molecular profiling of soil animal diversity in natural ecosystems: Incongruence of molecular and morphological results. Soil Biology and Biochemistry 41(4):849-857 doi:http://dx.doi.org/10.1016/j.soilbio.2009.02.003.

Wu, T., E. Ayres, R. D. Bardgett, D. H. Wall & J. R. Garey, 2011. Molecular study of worldwide distribution and diversity of soil animals. Proceedings of the National Academy of Sciences of the United States of America 108(43):17720-5 doi:10.1073/pnas.1103824108.

Zhang, Y., Z. Zhao, C. T. Chen, K. Tang, J. Su & N. Jiao, 2012. Sulfur metabolizing microbes dominate microbial communities in Andesite-hosted shallow-sea hydrothermal systems. PloS one 7(9):e44593 doi:10.1371/journal.pone.0044593.

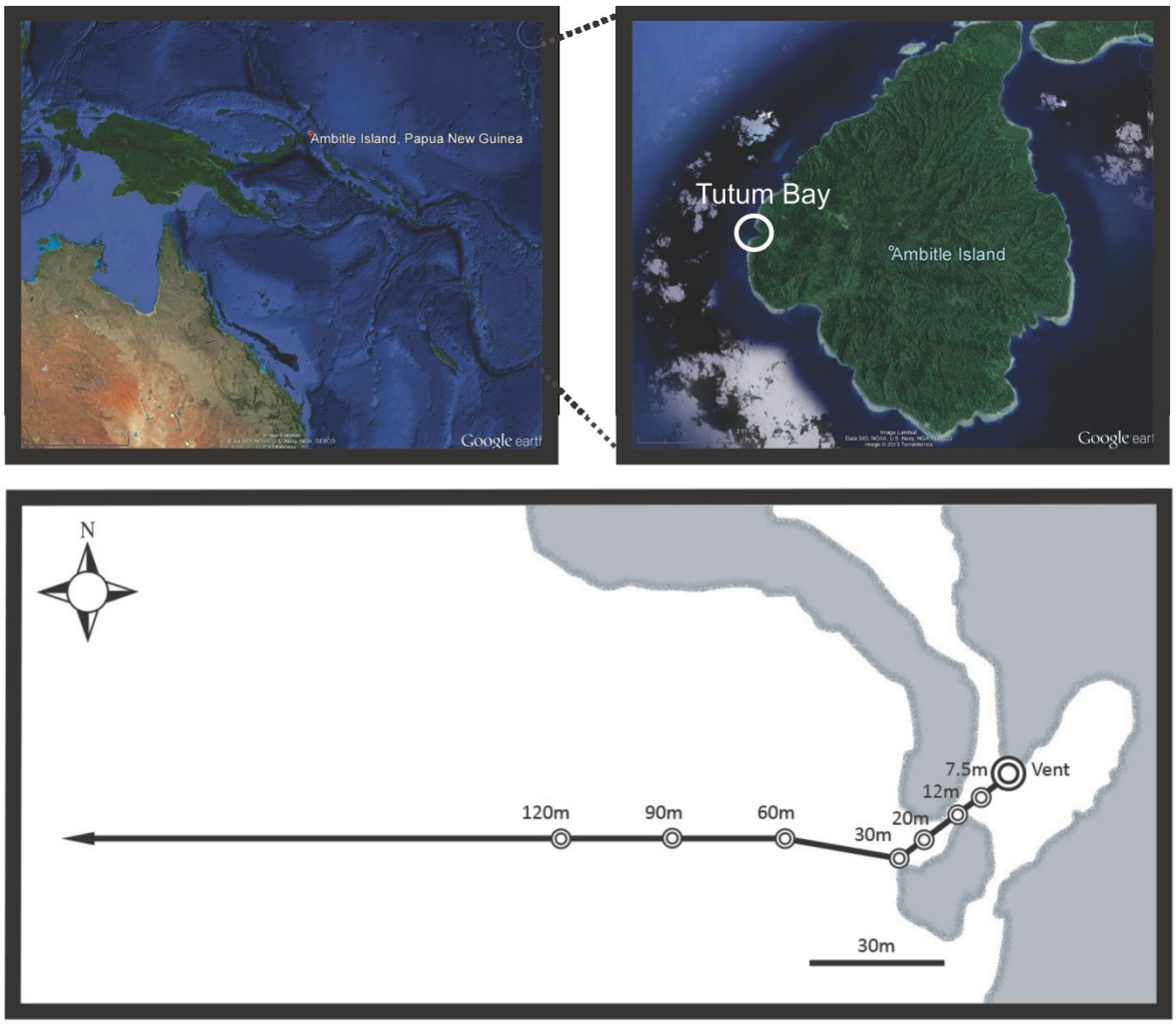

Figure 3.1. Maps showing Ambitle Island and Tutum Bay with Tutum Bay transect and sample sites. From the vent, the transect extended southwest to avoid reef outcroppings before extending 300 meters west.

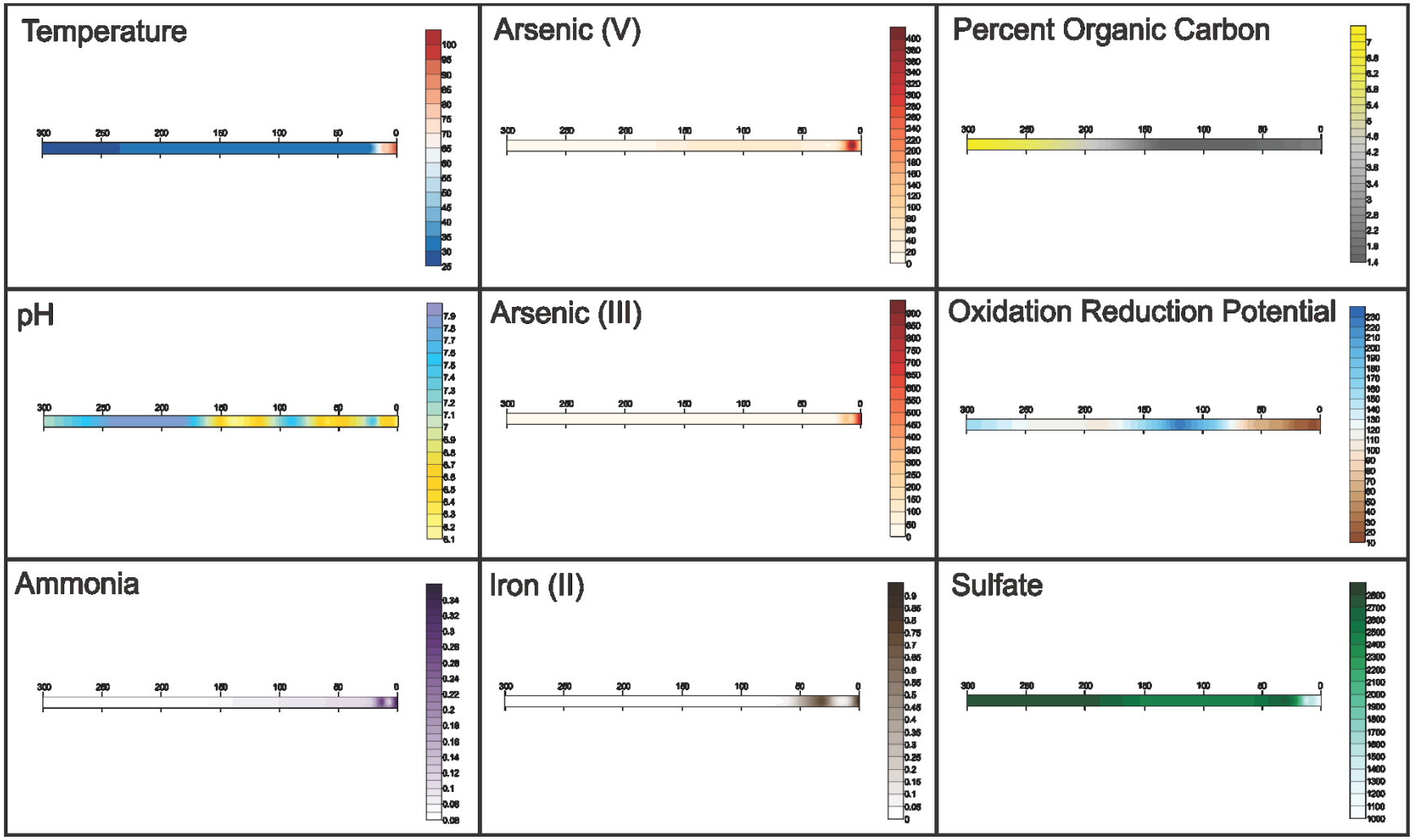

Figure 3.2. Abiotic factors as shown along the transect. The transect is labeled in meters away from vent. Values between sample sites were interpolated within the Surfer program. Contour maps from left to right: Temperature (pH), Arsenic (V) in µg L^{-1}, Percent organic carbon, pH, Arsenic (III) in µg L^{-1}, Oxidation Reduction Potential (mV), Ammonia (aq) in mg L^{-1}, Fe (II) in µg L^{-1}, Sulfate in mg L^{-1}.

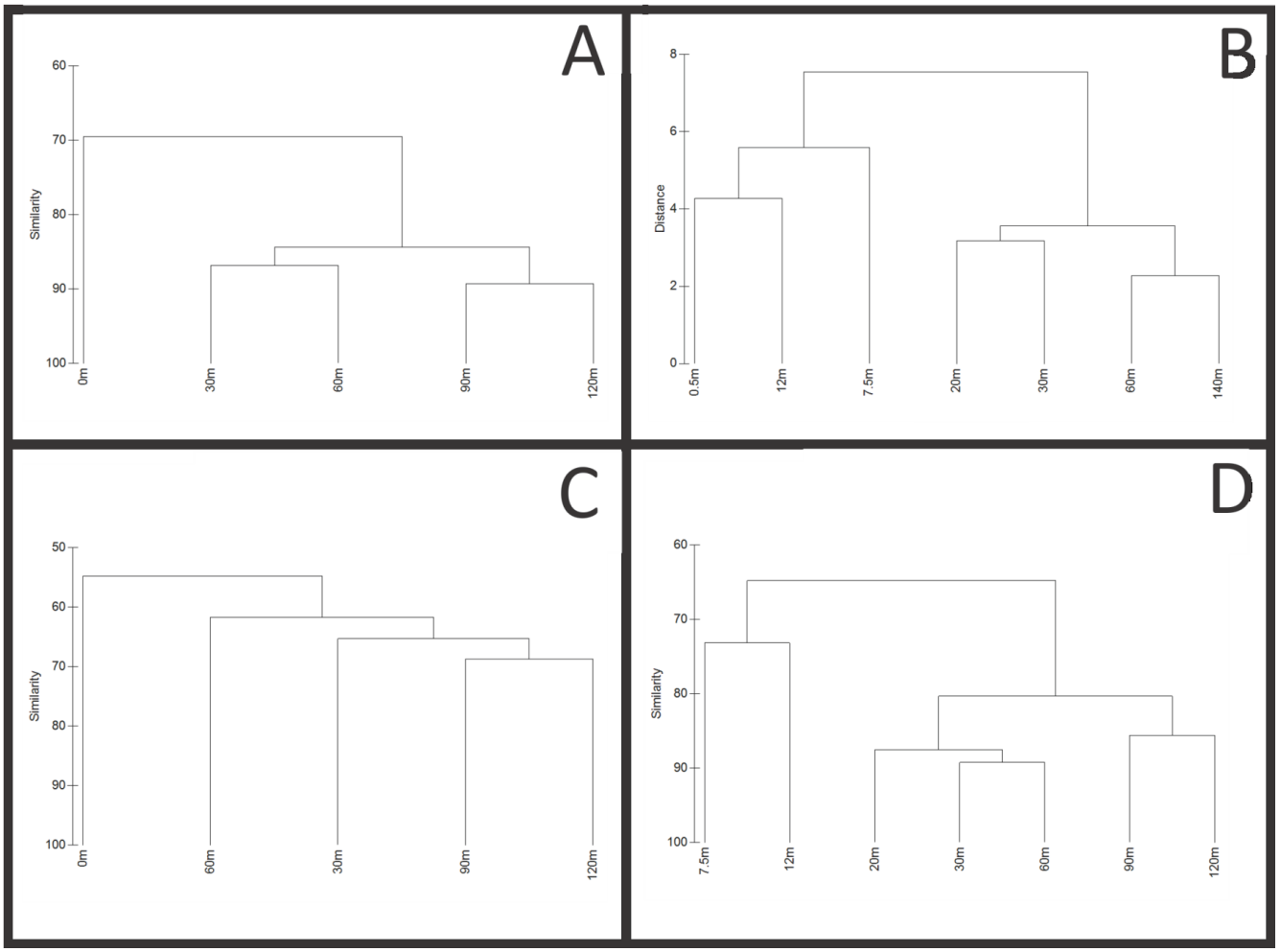

Figure 3.3. Cluster analysis of abiotic and biotic data. Biotic samples were standardized by total, transformed by square root and had resemblance calculated using Bray-Curtis similarity. Abiotic factors were normalized and clustered based on Euclidean distance. (A) Macrofauna and Meiofauna dendogram showing similarity among transect sites. (B) Dendogram of abiotic factors showing similarity along transect sites. (C) Eukaryotic sequence dendogram, showing similarity among transect sites. (D) Bacterial sequence dendogram, showing similarity among transect sites.

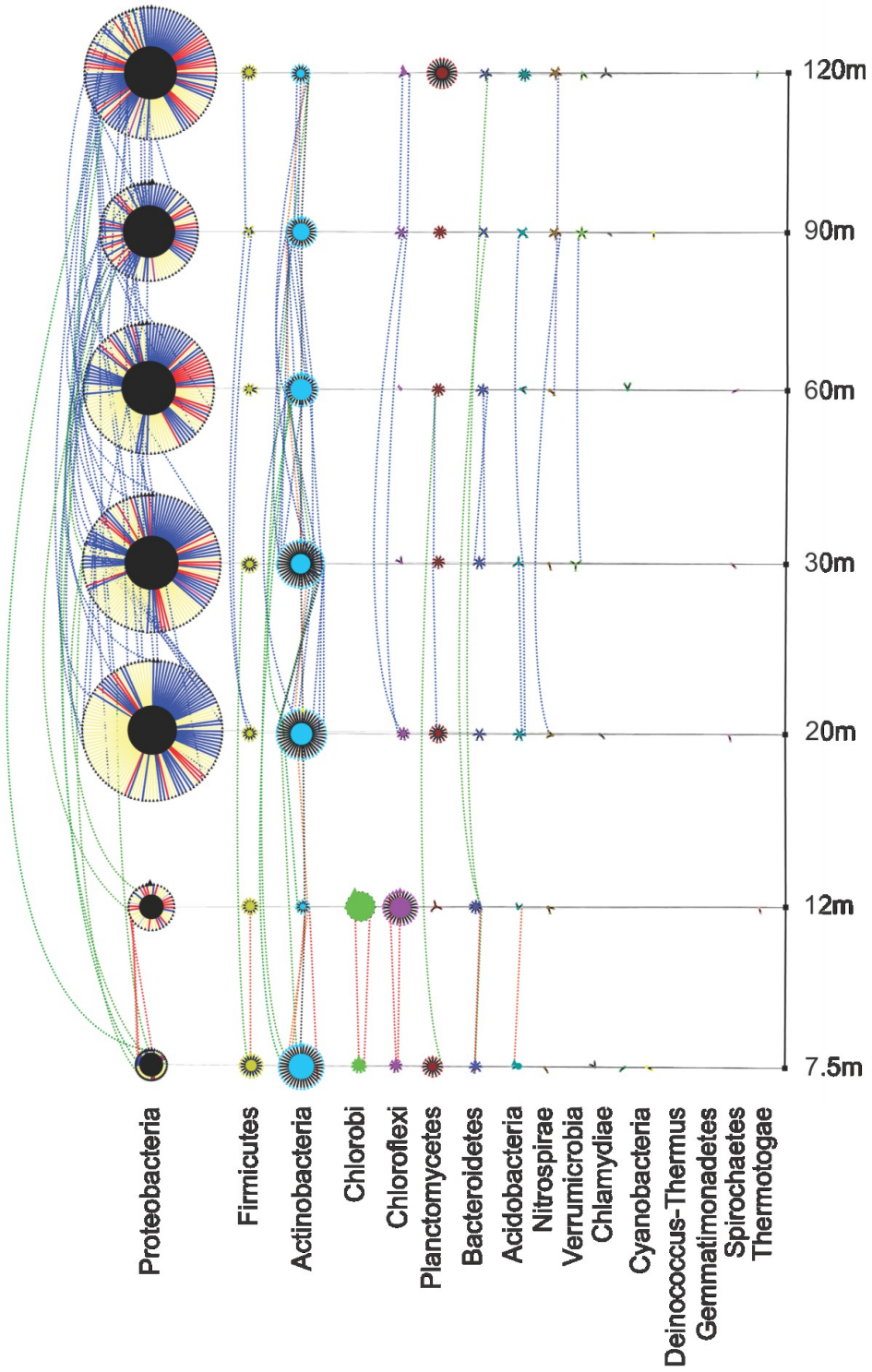

Figure 3.4. Phylogenetic network showing richness, abundance and distribution of phyla at each site. Transect nodes (square) designate sample sites (right). Edges connect transect nodes to phyla nodes (circles). Phyla nodes are connected to individual species nodes (triangles). This connection is colored in Proteobacteria to designate class (α – red, β – gray, δ – yellow, ε - pink ,γ- blue, ζ – teal). Phyla and species node sizes are proportional to relative abundance. Species nodes are connected by dotted edges if they are found at more than one site. These distribution edges are orange (near vent), blue (away from vent), green (near and away from vent) or black (all sites) to show any homogeneity across the transect. Phyla nodes are color coded to facilitate differentiation.

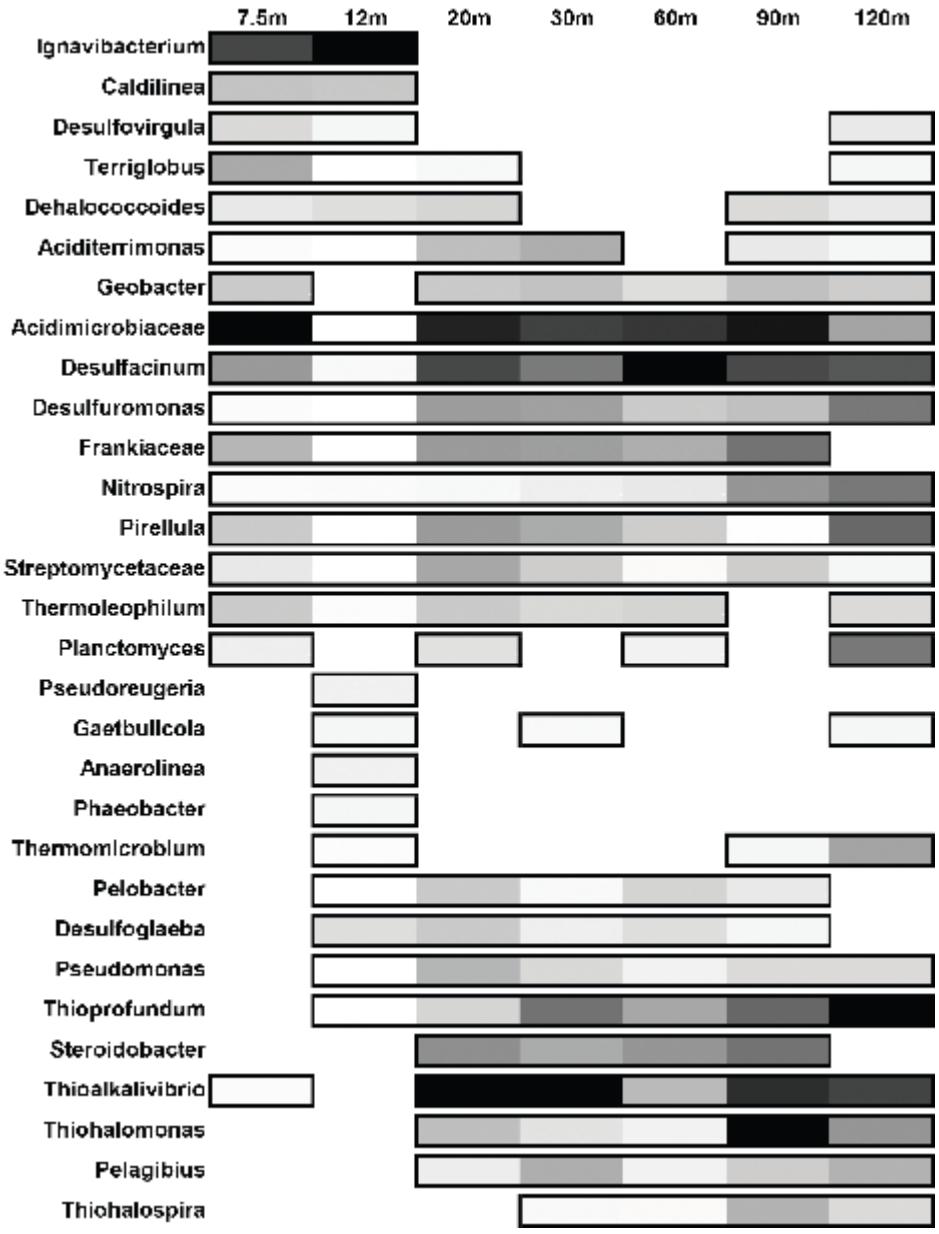

Figure 3.5. Distribution of the most abundant bacterial taxa across each site. The shading is determined by relative abundance where lighter colors represent a lower abundance in respect to the given site. Non-boxed regions represent an absence of the genus at that site.

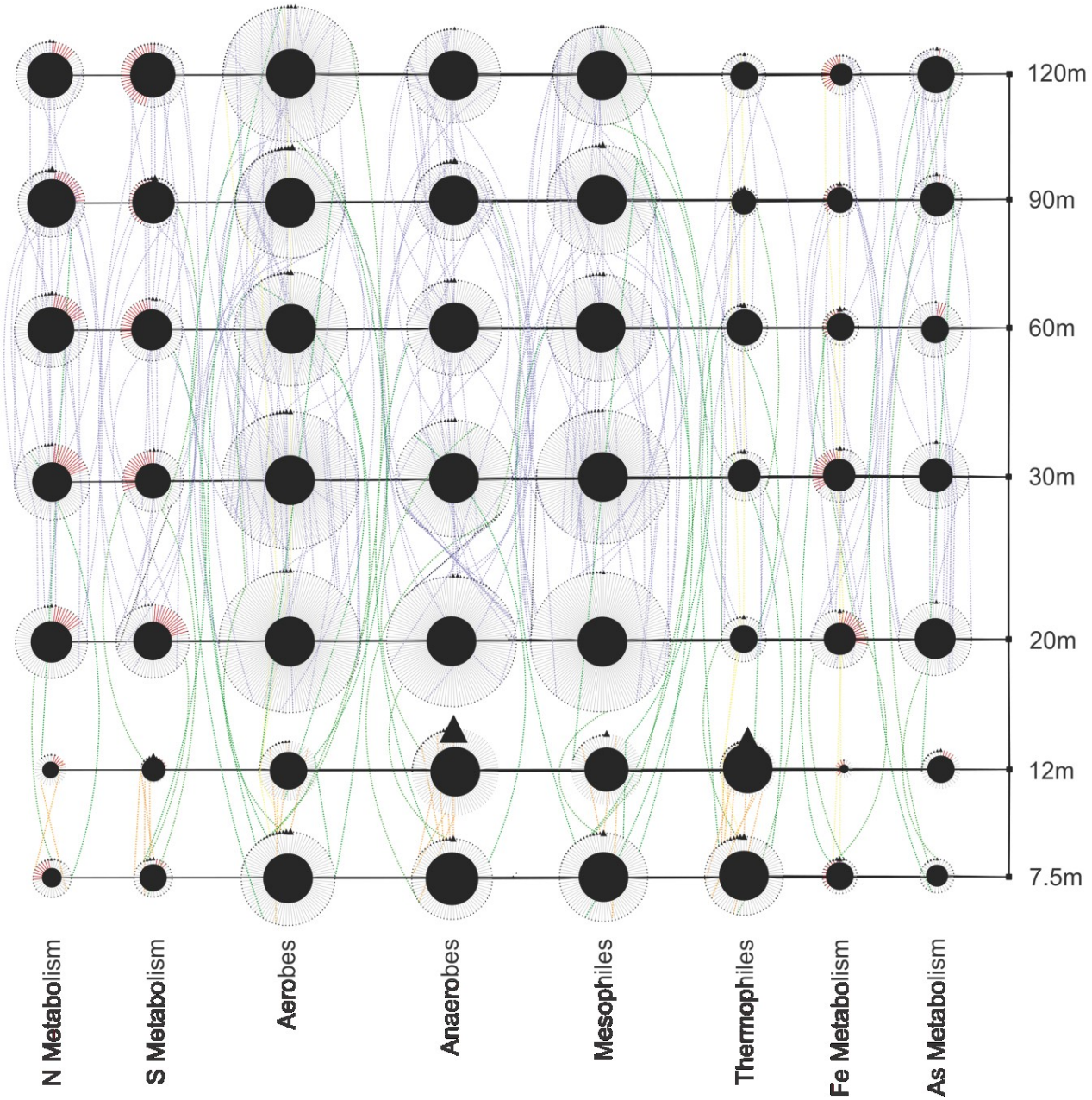

Figure 3.6. Functional guild network showing richness, abundance and distribution at each site. Red edges represent oxidizers within metabolic guilds. Transect nodes (square) designate sample sites (right). Edges connect transect nodes to guild nodes (circles). Guild nodes are connected to individual species nodes (triangles). Species nodes are connected by dotted edges if they are found at more than one site. These distribution edges are orange (near vent), blue (away from vent), green (near and away from vent) or yellow (all sites) to show any homogeneity across the transect.

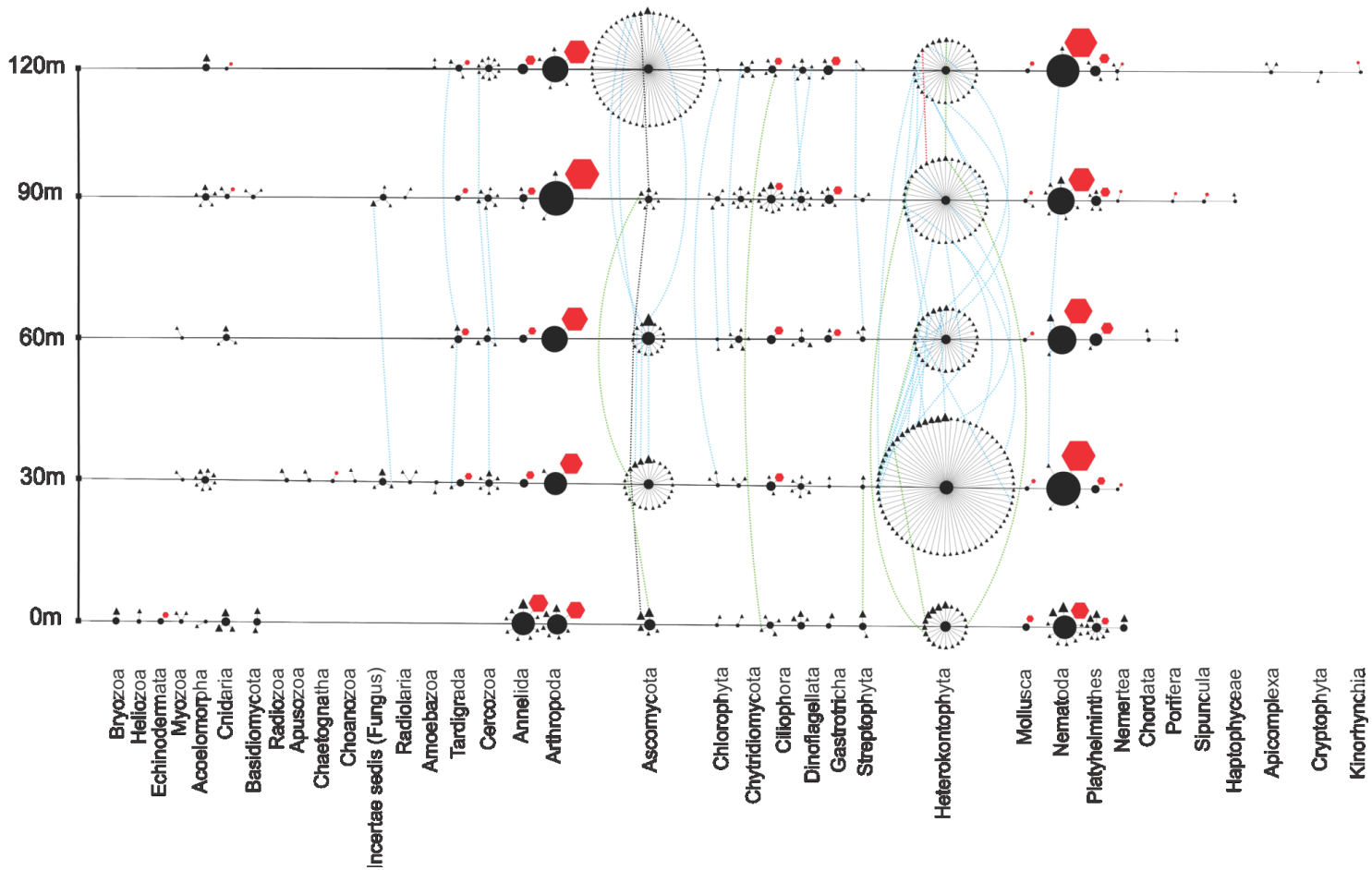

Figure 3.7. Eukaryote phylogenetic network showing richness, abundance and distribution of phyla at each site. Transect nodes (square) designate sample sites (left). Edges connect transect nodes to phyla nodes (circles). Phyla nodes are connected to individual species nodes. Species nodes are either triangles or octagons to describe the method of identification as either sequencing or scoring, respectively. Phyla and species node sizes are proportional to relative abundance. Species nodes are connected by dotted distribution edges if they are found at more than one site. These distribution edges are blue if found far from vent (30 meters to 120 meters), green if found both near-vent (0 meters) and any other site or black (all sites) to show any homogeneity across the transect.

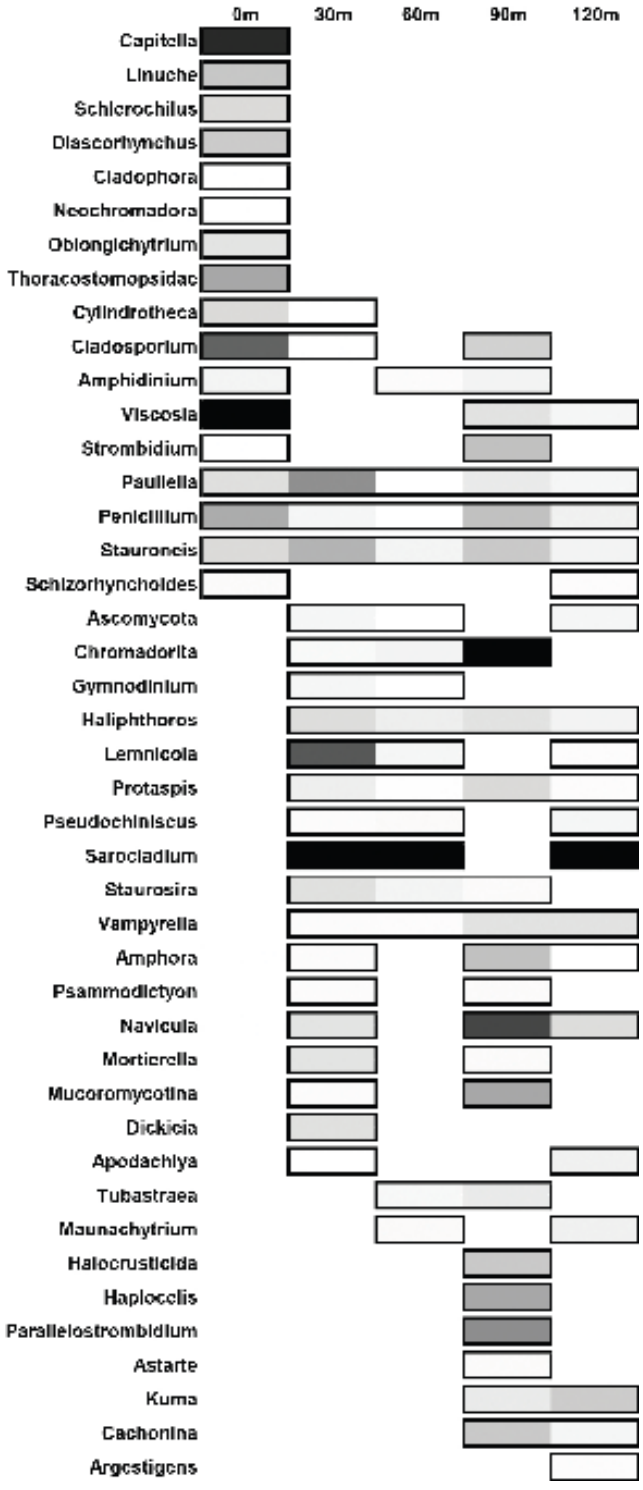

Figure 3.8. Distribution of the most abundant eukaryote genera across each site. The shading is determined by relative abundance where lighter colors represent a lower abundance in respect to the given site. Non-boxed regions represent an absence of the genus at that site.

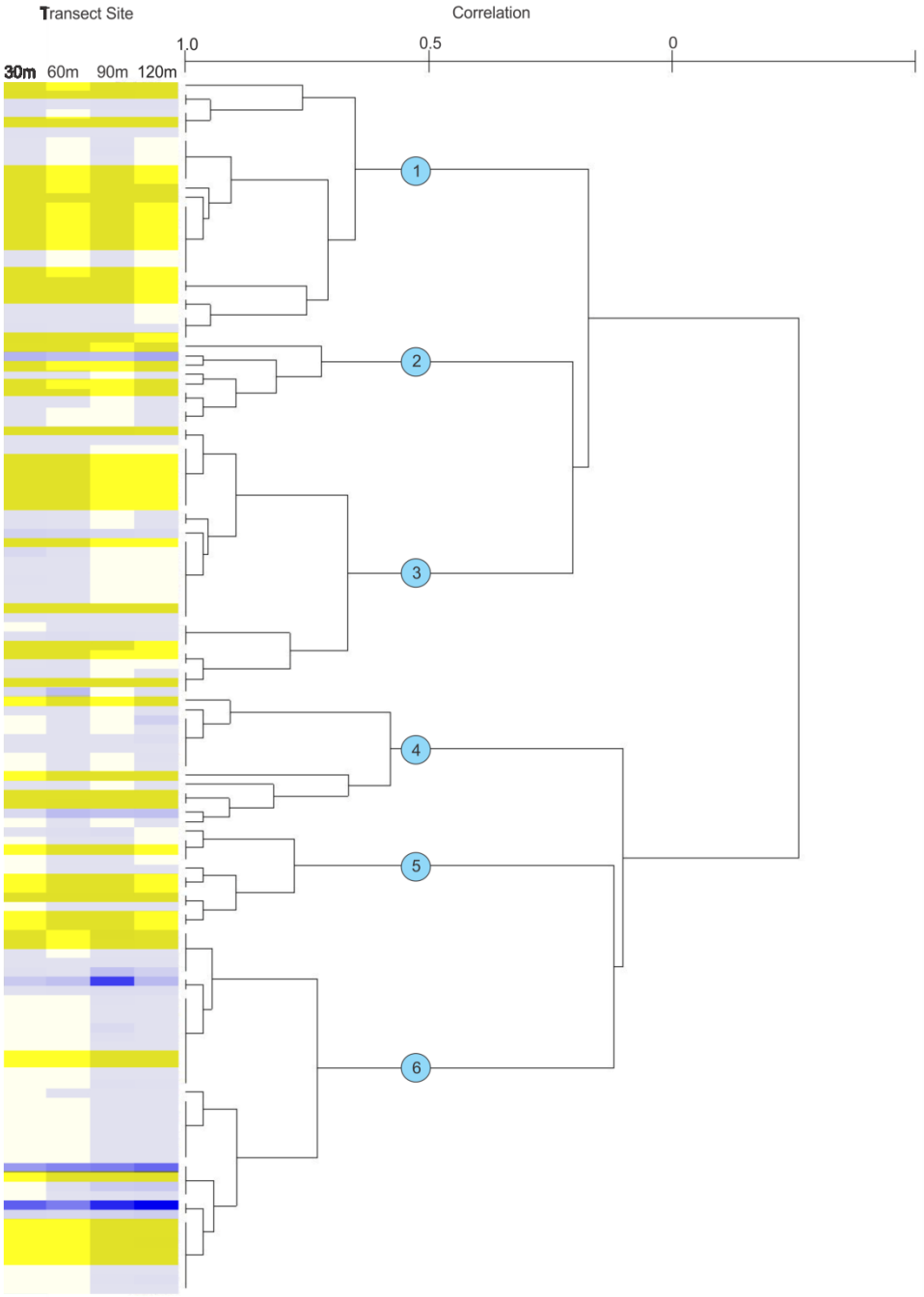

Figure 3.9. Association Meta Analysis between bacteria and eukaryotes. Bacterial species are highlighted in yellow while eukaryotic species are colored purple. Six nodes (correlation values > 0.5) are depicted with blue circles and represent species with similar distribution patterns. The heat map shows raw abundance values for each species represented. Only species found together at more than one site were used in this analysis.

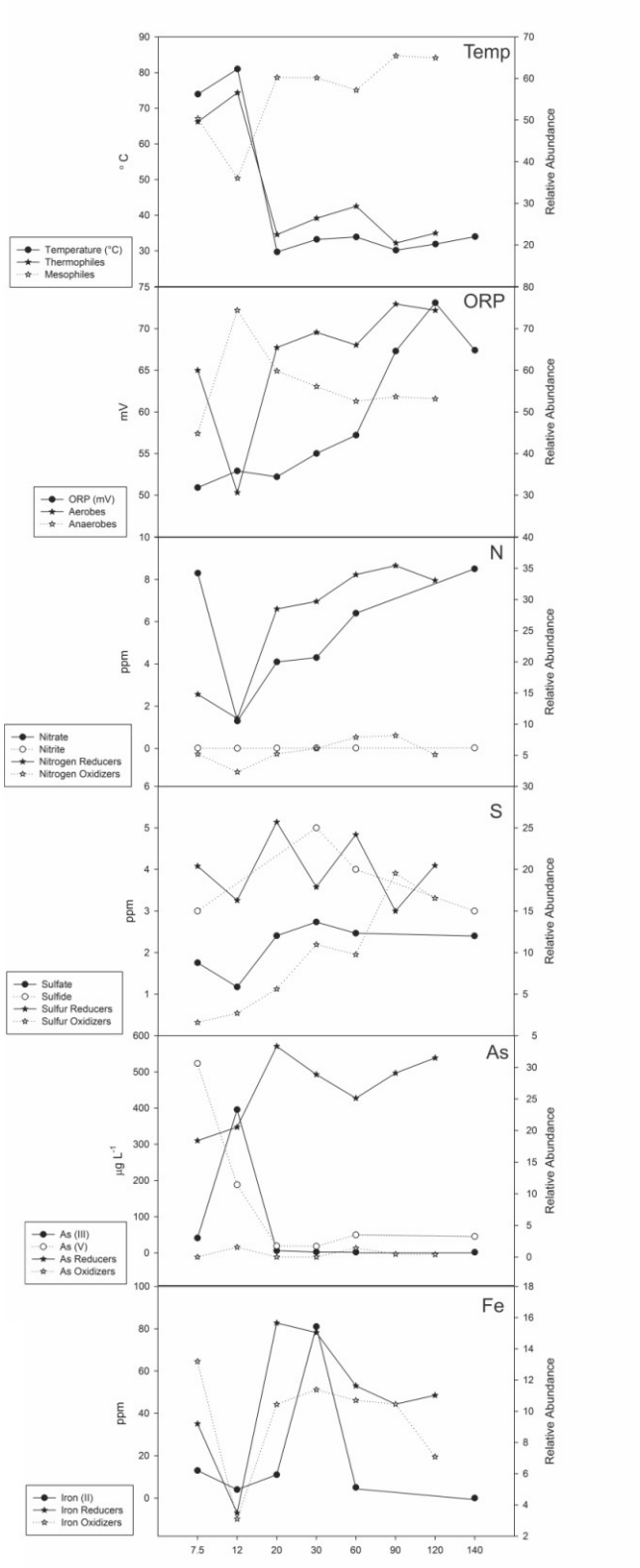

Figure 3.10. Geochemical measurements and functional guild relative abundance values. Temperature (°C), oxidation-reduction potential (mV), nitrogen (ppm), sulfur (ppm), arsenic (μgL^{-1}) and iron concentrations (ppm) are plotted against related functional guilds.

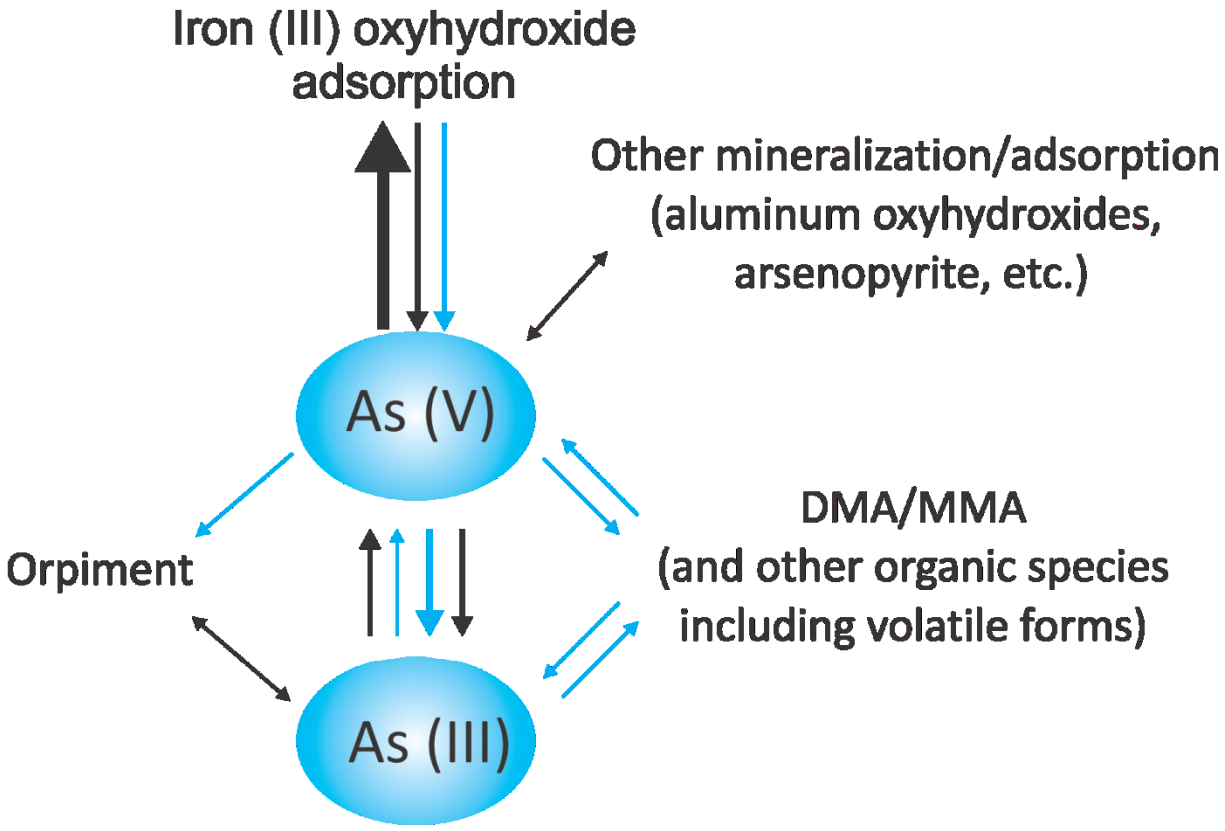

Figure 3.11. Proposed arsenic cycle of Tutum Bay. Abiotic processes are shown as black arrows. Biotic processes are shown with blue arrows. The sizes of the arrows propose a relative rate at which the processes occur. DMA and MMA represent mono- or di-methylated forms of arsenic.

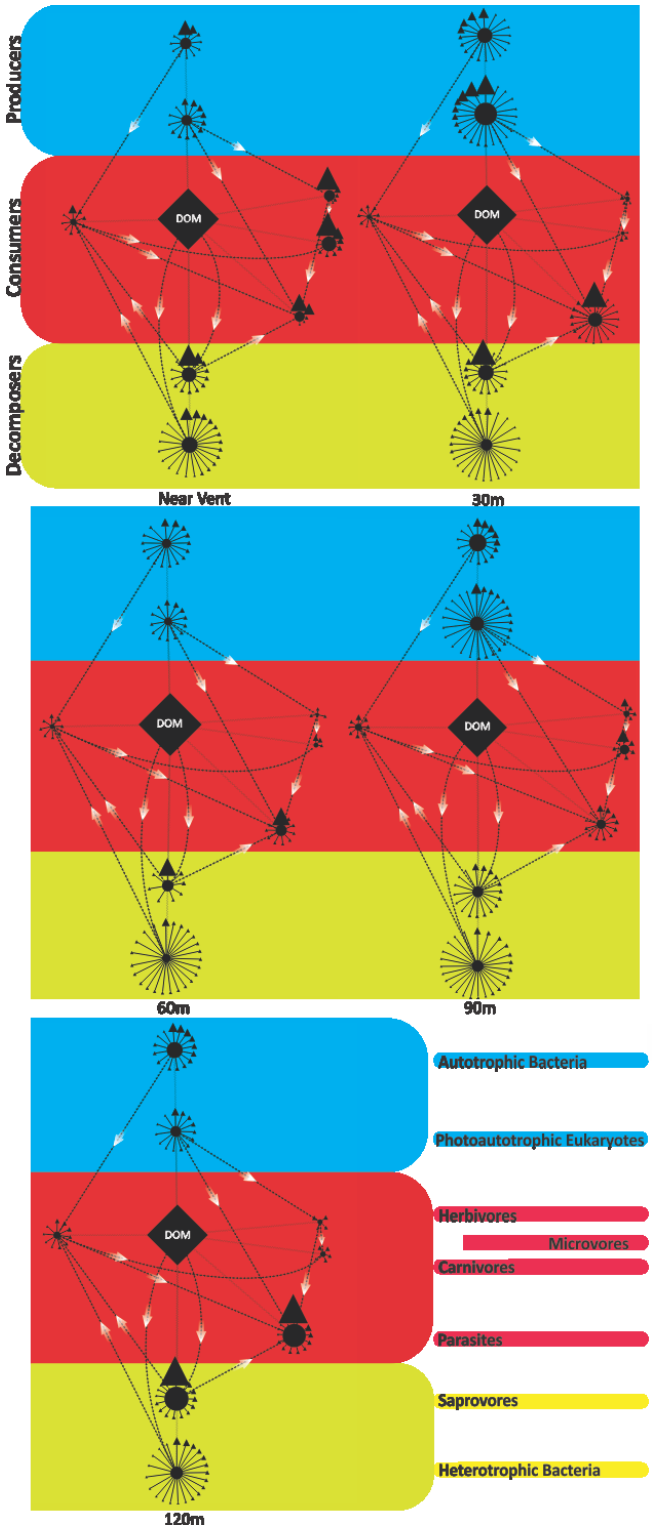

Figure 3.12. Food networks of functionally relevant guilds at each site. Species are represented by triangles which are attached to their respective guilds that are represented as circles. The size of the nodes correspond to their relative abundance. Each network has Dissolved Organic Material (DOM) in the center with lines connected to each guild signifying their contribution. Dotted lines represent carbon flow and are highlighted with white arrows indicating the direction of flow. Background color signifies Producers (blue), Consumers (red), and Decomposers (yellow). Guilds are listed horizontally at the end of the figure with Microvores found on the left side of each network.

APPENDICES

Appendix A: Functional guild and trophic group classification methodology

Bacteria were classified to the genus level whenever possible for classification into functional guilds. Each genus was researched fully in the primary literature and in Bergey's Manual of Systematic Bacteriology. Information was recorded based on culture data from publications that first describe a type species of the genus or, when referencing Bergey's, information for the genus was compiled for all species listed within the genus. The information collected included oxygen requirements (aerobic, anaerobic, facultative, etc.). If an organism was considered facultative in regards to oxygen requirements it was scored into both aerobic and anaerobic categories. Information was also recorded for sulfur metabolism. If an organism was listed as being able to reduce any sulfur compound it was scored as a sulfur reducer. Similarly, if an organism was listed as being able to oxidize any sulfur compound it was scored as a sulfur oxidizer. This was also the method used to record iron, nitrogen and methane metabolism. If an organism was not referenced as being tested for these capabilities, it was not scored into the respective category. Similarly, if an organism was listed specifically as not being able to do a particular metabolism, it was not scored into that category. Arsenic metabolism was determined differently from the aforementioned guilds, primarily because during culture experiments many do not include tests that test a microbe's ability to metabolize arsenic. Therefore, the enzymes arsenate reductase and arsenite oxidase were searched in the Integrated Microbial Genome database, which hosts non-redundant genomes of prokaryotes that have been fully sequenced, and subsequently

cultured, to date. Each genus of bacteria that was known to have either of the enzymes was compiled into a list. This list was then used to identify the genera within the study capable of arsenic reduction or oxidation. Trophic categories for the bacteria were only recorded when specifically mentioned either in a type species publication or in Bergey's. If the trophic group was not clearly stated, the genus was not scored into a functional guild based on trophic requirements. Temperature ranges were recorded for each genus. Thermophiles were considered any organism whose range overlapped with the temperatures normally associated with thermophilic organisms (i.e. - 45 to 122 °C). Mesophiles were considered any organism whose range overlapped with the temperatures normally associated with mesophilic organisms (i.e. - 20 to 45 °C).

Eukaryotic trophic group classification was based solely on primary literature and was examined at the genus level. In some cases, certain phyla of eukaryotes shared one common means of obtaining nutrition. In these cases, members of the phylum were scored based on the literature describing the phylum. More detailed trophic categories were recorded when possible but eventually were grouped into less specific categories such that only photoautotrophs, herbivores, carnivores, microvores, parasites, and saprovores were reported.

Appendix B: Jewfish Datasonde Data

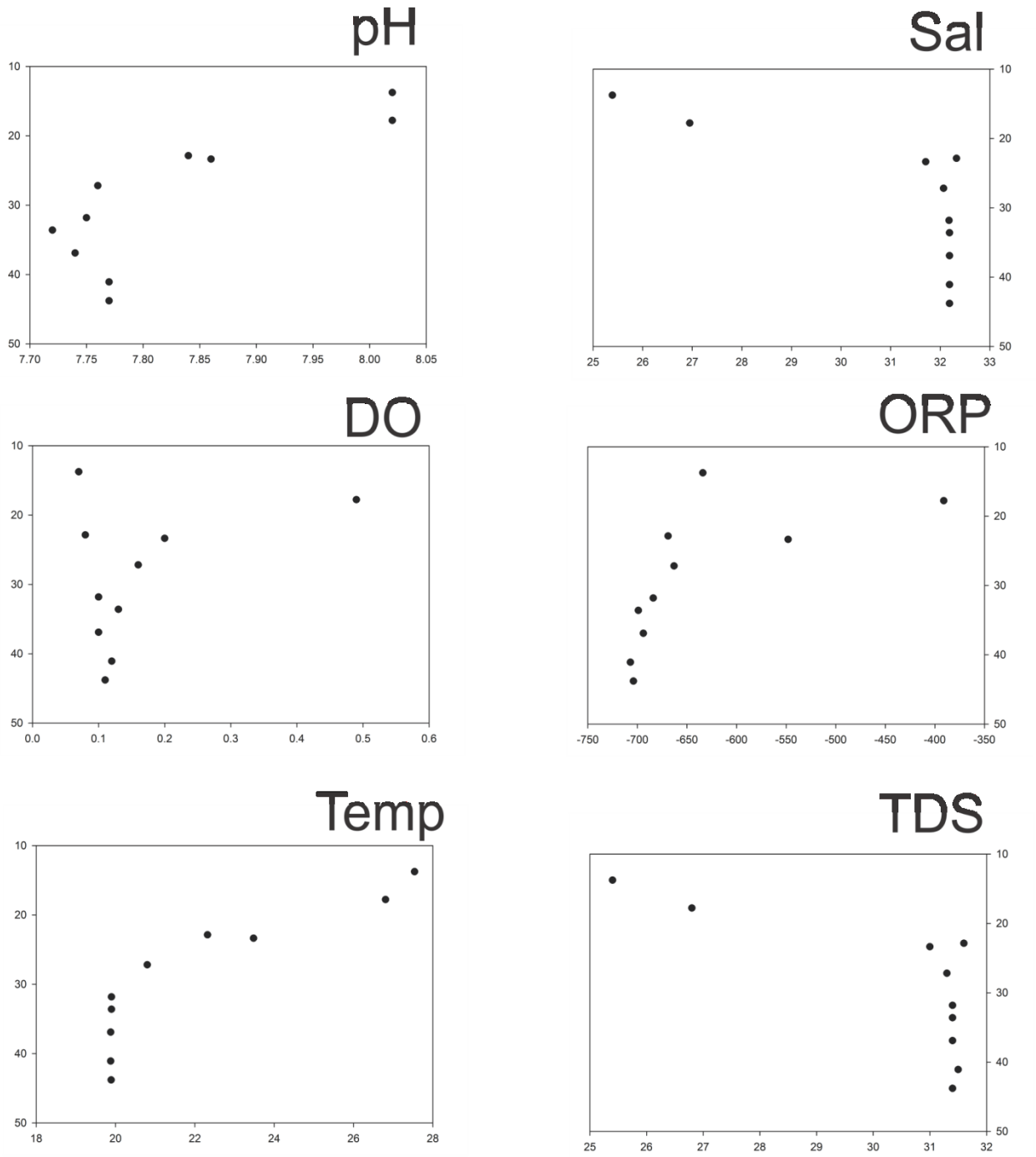

Figure A1. Water column data collected at Jewfish sink on September 17th, 2009. Depth within the sink is displayed on the y axis in meters. Temperature (Temp), Total Dissolved Solids (TDS), pH, Dissolved Oxygen (DO), Oxidation-Reduction Potential (ORP), and Salinity (Sal) are reported. Temperature is measured in degrees Celsius. TDS is measured in grams per liter. LDO is measured in milligrams per liter. ORP is measured in millivolts. Salinity is measured in parts per thousands.

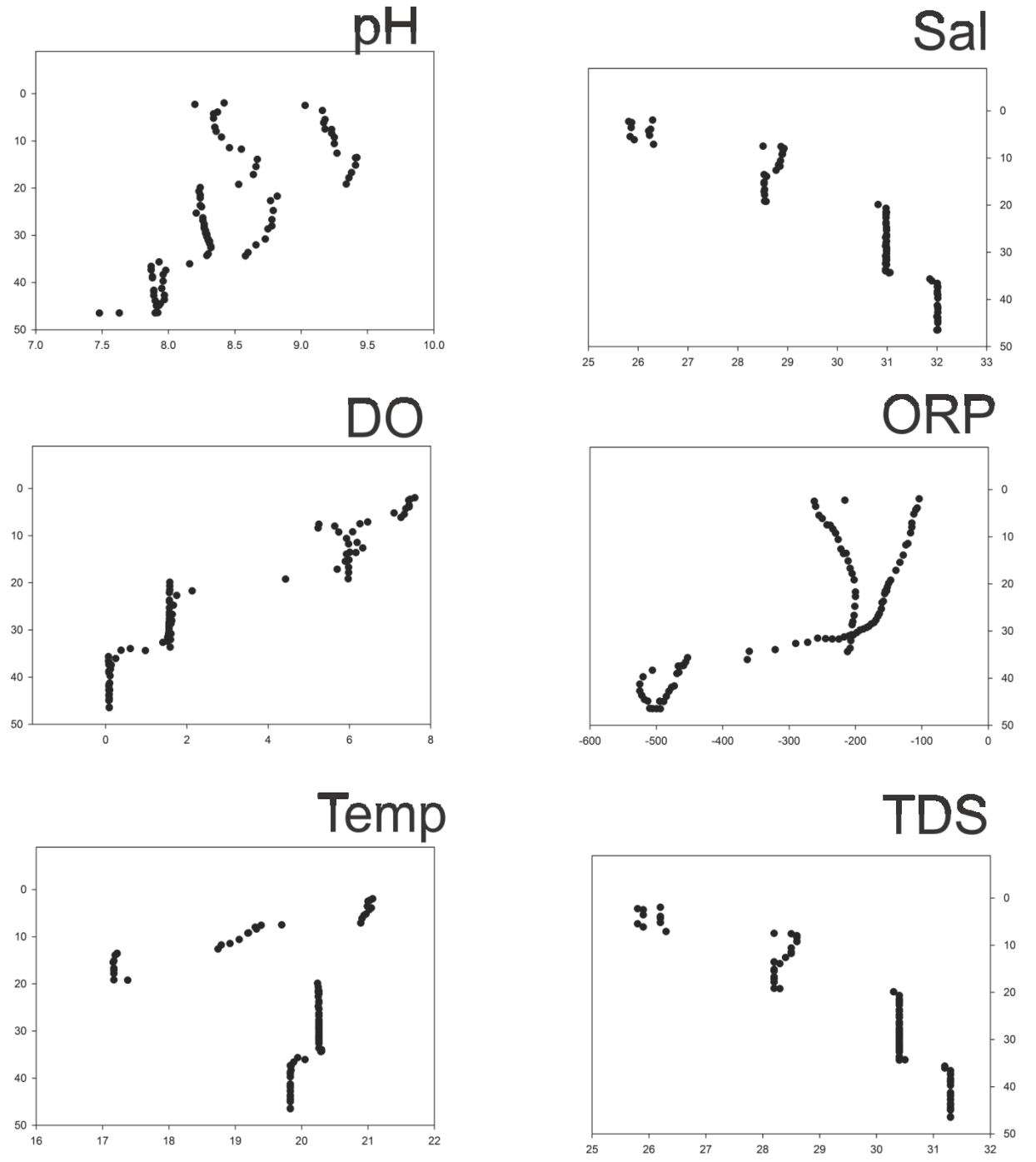

Figure A2. Water column data collected at Jewfish sink on December 13th, 2009. Depth within the sink is displayed on the y axis in meters. Temperature (Temp), Total Dissolved Solids (TDS), pH, Dissolved Oxygen (DO), Oxidation-Reduction Potential (ORP), and Salinity (Sal) are reported. Temperature is measured in degrees Celsius. TDS is measured in grams per liter. LDO is measured in milligrams per liter. ORP is measured in millivolts. Salinity is measured in parts per thousands.

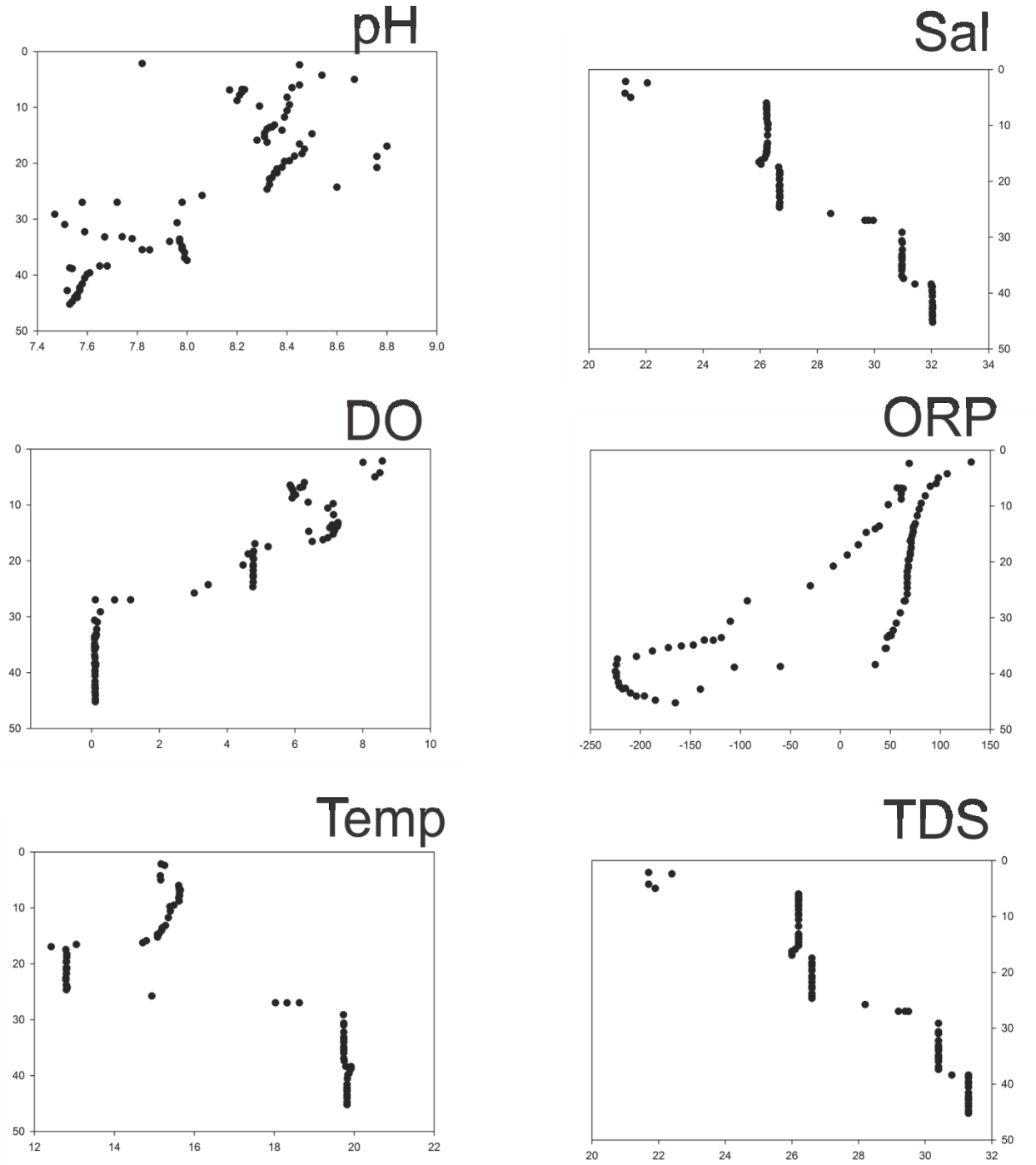

Figure A3. Water column data collected at Jewfish sink on January 29th, 2010. Depth within the sink is displayed on the y axis in meters. Temperature (Temp), Total Dissolved Solids (TDS), pH, Dissolved Oxygen (DO), Oxidation-Reduction Potential (ORP), and Salinity (Sal) are reported. Temperature is measured in degrees Celsius. TDS is measured in grams per liter. LDO is measured in milligrams per liter. ORP is measured in millivolts. Salinity is measured in parts per thousands.

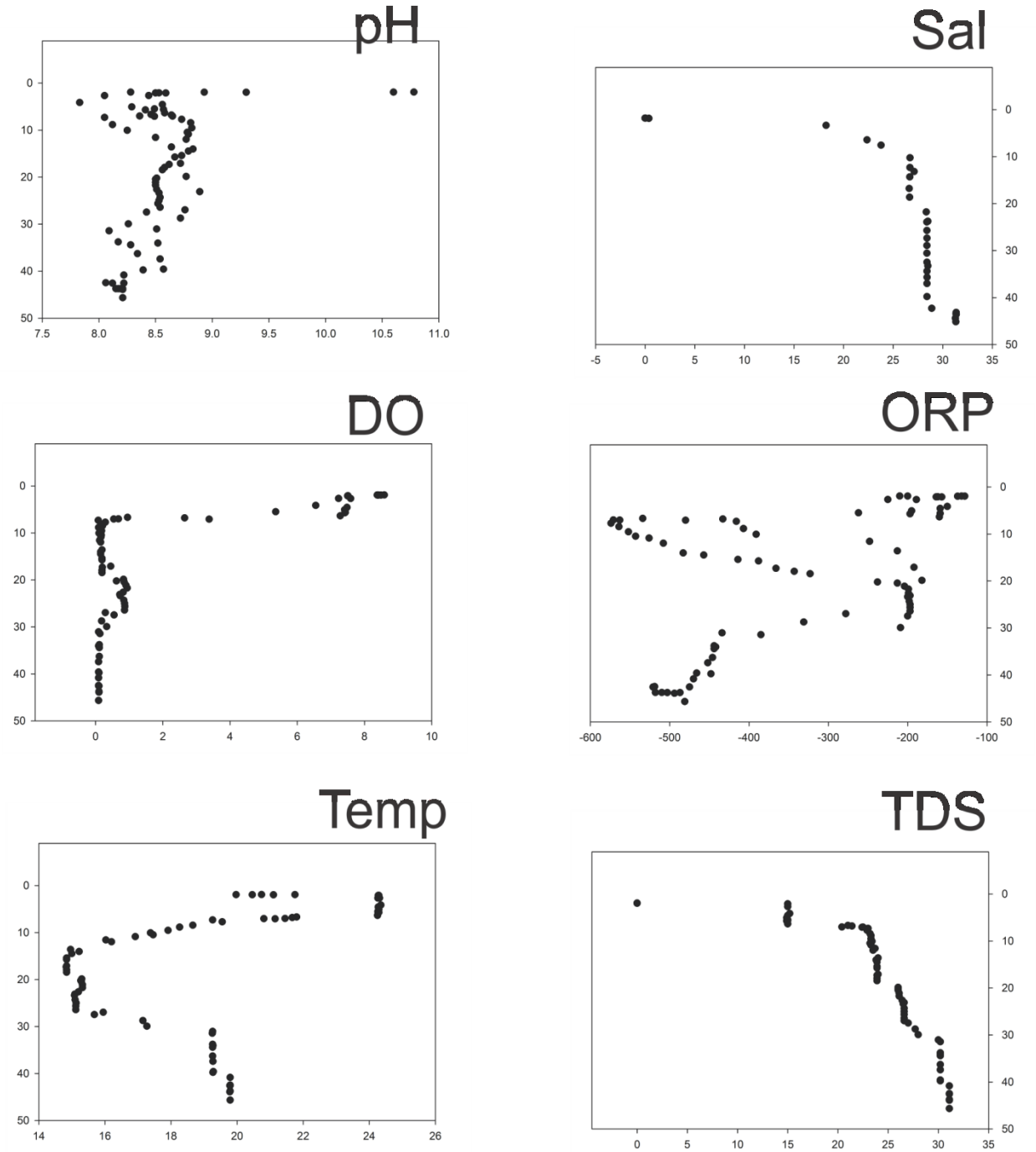

Figure A4. Water column data collected at Jewfish sink on April 23th, 2010. Depth within the sink is displayed on the y axis in meters. Temperature (Temp), Total Dissolved Solids (TDS), pH, Dissolved Oxygen (DO), Oxidation-Reduction Potential (ORP), and Salinity (Sal) are reported. Temperature is measured in degrees Celsius. TDS is measured in grams per liter. LDO is measured in milligrams per liter. ORP is measured in millivolts. Salinity is measured in parts per thousands

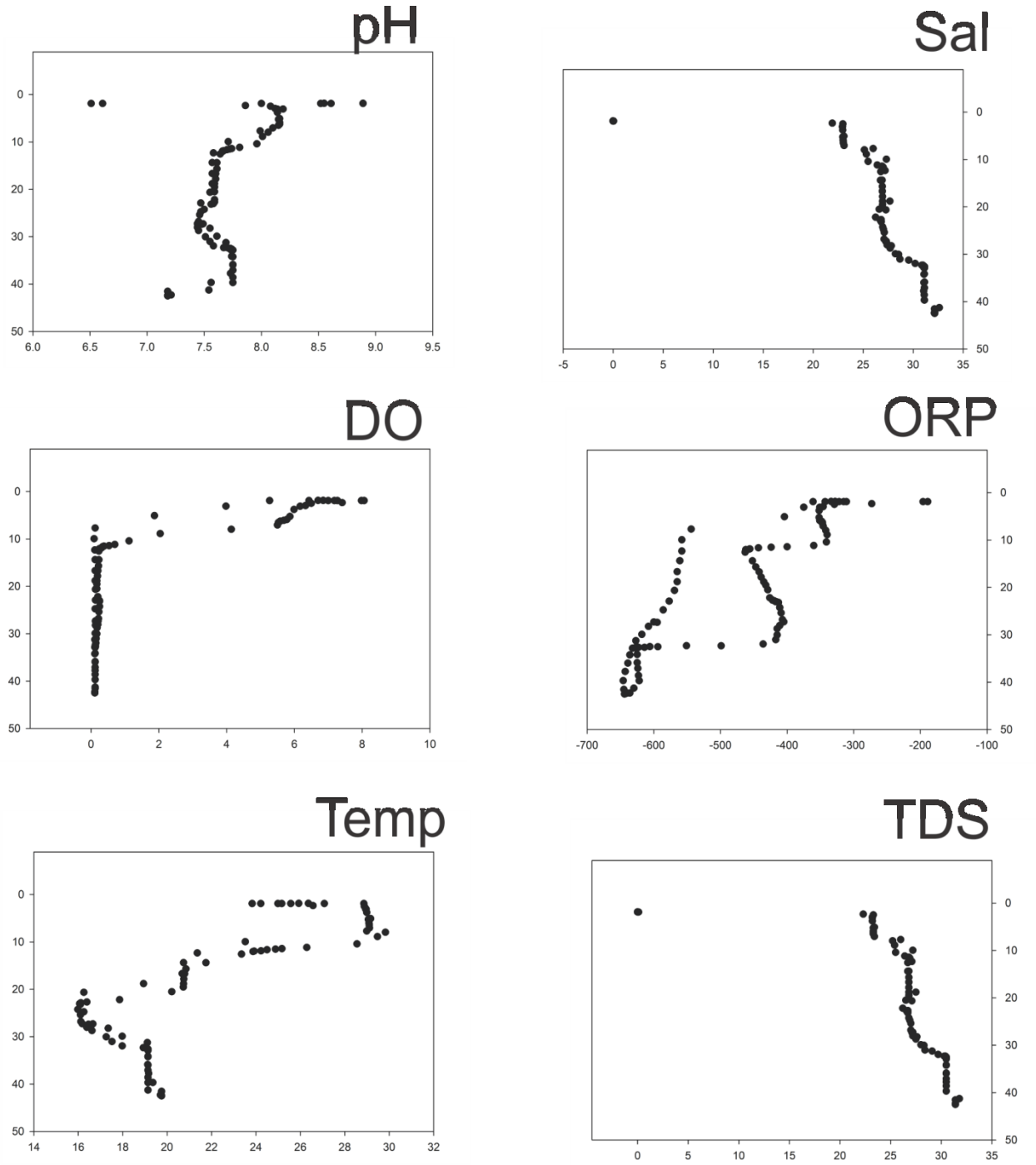

Figure A5. Water column data collected at Jewfish sink on June 9th, 2010. Depth within the sink is displayed on the y axis in meters. Temperature (Temp), Total Dissolved Solids (TDS), pH, Dissolved Oxygen (DO), Oxidation-Reduction Potential (ORP), and Salinity (Sal) are reported. Temperature is measured in degrees Celsius. TDS is measured in grams per liter. LDO is measured in milligrams per liter. ORP is measured in millivolts. Salinity is measured in parts per thousands.

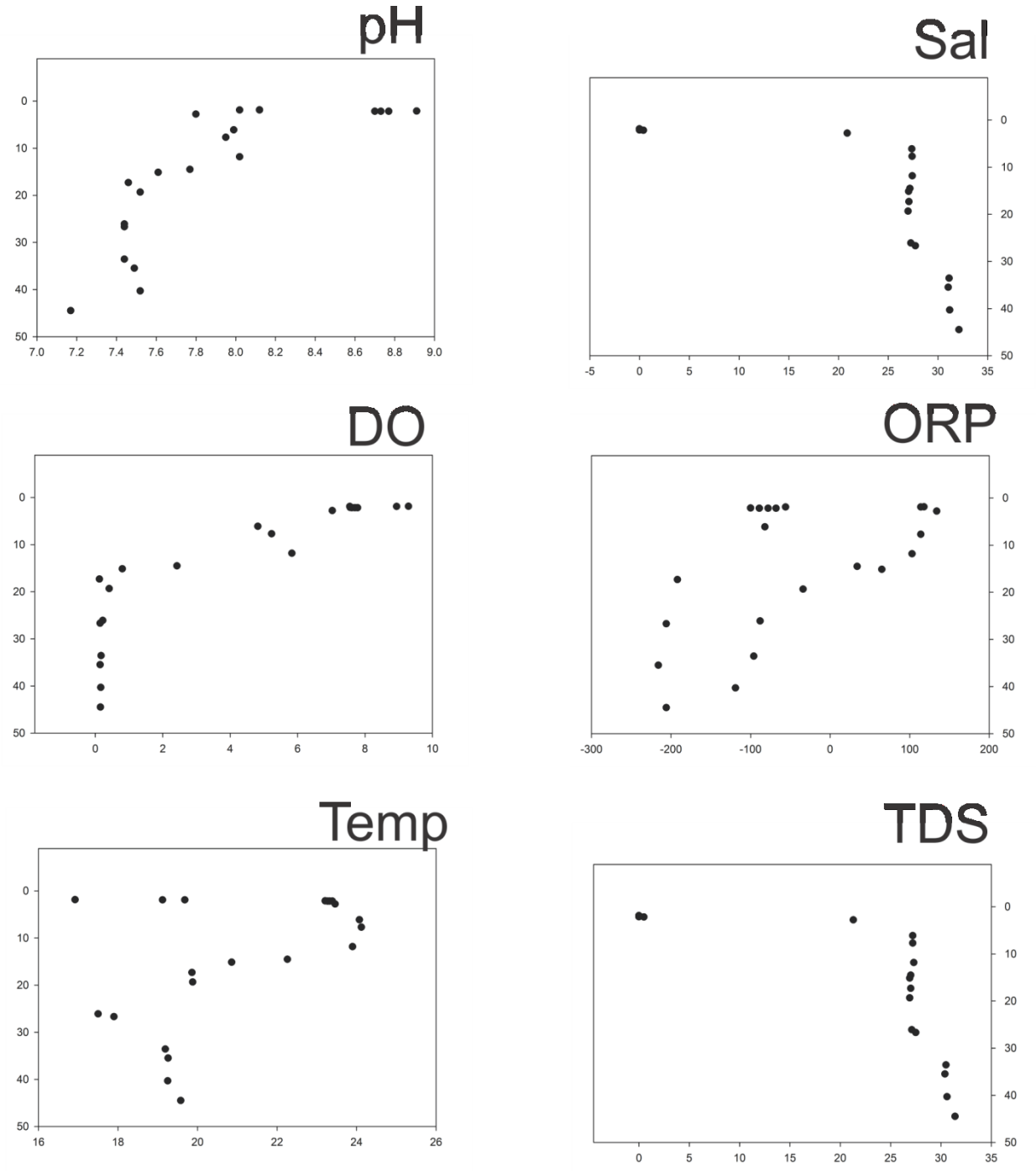

Figure A6. Water column data collected at Jewfish sink on October 22nd, 2010. Depth within the sink is displayed on the y axis in meters. Temperature (Temp), Total Dissolved Solids (TDS), pH, Dissolved Oxygen (DO), Oxidation-Reduction Potential (ORP), and Salinity (Sal) are reported. Temperature is measured in degrees Celsius. TDS is measured in grams per liter. LDO is measured in milligrams per liter. ORP is measured in millivolts. Salinity is measured in parts per thousands.

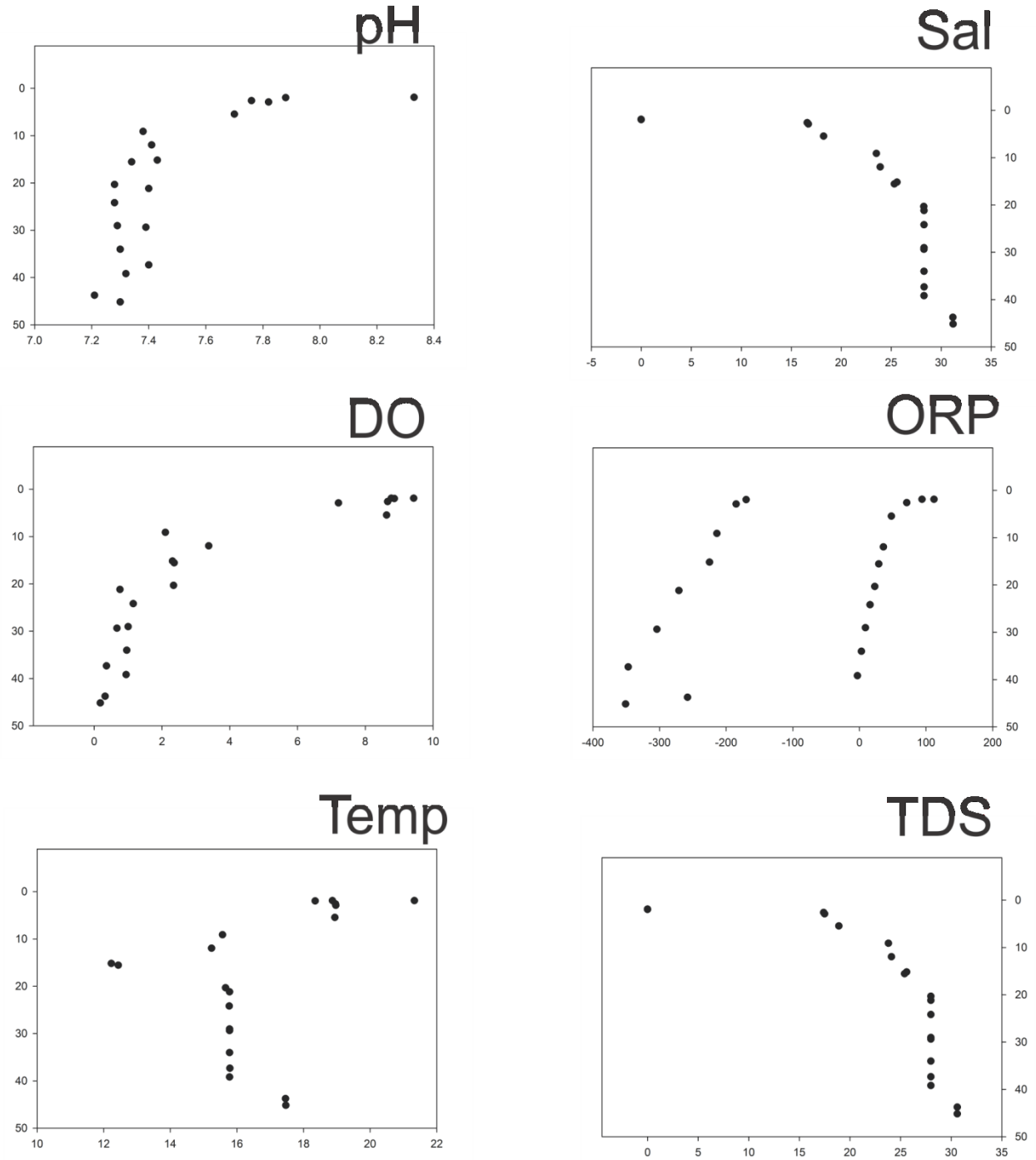

Figure A7. Water column data collected at Jewfish sink on February 19th, 2011. Depth within the sink is displayed on the y axis in meters. Temperature (Temp), Total Dissolved Solids (TDS), pH, Dissolved Oxygen (DO), Oxidation-Reduction Potential (ORP), and Salinity (Sal) are reported. Temperature is measured in degrees Celsius. TDS is measured in grams per liter. LDO is measured in milligrams per liter. ORP is measured in millivolts. Salinity is measured in parts per thousands.

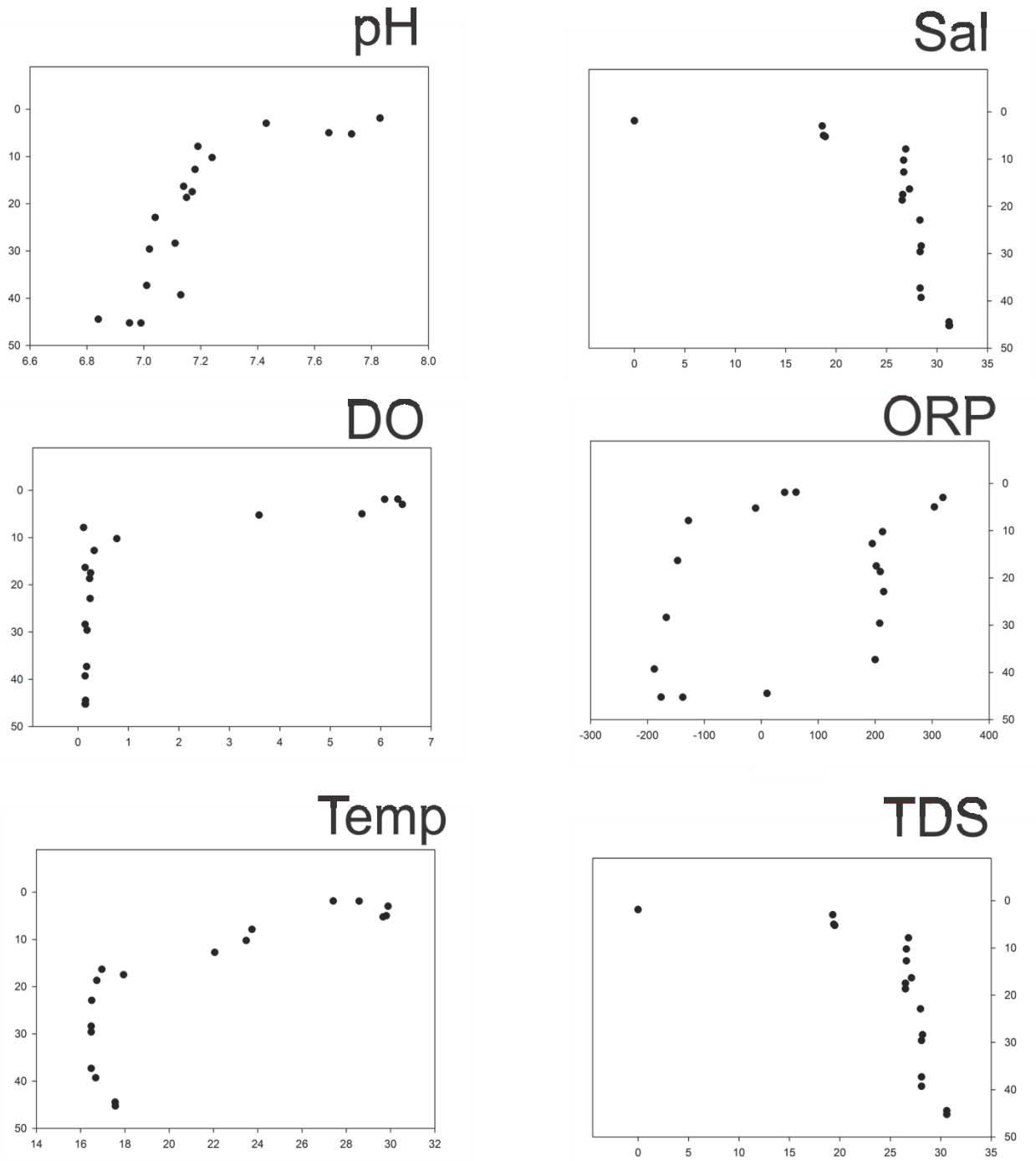

Figure A8. Water column data collected at Jewfish sink on June 18^{tn}, 2011. Depth within the sink is displayed on the y axis in meters. Temperature (Temp), Total Dissolved Solids (TDS), pH, Dissolved Oxygen (DO), Oxidation-Reduction Potential (ORP), and Salinity (Sal) are reported. Temperature is measured in degrees Celsius. TDS is measured in grams per liter. LDO is measured in milligrams per liter. ORP is measured in millivolts. Salinity is measured in parts per thousands.

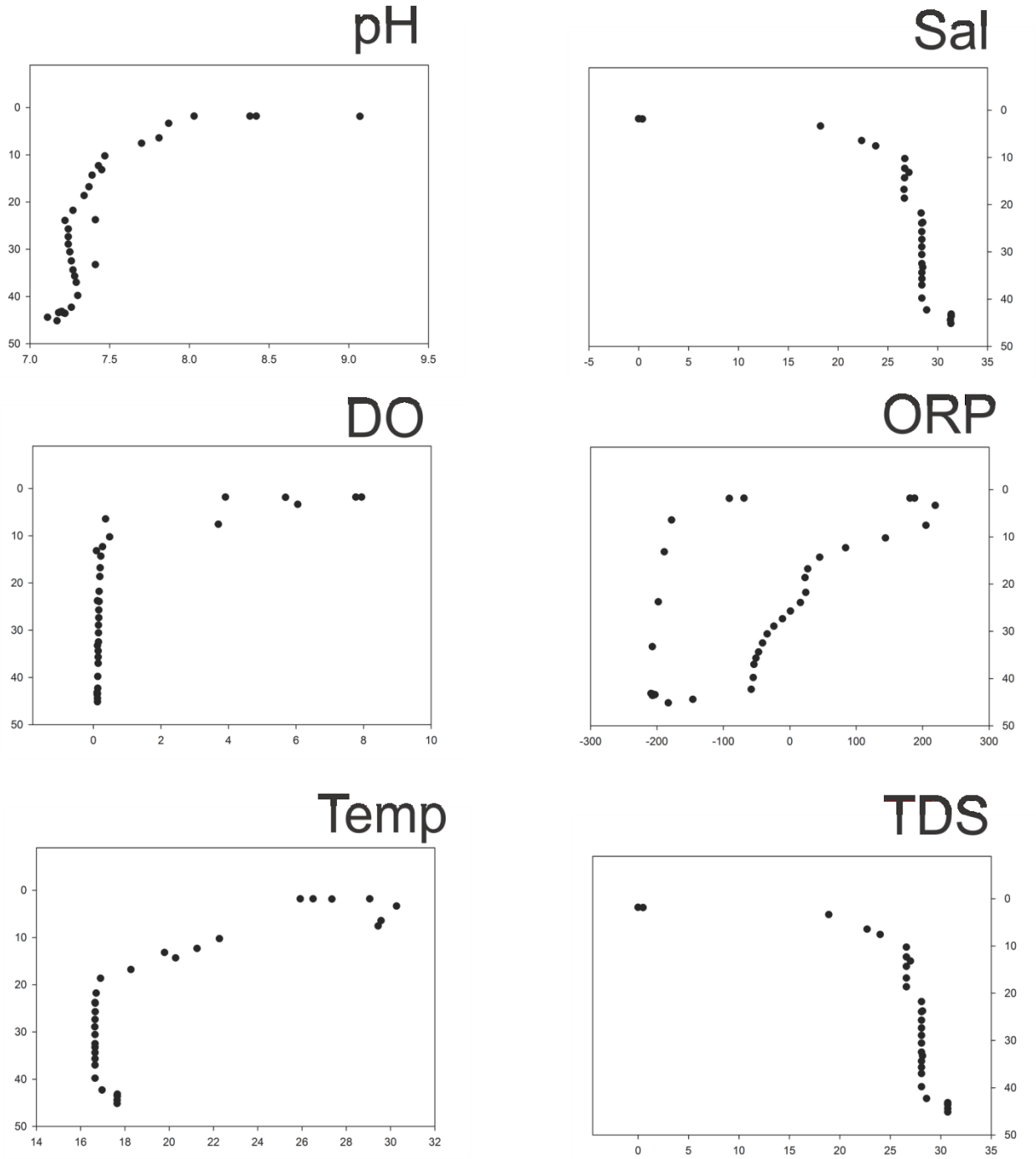

Figure A9. Water column data collected at Jewfish sink on August 23rd, 2011. Depth within the sink is displayed on the y axis in meters. Temperature (Temp), Total Dissolved Solids (TDS), pH, Dissolved Oxygen (DO), Oxidation-Reduction Potential (ORP), and Salinity (Sal) are reported. Temperature is measured in degrees Celsius. TDS is measured in grams per liter. LDO is measured in milligrams per liter. ORP is measured in millivolts. Salinity is measured in parts per thousands.